universität wien

DIPLOMARBEIT

Titel der Diplomarbeit

Monocyte Recruitment into the Central Nervous System

Verfasserin

Magdalena Heninger

angestrebter akademischer Grad

Magistra der Naturwissenschaften (Mag.rer.nat.)

Matrikelnummer:	0605587
Studienkennzahl lt. Studienblatt:	A490
Studienrichtung lt. Studienblatt:	Molekulare Biologie
Betreuerin:	Univ. Doz. Dr. Monika Bradl

Wien, am 31. August 2011

Abstract

There has been a debate about the origin of adult microglial cells which lasted for decades. A group of researchers supported the theory of a myeloid/monocytic ancestor, whereas another circle of researchers believed in the origin of a mesodermal precursor during early fetal development. Recently, it has been confirmed that fetal macrophages serve as progenitors of the resident microglia population found in adults. However, various groups of scientists described a second microglia population, exhibiting amoeboid morphology in the corpus callosum during postnatal development. These cells appear from one week before until ten days after birth and then gradually disappear from the white matter. Their function and fate - whether they leave, differentiate, or undergo apoptosis - are still unknown.

As a first step towards the identification of function and fate, the recruitment of myeloid cells isolated from blood and spleen into the central nervous system (CNS) was assessed. To unequivocally identify these cells and their derivatives, a genetic label was used and the myeloid cell population was isolated from transgenic Lewis rats expressing the green fluorescent protein (GFP) in all of their cells. GFP-expressing cells from adult transgenic Lewis rats were administered via intra peritoneal injection into neonatal Lewis rats. Additionally, expression of cell adhesion molecules on myeloid cells was investigated on messenger RNA and protein level. Results from the injection experiments showed that the cells did not enter into the CNS. This is probably due to administration into the peritoneum. Intravenous injection might present a more promising approach.

Kurzfassung

Der Ursprung adulter Mikrogliazellen war Thema einer jahrzehntelangen Debatte. Während ein Forscherkreis an einem monozytischen Ursprung festhielt, beharrte die gegnerische Front auf einem früheren, mesodermalen Mikroglia-Vorläufer. Erst vor Kurzem wurden fetale Makrophagen mesodermalem Ursprungs als Vorläufer bestätigt. Unterschiedliche Forschergruppen entdeckten allerdings noch eine zweite Mikrogliapopulation in der weißen Substanz des Corpus Callosum, welche amöboide Morphologie aufweist und in der perinatalen Phase zwischen einer Woche vor bis zehn Tage nach der Geburt auftritt. Die Funktion dieser Zellen ist noch nicht aufgeklärt. Des Weiteren ist noch nicht bekannt, ob diese Zellen das zentrale Nervensystem (ZNS) wieder verlassen, ausdifferenzieren, oder Apoptose durchlaufen.

In einem ersten Schritt zur Aufklärung der Funktion und des Schicksals dieser Zellen wurde die Rekrutierung myeloider Zellen aus dem Blut und der Milz in das ZNS untersucht. Zur Identifizierung der verabreichten Zellen diente ein genetischer Marker, das grün-fluoreszierende Protein (GFP), welches in jeder Zelle der transgenen Lewisratte exprimiert wird. GFP positive myeloide Zellen wurden aus transgenen adulten Lewisratten isoliert und neugeborenen Lewisratten intra peritoneal verabreicht. Zusätzlich wurde die Expression

verschiedener Zelladhäsionmoleküle auf myeloiden Zellen auf Boten-RNA und Proteinebene überprüft. Aus den Injektionsexperimenten ging hervor, dass die untersuchten Zellen nicht in das ZNS einwandern. Die Abwesenheit dieser Zellen könnte auf die Injektion in das Peritoneum zurückzuführen sein. Daher stellt intravenöse Verabreichung eine vielversprechende Alternative dar.

Table of contents

Introduction

2.1. Hematopoiesis

Hematopoiesis, the generation of blood cells, is a process that starts during fetal development in the blood islands of the yolk sac and the aorta-gonad-mesonephrons, and is taken over by the liver during late fetal development. Subsequently, the function of blood cell production is gradually adopted by the bone marrow, marking the onset of definitive hematopoiesis. In the adult organism, the bone marrow is the main site of hematopoiesis ((Mikkola and Orkin, 2006); Abbas et al. Cellular and Molecular Immunology 6th edition).

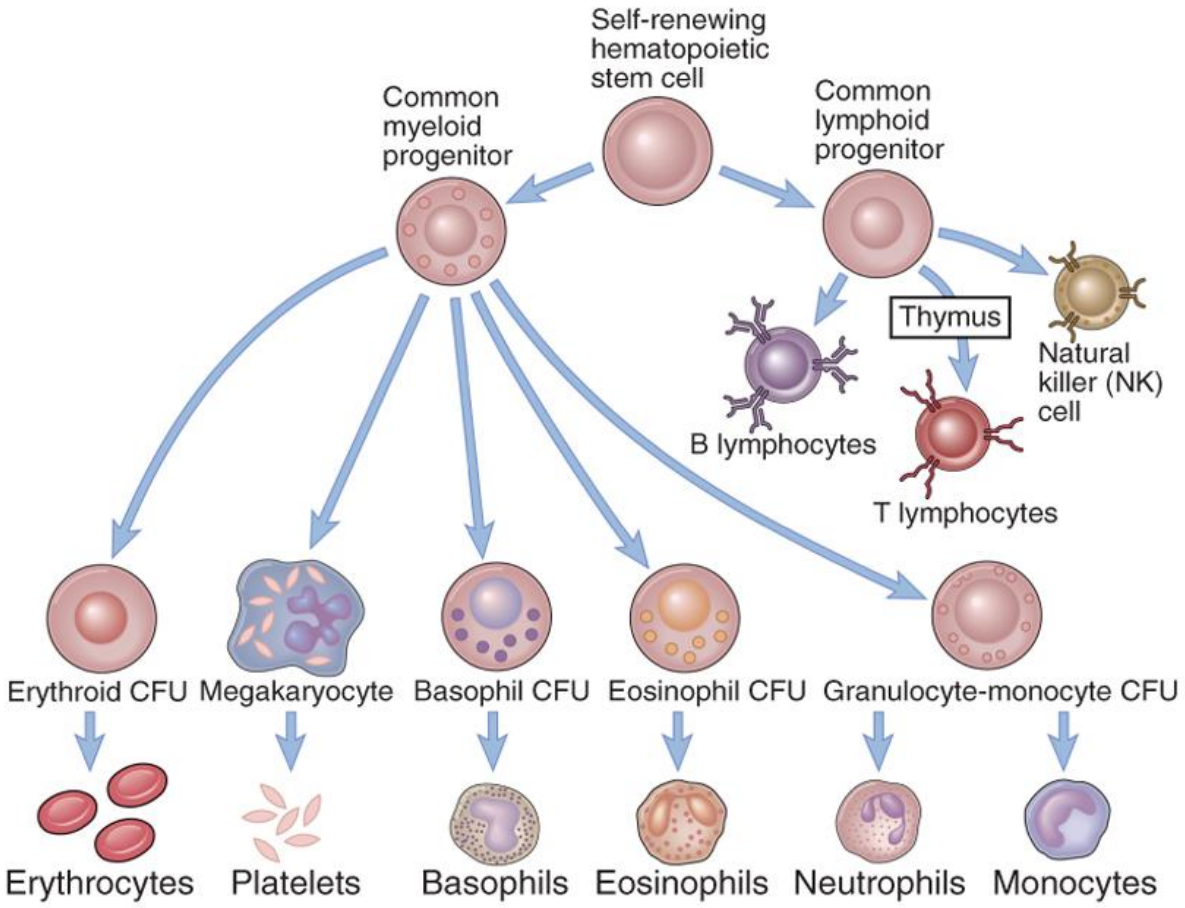

Figure 1: A highly proliferative common hematopoietic stem cell which resides in the bone marrow can commit to two different lineages, the common myeloid progenitor (CMP) and the common lymphoid progenitor (CLP) lineage. The CMPs eventually give rise to erythrocytes, platelets, granulocytes and monocytes. The CLPs differentiate to natural killer cells and lymphocytes. Figure taken from Abbas et al: Cellular and Molecular Immunology, 6th edition.

2.2. Leukocytes

Leukocytes constitute a diverse group of cell types that mediate innate and adaptive immune responses (Geissmann et al., 2010). The phagocytic cells can be divided into two categories. The polymorphonuclear granulocytes, which are cells of innate immunity, comprise basophils, eosinophils and neutrophils. The mononuclear phagocyte system consists of circulating monocytes, tissue macrophages and various subtypes of dendritic cells (Sunderkotter et al., 2004; Van Furth et al., 1972).

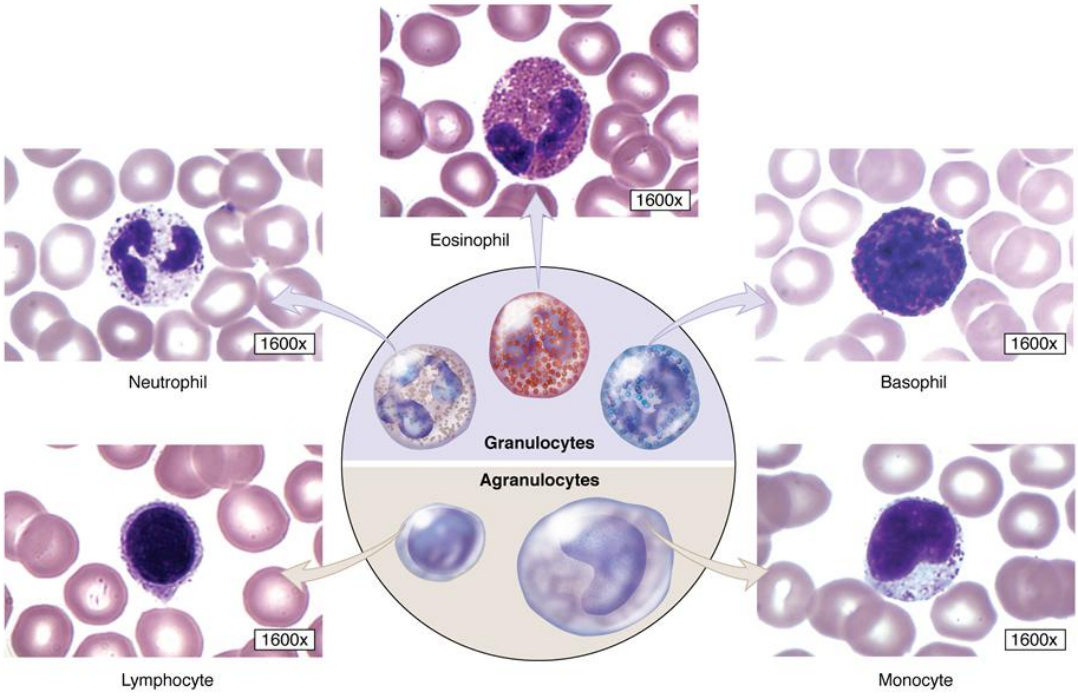

Figure 2: Leukocytes can be divided into granulocytes and agranulocytes. The granular leukocytes can be divided into neutrophilic, eosinophilic, and basophilic granulocytes. The agranular leukocytes comprise the mononuclear monocytes and lymphocytes. Figure taken from Junqueira's Basic Histology 12th edition, Anthony L. Mescher.

Monocytes are the most dynamic and versatile cell population of the mononuclear phagocyte system (Varol et al., 2009). They constitute about 10 % of peripheral leukocytes and are characterized by a high cytoplasm-to-nucleus ratio, irregular cell morphology and their most remarkable feature, the horse-shoe, or kidney bean-shaped nucleus. They commonly express CD11b, CD11c, M-CSF or CD115 and F4/80 (Geissmann et al., 2003) (see other cell surface markers in Table 1).

2.2.1. Monocyte Subsets

Monocytes are a heterogenous cell population. According to their morphology, size, granularity, transcriptome, and antigen expression two major subsets can be distinguished (Geissmann et al., 2003; Yona and Jung, 2010). The dichotomy of monocyte subsets is conserved among humans, rats, mice and has also been described in other mammals (Geissmann et al., 2003; Yona and Jung, 2010; Yrlid et al., 2006).

Mouse (Yona and Jung, 2010)	**Rat** (Yrlid et al., 2006)	**Human** (Ziegler-Heitbrock, 2000)
Inflammatory subset		
Ly6C^{high}, CX3CR1^{low}, CCR2^{+}, CD62L^{+}	CCR2^{high}, CX$_3$CR1^{low}, CD43^{low}, CD62L^{+}	CD14^{high}CD16^{-}
Resident subset		
Ly6C^{low}, CX$_3$CR1^{high}, CCR2^{-}, CD62L^{-}	CCR2^{low}, CX$_3$CR1^{high}, CD43^{high}, CD62L-	CD14^{low} CD16^{high}

Table 1: Dichotomy of monocyte subsets.

The first subset is described as “inflammatory subset” in rodents, analogous to the human “classical population”. The second subset is often referred to as the “resident”, “surveilling” population (Geissmann et al., 2003; Varol et al., 2009). In mice and humans, a third population, the “transitional” or “intermediate” monocytes are described (Tacke and Randolph, 2006).

Ly6C^{high} monocytes are larger, more granular, and have a shorter half life than the Ly6C^{low} subset (Geissmann et al., 2003). The two subsets are believed to be developmentally interlinked. Ly6C^{high} monocytes descend from dividing macrophage/dendritic cell progenitors (MDP), which reside in the bone marrow and are subsequently released as non-dividing cells (Akashi et al., 2000b). It has been suggested by some groups, that in absence of inflammatory cues, Ly6C^{high} monocytes return to the bone marrow, where they acquire the Ly6C^{low} subset features (Sunderkotter et al., 2004). These monocytes possibly serve as emergency pool that can be mobilized to accommodate the organisms need. This conversion raises the question whether Ly6C^{low} monocytes originate from MDPs, or if they require Ly6C^{high} as an intermediate state (Varol et al., 2009) (see Figure 3).

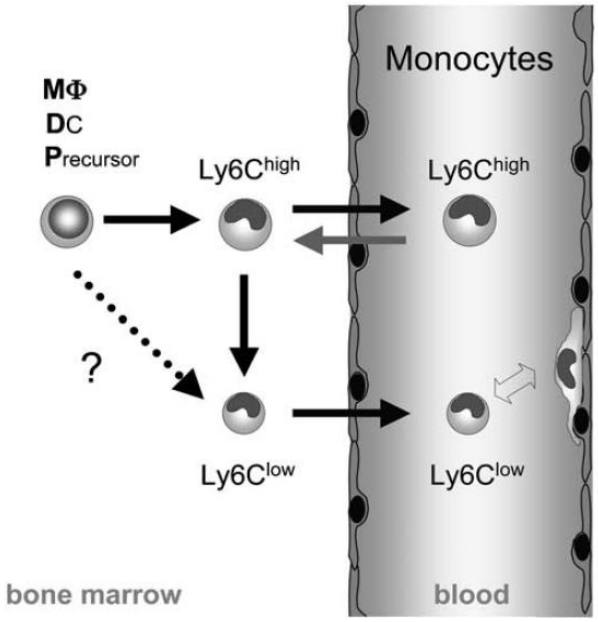

Figure 3: The origin of the two main monocyte subsets. It remains to be elucidated, whether Ly6C^{low} are directly derived from MDP, or whether they require an intermediate monocytic stage (Varol et al., 2009). Ly6C^{low} monocytes express a variety of chemokine receptors and integrins (Shang et al., 1998), allowing long-range crawling along the endothelium (Auffray et al., 2007). Figure taken from Varol et al., 2009.

2.2.2. Fate and functions of blood monocytes

Monocyte heterogeneity is also reflected in the functions and fates of the subsets. Ly6C^{high} monocytes are recruited to sites of inflammation in a CCR2-dependent manner (Geissmann et al., 2003; Serbina and Pamer, 2006). Their counterparts, Ly6C^{low} monocytes, home to non-inflamed tissues, a recruitment dependent on fractalkine (CX3CL1), which is associated with tissue repair (Geissmann et al., 2003). It has recently been discovered that Ly6C^{low} monocytes are patrolling along the resting blood vessel endothelium, a migration mediated by integrin LFA-1 and fractalkine receptor (CX3CR1). Upon inflammatory insults, they can be rapidly recruited to the affected location, even outpacing Ly6C^{high} cells. (Auffray et al., 2007; Varol et al., 2009)

Monocytes are ephemeral, short-lived cells (Van Furth and Cohn, 1968). This observation nourished the hypothesis that monocytes act as a transient reservoir of precursors, which can enter the tissue and replenish local macrophage and dedritic cell pools (Yona and Jung, 2010). In vitro differentiation of monocytes into macrophages and dendritic cells has been achieved by treatment with specific cytokines, however this does not reflect the situation in the in vivo steady state (Geissmann et al., 2003). Under normal conditions, resident tissue macrophage populations, such as liver Kupffer cells, splenic white pulp, alveolar, and metallophilic macrophages are largely maintained through local proliferation. Ly6C^{low} monocytes are likely candidates for replenishment of tissue macrophages, however their exact contribution still remains a subject of investigation. Several studies give strong

evidence that Ly6C^{high} monocytes give rise to various tissue macrophages and dendritic cells under pathological conditions (Tacke and Randolph, 2006; Yona and Jung, 2010).

2.2.3. Monocyte reservoirs

Monocytes are commonly described as circulating blood cells, but as mentioned before, they can also shuttle back to the bone marrow and serve as a monocytic reservoir. Recently, the spleen has been described as another harbor for large numbers of monocytes. These "reservoir monocytes" can be rapidly mobilized upon injury and inflammation, even outnumbering their equivalents in the periphery. Spleen monocytes resemble their blood counterparts morphologically, genetically, in their origin and fate, as they potentially give rise to DCs and macrophages. (Swirski et al., 2009; Yona and Jung, 2010)

2.3. Microglia

2.3.1. Morphology and Phenotype

Microglia are brain-resident phagocytes and are ubiquitously distributed throughout the grey and white matter. As sensors of CNS pathologies, they are the only CNS-based innate immune effector cells and constitute the first immunological barrier against pathogens and environmental insults (Kreutzberg, 1996; Mildner et al., 2007).

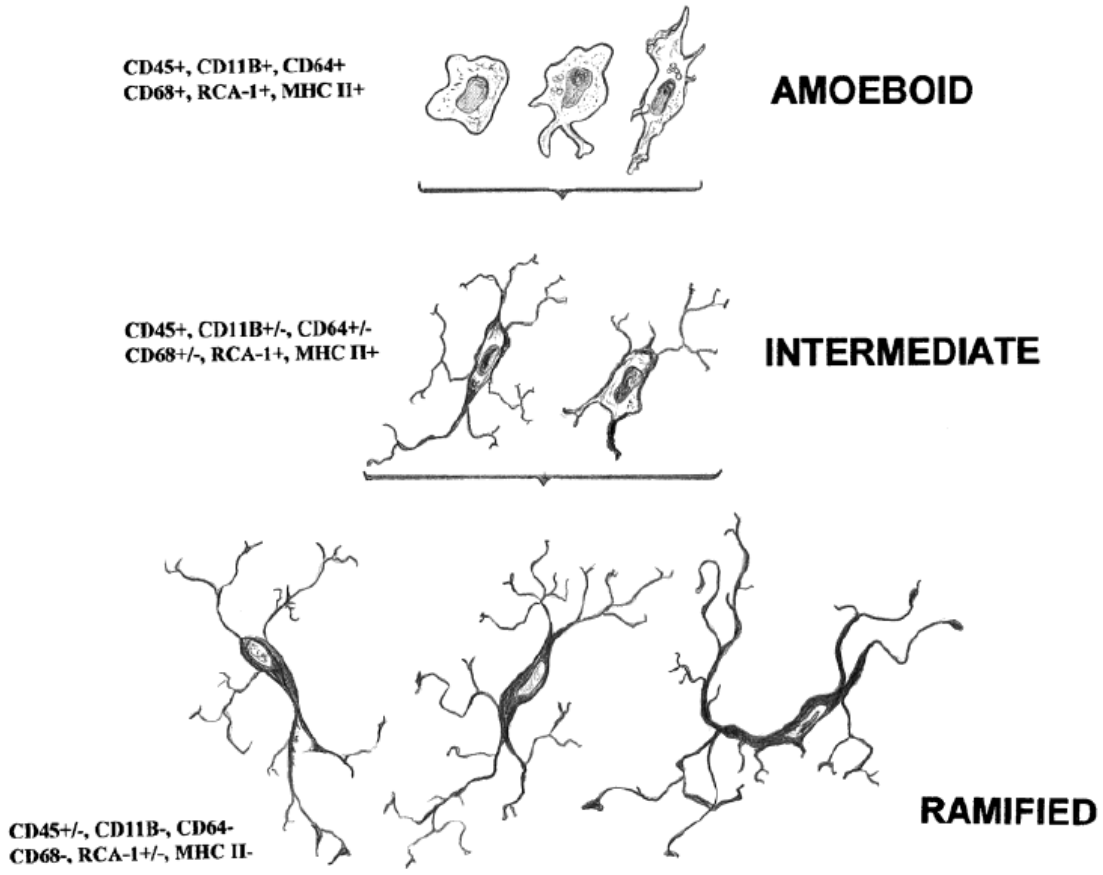

Figure 4: Microglia activation is a graded process. According to phenotype and morphology, 3 different states can be distinguished: the amoeboid, intermediate, and ramified microglia. Figure modified from Rezaie et al. 1999. (Rezaie and Male, 1999)

Microglial cells exhibit a specialized morphology and surface marker expression which is highly dependent on their microenvironment (Perry et al., 1993). They can be activated upon extracellular stimulation, whereas they respond in a graded fashion (Chan et al., 2007) (see Figure 4). In the quiescent state, microglia appear as ramified, arborized resting cells, whereas the notation "resting" is not quite accurate, as microglia possess highly motile filopodia (Davalos et al., 2005) which constantly protrude and retract, while microglia are scavenging their surroundings for physiological changes (Neumann et al., 2009). Ramified microglia down-regulate molecules essential for antigen-presentation. Upon environmental stimulation, they become activated, assume an arborized appearance and upregulate their

immunophenotype, converting them into potent antigen-presenting cells comparable to dendritic cells (Akashi et al., 2000a; Hoftberger et al., 2004; Stoll et al., 2006; Tambuyzer et al., 2008). Under persistent stimulation, microglia acquire the ameboid phenotype and become functional, phagocytic cells (Tambuyzer et al., 2008).

2.3.2. Functions

Under pathological conditions, like brain injury, inflammation, and neurodegeneration microglia carry out essential immune effector and immune modulating functions and they are critical contributors to repair and tissue homeostasis in the resting state (Mildner et al., 2007; Neumann et al., 2009). As immune-modulatory cells they can secrete trophic factors, cytokines, and chemokines to attract secondarily recruited immune cells. (Tambuyzer et al., 2008). Activated microglia can also release cytotoxic mediators, which have deleterious side-effects on neurons (Neumann et al., 2009; Polazzi and Monti, 2010). Following resolution of inflammatory response, microglia, by virtue of their phagocytic potential, engulf tissue debris and thus create a pro-regenerative microenvironment (Neumann et al., 2009).

2.3.3. Origin of microglia

Up to date it is known that the adult resident microglia population derives from primitive macrophages originating from the yolk sac in an early embryonic stage. In a first wave of microglia colonization they seed the brain rudiment around embryonal day 9 (E9), where they proliferate rapidly to establish the microglia population (Alliot et al., 1999; Alliot et al., 1991; Ginhoux et al., 2010; Takahashi and Naito, 1993). Yet, the quest for the origin of microglia has not been an easy task, bringing up a controversial debate which lasted for decades. The paradigm that microglia may have a monocytic origin was supported by numerous studies performed in the last decades.

In 1978, Ling and his colleagues observed the presence of carbon particle-labeled monocytes in the corpus callosum of perinatal rats. The cells differentiated into amoeboid and later on ramified microglial cells (Tambuyzer et al., 2008).

Roughly ten years later, Chugani et al. exploited the presence of ribonucleoprotein particles, the so called vaults in macrophages to observe the entry of microglial precursors into the brain. They had an amoeboid morphology in the corpus callosum until postnatal day 14, and progressively assumed a ramified morphology, while leaving the white matter area (Chugani et al., 1991a).

Mildner et al. found that CCR2+ monocytes enter the mouse brain upon irradiation, and this engraftment is enhanced in CNS pathology. They suggested that these “inflammatory” monocytes serve as circulating precursors and engraft the adult brain in a CCR2-dependent manner and give rise to microglia-like cells. However, the microglial engraftment turned out to be an irradiation artifact. Irradiation of CNS induces vascular changes, compromising the

competence of the blood brain barrier (Ransohoff, 2007). CCL2, the ligand of CCR2 is notoriously upregulated in irradiation (Klopp et al., 2007) and inflammation (Conductier et al., 2010; Ohno et al., 2000), thus it is not surprising that CCR2+ expressing monocytes are preferentially recruited into the CNS. In the negative control, when the head was shielded from irradiation, migroglial engraftment could no longer be observed (Mildner et al., 2007). These results suggest that monocyte recruitment only occurred upon conditioning, which does not mimic the situation under normal, physiological conditions.

Bone marrow chimeras with EGFP (enhanced green fluorescent protein)-expressing hematopoietic cells displayed microglial engraftment after four weeks of chimerism. In lesion models for stroke, cholinergic fiber degeneration and facial-nerve axotomy, a massive infiltration of EGFP-labeled round-shaped cells was observed. These cells were identified as microglia by expression of the microglia/macrophage marker Iba1 (ionized calcium binding adaptor molecule 1) (Priller et al., 2001).

The results of these studies are consistent with the proposition, that monocytes serve as tissue macrophage precursors under pathological conditions. However there is no definite evidence consolidating the hypothesis of a monocytic origin.

Based on the observation that microglia colonize the CNS in early development, before establishment of the vascular system, Takahashi and Naito proposed that microglia derive from a separate mesodermal lineage, namely primitive macrophages originating from the yolk sac (Takahashi and Naito, 1993).

Experiments, conducted in parabiotic animals, revealed that microglia are not replenished by bone marrow-derived progenitors, but are maintained by local proliferation (Ajami et al., 2007). Further, kinetic studies showed that microglia turn over at much lower pace than other tissue macrophages (Kennedy and Abkowitz, 1997). A bone marrow transplantation experiment indicated a higher rate of CNS macrophage turn over, however these CNS-resident phagocytes turned out to be perivascular macrophages (Hickey and Kimura, 1988). Together with meningeal and choroid plexus macrophages they are now known to be periodically replenished by circulating hematogenous precursors (Polfliet et al., 2001). Adult microglia are maintained by local proliferation and only under pathological conditions, or after injury, microglia population is supported by recruited blood-borne monocytes.

Recently, data from in vivo lineage tracing studies conducted by Ginhoux et al. provided final evidence, that adult microglia derive from primitive yolk sac macrophages which arise before embryonic day 8 (E8), right before onset of vascularisation around E9. In their extensive studies, they also confirmed that precursors from definitive hematopoiesis, including monocytes, contributed only to a minor extent to adult microglia population in bone marrow chimeric and parabiotic animals and therefore do not substantially contribute to adult microglial engraftment in the steady state. As already highlighted in previous studies, the

results suggest that microglia are maintained by self-renewal of a local microglial precursor population (Alliot et al., 1999; Ginhoux et al., 2010).

2.3.4. The fountain of microglia

In the CNS, two different microglia populations have been described on the basis of marker expression, morphology, and location in cerebrum. One peripheral population exhibits ramified morphology with a resting phenotype, and the second one displays an amoeboid morphology and abides within the ventricular zone, subventricular zone and corpus callosum until the beginning of the third gestational trimester. The ramified, parenchymal microglia take up residence early during development, whereas the amoeboid microglial cells suddenly appear in the perinatal phase in the “fountain of microglia” zones. On this occasion, a dual lineage for microglia has been proposed (Rezaie, 2004).

Now that the origin of adult, parenchymal microglia has been unraveled, there still remains a question mark to the origin of a second wave of microglia recruitment in the perinatal stage. This timed invasion and persistence of amoeboid microglia is restricted to areas of the cingulum and the supraventricular corpus callosum and they appear in rodents from one week before until ten days after birth (Hristova et al., 2010). Experiments with transgenic mice carrying EGFP under the control of the Iba1 promoter led to the detection of a fluorescent signal in respective areas of the CNS. At postnatal day 6 (P6), they found clear EGFP signals from amoeboid cells in the supraventricular corpus callosum. The number of EGFP-positive cells decreased in this area and failed to be detected at postnatal day 14 (P14). Further, a progressive maturation of EGFP-positive cells into ramified microglia in the cortical parenchyma could be observed (Hirasawa et al., 2005).

Preliminary data from immunohistochemical experiments in our lab revealed iron-positive cells with ameboid morphology in the area of the corpus callosum between day of birth (P0) and postnatal day 7 (P7), where the “fountain of microglia” has been described (see Figure 7). A peak of iron positive cells was observed at P14. Further, a time study from P0 to P14 revealed a correlation between a decrease of iron-positive cells in the stem cell zone with a rise of iron-positive cells in the corpus callosum (unpublished data). After successful double staining with Iba-1, iron-positive cells could be classified into the myeloid lineage (unpublished data not shown). From this observation we hypothesized that mononuclear phagocytes enter from the ventricle and eventually migrate towards the corpus callosum.

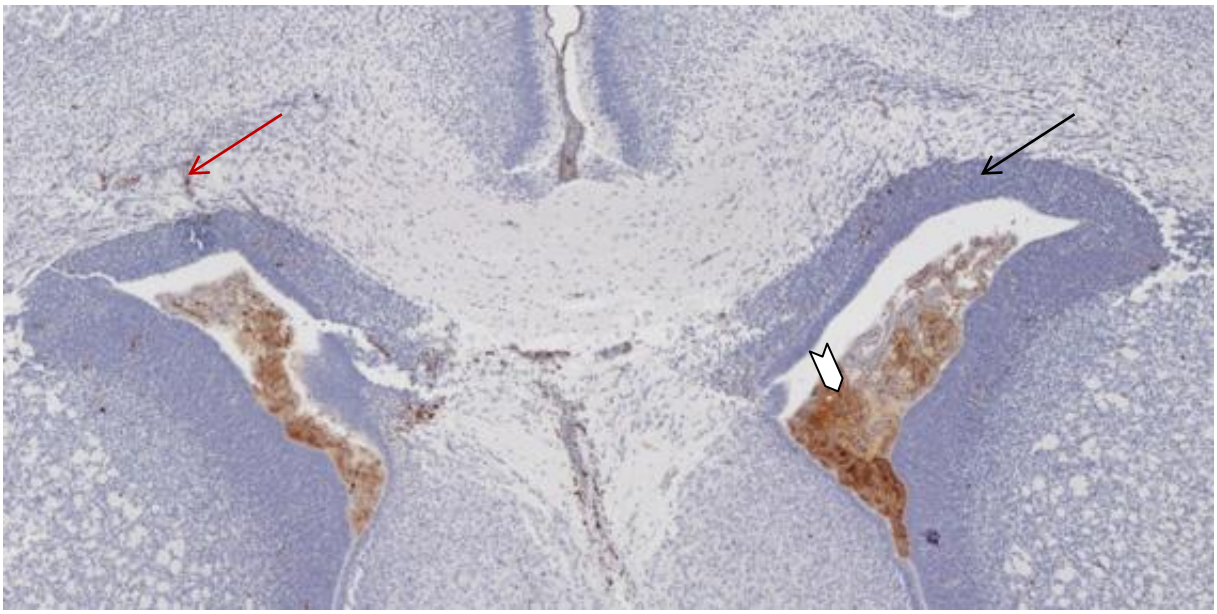

Figure 5: Brain section of a P0 rat pup, stained for iron with DAB-enhanced Turnbull Blue. The black arrow indicates the stem zell zone of the lateral ventricle. During postnatal development, iron positive microglia-like cells are found in the stem cell zones and the supra- and periventricular corpus callosum (see red arrow). Cell nuclei are stained in blue. The choroid plexus stains for iron (white arrow head).

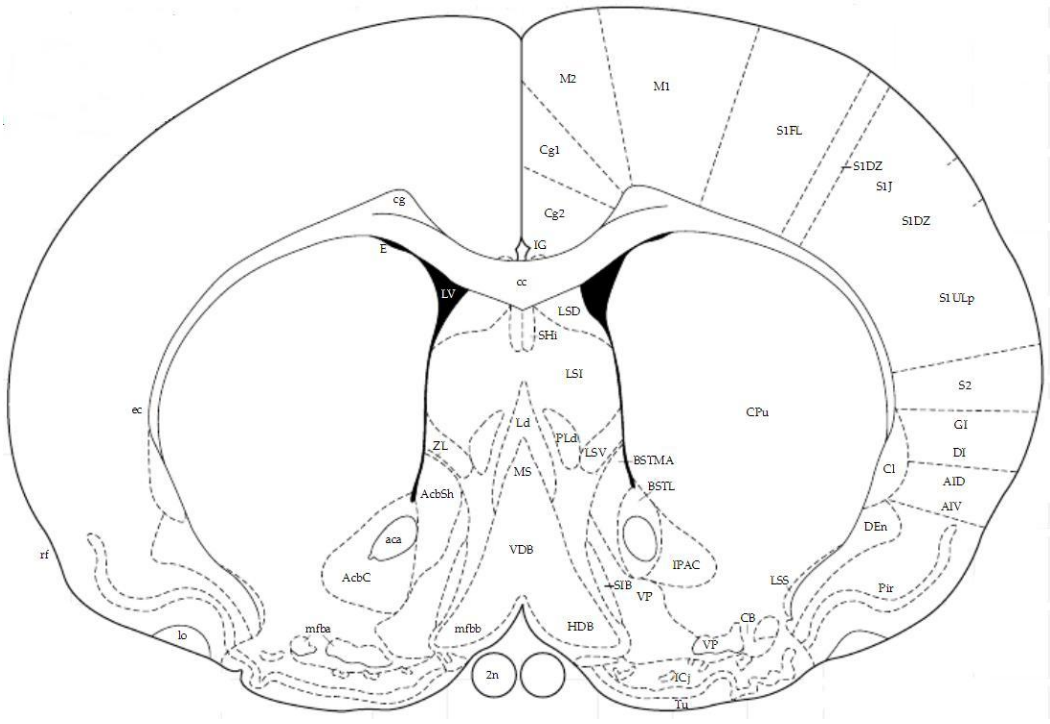

Figure 6: This figure illustrates the brain section of interest (Figure 16) from the rat brain atlas[1].

[1] http://www.scribd.com/doc/22822097/Rat-Brain-Atlas

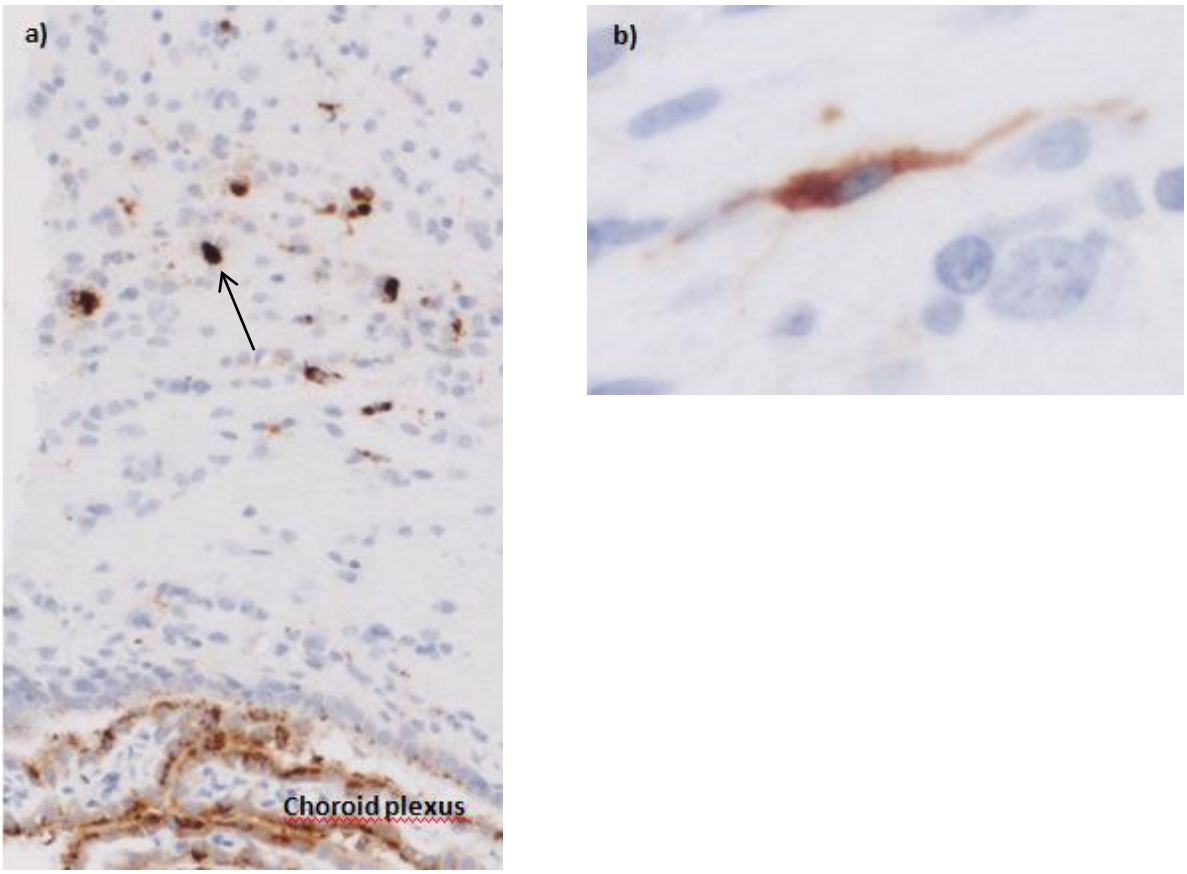

Figure 7: a) DAB enhanced - Turnbull Blue staining (brown) of iron-containing cells, which display amoeboid morphology (see black arrow). Iron positive cells are located in the supraventricular corpus callosum. Cell nuclei are stained blue. Choroid plexus displays brown iron staining (× 250). b) Higher magnification of an iron positive cell (× 400).

2.4. Aim of the thesis

In this study, we aim to elucidate the source of the observed fountain of microglia cells. To address the hypothesis of a monocytic origin, isolated and GFP-labeled blood cells are injected into the peritoneum of newborn Lewis rats. Based on unpublished data from our lab, amoeboid phagocytes contain iron. Therefore it is also investigated, whether iron-containing cells of myeloid lineage are recruited into the CNS. Our source of these cells is the spleen. In case one of these cell types enter into the predicted area (see Figure 5), it can further be assessed how long these cells persist in the CNS, whether they undergo apoptosis, emigrate, or differentiate and contribute to the parenchymal microglia population.

Materials and Methods

3.1. Isolation of peripheral blood mononuclear cells

3.1.1. Materials

- 50 ml syringe Luer-Lok™ (BD Plastipak™)
- Needle, Microlance™ 3, 18G, 1,2 x 44 mm (BD)
- Needle, Microlance™ 3, 19G, 1,1 x 40mm (BD)
- 10mM PBS (phosphate buffered saline)/EDTA
    - 137 mM NaCl (Merck) 80 g
    - 10 mM Na_2HPO_4 x $2H_2O$ (Merck) 17.8 g
    - 1.7 mM HK_2PO_4 (Merck) 2.4 g
    - 2.7 mM KCl (Merck) 2 g
    - 2.7 mM EDTA (Merck) 7.9 g (10 x stock)

  For 1 x dilute 10 x stock 1:10 with dH_2O.
- Perfusion buffer
    - 10 mM PBS
    - Heparin ammonium salt (0.452 mg/ml) (Sigma-Aldrich)
- Isolation buffer
    - 10 mM PBS
    - 1 % Bovine Serum Albumine, pH 7 (PAA)
- Percoll 82 (sterile filtered)
    - 1.5 M NaCl (Merck)
    - Percoll (GE Healthcare) (density: 1.130g/ml)
- H_2O (Ampuwa®)
- ACK lysis buffer
    - 0.15 M NH_4Cl (Merck)
    - 1 mM $KHCO_3$ (Merck)
    - 0.1 mM Na_2EDTA (Merck)

  adjust to pH 7.4 with HCl.

- RPMI 1640 Bio Whittaker ® without L-glutamine (Lonza)
- Bio Whittaker ® Phosphate buffered saline (PBS) (Lonza)
- Rat serum (self-prepared)

3.1.2. Method

Adult Lewis rats, overexpressing the green fluorescent protein (GFP) under the control of the β-actin promoter were used as a source for genetically labeled cells. The animals were bred at the Decentral Facilities of the Institute of Biomedical Research (Medical University Vienna).

The protocol was adapted from Scriba et al. (Scriba et al., 1996), Repnik et al. (Repnik et al., 2003), and Zassler et al. (Zassler and Humpel, 2006). The GFP transgenic animals were sacrificed by inhalation of CO_2. The thorax was opened and the heart was perfused with 100ml perfusion buffer by slowly introducing the solution into the left heart ventricle and withdrawing the effluent from the right ventricle (Figure 8).

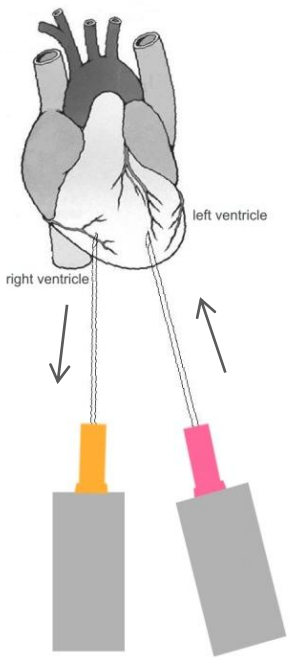

Figure 8: Schematic illustration of rat heart perfusion procedure. 19G syringe was inserted into the right ventricle, 18G syringe was inserted into the left heart ventricle. Figure modified from [2].

[2] http://kentsimmons.uwinnipeg.ca/16cm05/16labman05/lb8pg12.htm

The following procedure was performed under sterile conditions in the laminar flow hood. All centrifugation steps occurred at 4°C, and the samples were always kept on ice. The perfusate was centrifuged for 10 minutes at 600g. The blood plasma was aspirated and blood cell pellets resuspended in isolation buffer. The blood perfusate was carefully loaded onto 14ml Percoll82 solution, and centrifuged at 600g for 30 minutes (acceleration 1, deceleration 0). After centrifugation, the Percoll gradient comprised 3 different layers, the blood plasma, buffy coat and erythrocytes (Figure 9).

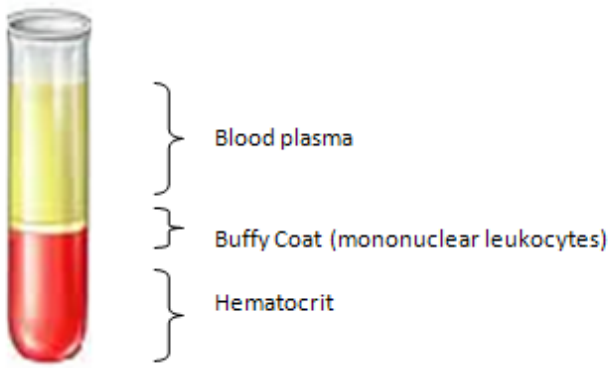

Figure 9: Centrifugation in a Percoll gradient results in 3 separate layers of blood components: The plasma forms the uppermost layer, while erythrocytes precipitate in the tube bottom. Hematocrit and blood plasma are flanked by a thin, grayish layer of platelets and leukocytes, called the "buffy coat". Figure modified from [3].

After harvesting the buffy coat, the cell suspension was centrifuged at 550g for 10 minutes. Erythrocyte lysis was achieved by incubation in ACK lysis buffer for 5 minutes. After centrifugation at 550g for 10 minutes, the pellet was washed twice in isolation buffer and an aliquot was taken for cell counting in a counting chamber (Reichert Bright-line Hemacytometer).

A cytospin (Shandon CytoSpin III) of $5x10^5$ – 10^6 cells at 1000 rpm for 10 minutes was performed and stained with May-Grünwald/Giemsa according to a well-established standard protocol to assess the quality and morphology of the buffy coat cells. The cells were resuspended in RPMI/ 1% rat serum for subsequent injection into neonates (P0).

[3] http://www.biosbcc.net/doohan/sample/htm/Blood%20cells.htm

3.2. Spleen Homogenization

3.2.1. Materials

- RPMI 1640 BioWhittaker® without L-glutamine (Lonza) supplemented with 40 µg/ml DNase I (Roche)
- Cell strainer (BD Falcon™) nylon mesh pore size 100µm
- Cell strainer (BD Falcon™) nylon mesh pore size 40 µm
- Razor blade
- ACK lysis buffer

3.2.2. Method

Spleen was excised from GFP transgenic Lewis rat and stored in RPMI 1640 on ice. All following steps were performed at 4°C. Spleen was minced with razor blades, forced through a 100 µm cell strainer, washed with supplemented medium, and forced through a 40 µm cell strainer to dissociate tissue clots and cell aggregates. The homogenate was centrifuged at 600g for 5 minutes, resuspended in ACK lysis buffer and incubated for 5 minutes. The suspension was diluted with isolation buffer and centrifuged at 600g for 10 minutes. For subsequent buffy coat injections, pellet was resuspended in RPMI 1640 containing 1% rat serum.

3.3. Magnetic Cell Sorting (MACS)

The MACS technology is based on a simple, straightforward principle. The target cells are magnetically labeled with MicroBeads and run through a column, which is placed in a strong magnet, the separator. The labeled cells are retained in the magnetic field of the column, while unlabeled cells run through. The column is removed from the separator, and labeled cells are eluted as an enriched, positively selected cell fraction.

3.3.1. Materials

- RPMI 1640 BioWhittaker ® without L-glutamine (Lonza)
- MACS buffer
  - 10 mM PBS (phosphate buffered saline), pH 7.2
  - 0.5 % BSA
  - 2 mM EDTA
- LS MACS column (Miltenyi Biotec)
- Midi MACS separator (Miltenyi Biotec)

Figure 10: MACS separator and column (Miltenyi Biotec)

- Monoclonal mouse anti-rat CD11b::FITC from Ox42 clone (Serotec), recognizes the epitope on tissue macrophages, dendritic cells, granulocytes and microglial cells.
- Anti-FITC MicroBeads (Miltenyi Biotec)

3.3.2. Method

Using a FITC-conjugated primary antibody targeting CD11b surface antigen, monocytes could be indirectly labeled with anti-FITC MicroBeads. To determine the ideal antibody dilution, concentrations ranging from 1:10 to 1:500 were tested in a titration experiment and evaluated by flow cytometry. The results suggest an optimal antibody dilution of 1:100 (see Figure 18).

Magnetic Sorting of monocytes

To meet optimal monocyte requirements, all centrifugation and incubation steps were performed at 4°C. Freshly isolated buffy coat cells (see 3.1.2) were centrifuged at 300g for 5 minutes, resuspended in MACS buffer and blocked for 5 minutes. The centrifugation step was repeated and mouse anti-rat CD11b::FITC (1:100 dilution in MACS buffer) was added to cell pellet and mixed thoroughly. After 20 minutes of incubation, cell suspension was centrifuged at 300g for 5 minutes and washed with MACS buffer twice. For labeling of 10^7

cells, 10 µl of anti-FITC MicroBeads were added. The mixture was centrifuged at 100g for 5 minutes to collect cells and MicroBeads in the pellet, then resuspended properly and centrifuged again. This step was followed by incubation for 10 minutes. After centrifugation at 300g for 5 minutes supernatant was discarded, cells were washed, and subsequently resuspended in MACS buffer.

The column was placed in the Midi MACS Separator and rinsed with MACS buffer, before applying the cell suspension. The flow-through was collected and again loaded onto the column. The column was rinsed 3 times with MACS buffer to wash unlabelled cells through. Eventually, the magnetically labeled cells retained in the column were eluted by removing the column from the separator and firmly applying a plunger. The collected eluate contained magnetically labeled CD11b-positive cells, whose purity was assessed by flow cytometry. Additionally some drops of the different MACS fractions from adult Lewis rat (~ 9 months) and a P3 rat pup were distributed on a coated cover slip to examine the receptor profile immunohistochemically. For RNA isolation aliquots of 10^6 cells were frozen at – 80°C.

Magnetic Sorting of metallophilic and splenic red pulp macrophages

In order to retrieve marginal zone metallophilic macrophages and red pulp macrophages from spleen of GFP transgenic rats, the spleen homogenate was applied onto a MACS column without prior antibody labeling. With their ability to recycle and store iron, these macrophages were retained in the column as a consequence of ferromagnetism. Upon removal from the separator, the iron-bearing cells were collected in the eluate. In order to investigate the receptor profile of spleen cells derived from an adult Lewis rat and P3 Lewis pup, some drops were applied onto coated cover slips and cells were stained with Turnbull Blue, to detect ferrous iron. Aliquots of 10^6 cells from both time points were frozen at – 80°C for RNA isolation.

3.4. Injection of GFP transgenic blood and spleen cells into neonates

3.4.1. Materials

- 1 ml syringe Luer-Lok™ Tip (BD)
- Needle, Microlance™ 3, 27G, 0.4 x 19 mm (BD)
- RPMI 1640 Bio Whittaker ® without L-glutamine (Lonza), supplemented with 1 % rat serum

3.4.2. Method

In early experiments, buffy coat (~ 200×10^6 cells/animal) and spleen homogenate (~ 400×10^6 cells/animal) were injected into the peritoneum of new born Lewis animals. For buffy coat injections, 5 different time points - P1, P3, P7, P10, and P14 - were investigated. Spleen homogenate-injected animals were sacrificed at postnatal day 7 and 14. For each time point, at least one animal was injected with RPMI/1% rat serum to serve as negative control.

After establishing the MACS protocol, magnetically purified monocytes (approximately 10^6 cells/animal) and iron-positive spleen cells (approximately 2×10^6 cells/animal) were injected into the peritoneum of Lewis neonates. 2 time points, P3 and P7, were tested for monocytes. Spleen cell-injected animals were sacrificed on postnatal day 3.

3.5. Tissue Sampling and preparation

3.5.1. Material

- Needle, Microlance™ 3, 20G, 0.9 x 40mm (BD)
- 0.1 M PBS, pH 7.4
  - 0.04 M NaH_2PO_4 (Merck) 13.8 g
  - 0.16 M Na_2HPO_4 (Merck) 71.2 g
  - dH_2O

  Dilute 0.2 M stock solution 1:2 to obtain 0.1 M PBS.
- 4 % Paraformaldehyde (PFA) (Merck) in 0.1 M PBS
- Preparation instruments: tweezers, scissors, razor blade
- Embedding cassettes, Filter paper

3.5.2. Method

The pups were sacrificed by inhalation of an overdose CO_2 and intracardially perfused with 4 % PFA. The peripheral organs, namely thymus, lung, heart, liver, kidney, spleen, intestine were excised, the brain cortex was exposed and spinal cord was resected and stored in 4 % PFA for post-fixation. After 24 hours, organs, spinal cord and brain were rinsed with PBS, wrapped in filter paper and transferred to embedding cassettes for subsequent dehydration and paraffination. Depending on the consistency of the tissue, two different Autotechnicon® protocols were employed. The delicate organs of P1 and P3 pups were treated with the longer program, whereas program 1 was the method of choice for the more robust P7, P10 and P14 organs.

Autotechnicon® programs

	Program 1 (16,3 hours)		Program 2 (25,5 hours)	
Solutions	**Duration**	**Temperature (°C)**	**Duration**	**Temperature (°C)**
50 % EtOH	20	40	30	40
70 % EtOH	60	40	90	40
70 % EtOH	90	40	120	40
80 % EtOH	60	40	120	40
80 % EtOH	90	40	120	40
96 % EtOH	60	40	90	40
96 % EtOH	90	40	120	40
96 % EtOH	120	40	150	40
Xylene	30	40	60	40
Xylene	60	40	120	40
Paraffin	60	60	120	60
Paraffin	60	60	120	60
Paraffin	60	60	120	60
Paraffin	120	60	150	60

Dehydration and paraffination was followed by cutting of tissue with a razor blade to obtain the desired section planes. The brain was cut into 5 sections, whereas the plane of interest is located at the level of the optical chiasm, adjacent to the anterior pons (see Figure 6). The tissue sections were embedded in paraffin blocks (Thermo Scientific HistoStar) and serial sections were cut with a microtome.

3.6. Detection of Green fluorescent protein (GFP)-transgenic cells

3.6.1. Materials

- Antibodies
    - Primary antibody: Polyclonal rabbit anti-mouse GFP (produced by lab group of Professor Sieghart, Dept. of Biochemistry and Molecular Biology, Center for Brain Research (Medical University Vienna)), 1:5000 dilution in Dako/10% fetal calf serum (FCS)
    - Secondary antibody: Biotin-conjugated donkey anti-rat IgG (Jackson ImmunoResearch), 1:2000 dilution in Dako/10% FCS

- Citric acid buffer 10 mM, pH 6.2
    - 1M Citric acid (Fluka) 210.14 g
    - 1 liter dH_2O

  Adjust to pH 6.2 with NaOH.
  1:100 dilution of 1M stock solution with dH_2O to obtain 10 mM.

- 1x Dako buffer (Dako)
  1:10 dilution of 10 x stock with dH_2O.

- Fetal calf serum (FCS) (Lonza)

- 0.1 M Tris buffered saline (TBS)
    - 0.5 M Tris (AppliChem) 60.57 g
    - 500 ml H_2O

  Adjust to pH 7.5 with HCl and fill up with H_2O to 1 liter.
  For 0.1 M TBS dilute stock solution 1:20 and to 1 liter add 8.766 g NaCl.

- Avidin-Peroxidase (Sigma-Aldrich), 1:100 dilution in Dako/10 % FCS

- 3,3’ diaminobenzidine-tetra-hydrochloride (DAB) (Sigma-Aldrich)

- H_2O_2, 30 % (Merck)

- Methanol (BDH Prolabo)

3.6.2. Method

The slices were dewaxed in xylene two times for 20 minutes, treated with 0.03 % H_2O_2/MeOH to block endogenous peroxidases, and rehydrated in a descending alcohol series and dH_2O.
To retrieve epitopes, slices were steamed in citric acid buffer in a conventional kitchen steamer. Slides were rinsed with 0.1M TBS and incubated in Dako/10% FCS for 20 minutes in a wet chamber to block unspecific binding sites. After washing with TBS, slides were incubated overnight at 4°C with primary rabbit anti-mouse GFP antibody solution. Washing with TBS was ensued by incubation with biotinylated donkey anti-rat IgG solution for 1 hour, followed by Avidin-Peroxidase incubation for 1 hour at room temperature. Subsequent detection was accomplished by adding 3,3' diaminobenzidine-tetra-hydrochloride (DAB) containing 0.30% H_2O_2. The sections were then counterstained with Mayer's haematoxylin for 7 seconds, differentiated with HCl/EtOH, treated with Scott's Blueing reagent for 5 minutes, dehydrated in ascending alcohol series, and mounted in resin.

3.7. Detection of cell surface markers on monocytes and splenic macrophages

3.7.1. Materials

- Primary antibodies
    - Monoclonal mouse anti-rat ED3, recognizing CD169/Sialoadhesin on marginal metallophilic macrophages (Serotec), 1:100 dilution in Dako/10 % FCS
    - Biotinylated monoclonal mouse anti-rat CD11b, recognizing monocytes, macrophages and granulocytes (Serotec), 1:100 dilution in Dako/10 % FCS
    - Polyclonal rabbit anti-rat CCR2 (abcam, ab21667)
    - Polyclonal rabbit anti-rat CX3CR1 (abcam), 1:250 dilution in Dako/10 % FCS
    - Polyclonal rabbit anti-rat Iba1, recognizing tissue macrophages (Wako, 019-19741), 1:3000 dilution in Dako/10 % FCS

- Secondary antibodies
    - Biotinylated donkey anti-mouse (Jackson), 1:1500 dilution in Dako/10 % FCS
    - Biotinylated donkey anti-rabbit (Jackson), 1:2000 dilution in Dako/10 % FCS

- 1 x Dako buffer (Dako)

- Fetal calf serum (FCS) (Lonza)

- 0.1 M Tris buffered saline (TBS)

- Avidin-Peroxidase (Sigma-Aldrich), 1:100 dilution in Dako/10 % FCS

- 3,3’ diaminobenzidine-tetra-hydrochloride (DAB) (Sigma-Aldrich)

- H_2O_2, 30 % (Merck)

3.7.2. Method

Cell smears of isolated blood monocytes and iron-containing cells from spleen of P3 Lewis pups and adult Lewis rat were rehydrated in dH_2O. Endogenous peroxidases were blocked for 30 minutes with 0,03% H_2O_2/MeOH. After washing with TBS, slides were blocked for 20 minutes with Dako/10 % FCS. Primary antibody solution was added and slides were incubated over night at 4°C. Following a washing step with TBS, biotinylated secondary antibodies were added onto the cell lawn and incubated for 1 hour at room temperature. Washing with TBS was followed by a 1 hour incubation with Avidin-Peroxidase. Slides were washed with TBS and subsequently developed with DAB/0.30% H_2O_2. Detection was stopped by adding H_2O. Slides were counterstained for 10 seconds with Mayer’s haematoxylin,

differentiated twice in HCl/EtOH, treated with Scott's Blueing reagent for 3 minutes. Subsequently, slides were dehydrated in an ascending alcohol series, and mounted in resin.

3.8. Double staining with anti-GFP and anti-CD43

3.8.1. Materials

- Primary antibodies
  - Monoclonal mouse anti-rat CD43/Leukosialin, W3/13 clone (Serotec). Antibody recognizes Leukosialin on T cells, granulocytes, monocytes and some B lymphocytes. 1:50 dilution in Dako/10% FCS
  - Polyclonal rabbit anti-mouse GFP (produced by lab group of Professor Sieghart) 1:5000 dilution in Dako/10 % FCS

- Secondary antibodies
  - Alkaline phosphatase-conjugated donkey anti-mouse IgG (Jackson ImmunoResearch), 1:200 dilution in Dako/10 % FCS
  - Biotin-conjugated donkey anti-rat IgG (Jackson ImmunoResearch), 1:2000 dilution in Dako/ 10 % FCS

- Tris-EDTA buffer, pH 8.5
  - 10 mM Tris (AppliChem) 1.21 g
  - 1 mM EDTA (Merck) 0.37 g
  - 50 ml dH_2O

  Adjust to pH 8.5 with HCl.

  1:20 dilution of stock solution with dH_2O to obtain working solution.

- Fast Blue Reagent (for 50 ml)
  - 12,5 mg Napthol-AS-MX-phosphate (Sigma-Aldrich)
  - 25 mg Fast Blue BB salt (Sigma-Aldrich)
  - 615 µl N,N di-methylformamid (Fluka)
  - 0,1 M Tris HCl, pH 8.5, prewarmed to 37°C
  - 2 N HCl (Merck)
  - 4 % $NaNO_2$ (Merck)
  - Tetramisole hydrochloride (Levamisole) (Sigma-Aldrich)

- Geltol
  - 6 g glycerine
  - 2.4 g mowiol
  - 6 ml dH_2O
  - 12 ml Tris 0,2 M, pH 8.5

3.8.2. Method

For simultaneous detection of GFP-transgenic cells and T cells, DAB development (see 3.6.2) was preceded by development with Fast Blue reagent.

Tissue slides were deparaffinated according to 3.6.2 and subsequently steamed for 60 minutes in Tris-EDTA buffer. Thereafter tissue slides were blocked with Dako/10 % FCS for 20 minutes in a wet chamber. Primary antibody incubation with mouse anti-rat CD43 over night at 4°C was followed by secondary antibody incubation with alkaline phosphatase-conjugated anti-mouse IgG. For detection with Fast Blue reagent, Naphtol-AS-MX-phosphate was mixed with N,N dimethylformamid and warm TrisHCl. Fast Blue BB salt was dissolved in 2N HCl, and mixed with 4 % $NaNO_2$ and TrisHCl buffer (prewarmed at 37°C) until solution was clear. In the final step, 1 M Levamisole was added to block endogenous alkaline phosphatases. Thereafter, the solution was filtered, slides developed under the microscope and mounted with Geltol.

3.9. DAB-enhanced Turnbull Blue staining for detection of iron-containing cells

3.9.1. Materials

- $(NH_4)_2S$ (Merck)
- $K_3[Fe(CN)_6]$ (Merck)
- HCl 37% (Riedel-de-Häen)
- MeOH (BDH Prolabo)
- N_3Na (Fluka)
- 0.2 M Sörensen phosphate buffer
    - 71,2 g $Na_2HPO_4.2H_2O$ (Merck)
    - 13,8 g $NaHPO_4.H_2O$ (Merck)
    - 2,5 liter dH_2O
- 0,025 % DAB/0,005 % H_2O_2
    - Aliquot (25mg/ml) diluted in 0,1M Sörensen phosphate buffer
    - filter solution
    - add H_2O_2, 30% (Merck)
- Geltol

3.9.2. Method

Tissue slides were deparaffinated in xylene 2 times for 15 minutes and rehydrated in a descending alcohol series and dH_2O. Cell smear slides, which did not require this pre-treatment, were solely rehydrated in dH_2O. For Fe^{3+} reduction, tissue sections were incubated in 2 % $(NH_4)_2S$ for 1.5 hours. After rinsing with dH_2O, slides were incubated in 20 % $K_3[Fe(CN)_6]$/1 % HCl solution for 15 minutes. After washing with dH_2O, slides were incubated in 0.01 M N_3Na solution followed by a washing step with 0.1 M Sörensen phosphate buffer. Finally, tissue sections were developed for 20 minutes in 0,025 % DAB containing 0,005 % H_2O_2 and mounted with Geltol.

3.10. RNA isolation of Cell eluates and corpus callosum tissue

3.10.1. Materials

- RNeasy Mini Kit (Quiagen)
- QIAshredder™ spin column (Quiagen)
- 10 X Reaction Buffer with $MgCl_2$ (Fermentas)
- RiboLock™ RNase Inhibitor (Fermentas)
- DNase I (Fermentas)
- 25 mM EDTA (Fermentas)
- RNase free water (Invitrogen)
- 100 % EtOH
- 70 % EtOH

3.10.2. Method

MACSed spleen cell eluate and buffy coat eluate from P3 and adult rats were mixed with RLT buffer, supplemented with β-mercaptoethanol for cell lysis. Suspension was applied onto QIAshredder spin column and centrifuged for 2 minutes at full speed.
Corpus callosum tissue was excised from a brain of a P2 rat pup with a razor blade and mixed with RLT, supplemented with β-mercaptoethanol. Tissue was homogenized with an Ultra-Turrax. The following RNA isolation of MACS eluates and corpus callosum tissue was performed according to the manufacturer's instructions.

After RNA isolation, contaminating genomic DNA was removed by enzymatic digestion. To 50 µl RNA solution the following mix was added:

10 X Reaction Buffer with $MgCl_2$	7 µl
RiboLock Rnase Inhibitor	2 µl
Dnase 1	7 µl
Rnase-free water	4 µl

Upon adding DNA digestion mix, samples were incubated at 37°C for 30 minutes. Digestion was stopped by adding 7µl 25 mM EDTA to each sample and subsequent incubation at 65°C for 10 minutes.

DNA-free RNA samples were purified according to the "RNA Cleanup" protocol, again using the "RNeasy Mini Kit".

Afterwards, RNA concentration and purity were determined by UV-VIS spectrophotometric analysis using NanoDrop 2000 (Thermo Scientific).

3.11. Reverse transcription PCR

3.11.1. Materials

- M-MLV Reverse Transciptase, RNaseH, point mutant, 200 U/µl (Promega)
- M-MLV reverse transcriptase 5x reaction buffer (Promega)
- dNTPs (Roche)
- RNase inhibitor (SABiosciences Kit or Fermentas)
- T7-N7 primer (100 pmol/µl): 5' – CCA AGC TTC TAA TAC GAC TCA CTA TAG GGA GA (AGCT) (AGCT) (AGCT) (AGCT (AGCT) (AGCT) – 3'
- Mastermix (1x)

M-MLV RT buffer	10 µl
dNTPs	3 µl
RNase inhibitor	3 µl
ddH_2O	5 µl

3.11.2. Method

For reverse transcription, 2 µl T7 - N7 primers were added to 30 µl of RNA samples and incubated for 5 minutes at 70°C. Thereafter samples were incubated on ice for 5 minutes. After addition of the master mix, samples were incubated for 2 minutes at 40°C. In the end, reverse transcriptase was added, incubated for 10 minutes at room temperature, 50 minutes at 40°C, and 15 minutes at 70°C.

3.12. Polymerase Chain Reaction (PCR)

3.12.1. Material

- Primer sets (100 pmol/µl)

  GAPDH Forward: 5’ - GGC – ATT – GCT – CTC – AAT – GAC – ACC – 3’
  GAPDH Reverse: 5’ – TGA – GGG – TGC – AGC – GAA – CTT – TAT – 3’
  Annealing Temperature: 53°C

  CX3CR1 Forward: 5’ – ACT – CCC – TTG – TCT – TCA – CGT – TC – 3’
  CX3CR1 Reverse: 5’ – AGA – AGA – AAG – CAG – TCG – TGA – GC – 3’
  Annealing Temperature: 52 °C

  VCAM-1 Forward: 5’ – GAG – ACA – AAA – CAG – AAG – TGG – AAT – 3’
  VCAM-1 Reverse: 5’ – AGC – AAC – GTT – GAC – ATA – AAG – AGT – 3’
  Annealing Temperature: 55°C

  Integrin α_4 Forward: 5’ – CCC – AGG – CTA – CAT – CGT – TTT – GT – 3’
  Integrin α_4 Reverse: 5’ – AAA – GAC – GTG – CGA – GAC – ATC – CT – 3’
  Annealing Temperature: 52°C

  Integrin α_L Forward: 5’ – CAG – CTC – GCT – CTC – AGT – CTC – CT – 3’
  Integrin α_L Reverse: 5’ – TCC – GTT – TGA – AGA – AAC – CAA – CC – 3’
  Annealing Temperature: 52°C

  CCL2 Forward: 5’ – CAC – TCA – CCT – GCT – GCT – ACT – CAT – TCA – 3’
  CCL2 Reverse: 5’ – GCT – TGA – GGT – GGT – TGT – GGA – AAA – G – 3’
  Annealing Temperature: 60°C

  ICAM-1 Forward: 5’ – GGG – TTG – GAG – ACT – AAC – TGG – ATG – A – 3’
  ICAM -1 Reverse: 5’ – GGA – TCG – AGC – TCC – ACT – CGC – TC – 3’
  Annealing Temperature: 56°C

  CD169 Forward: 5’ – CCC – AGC – TAC – AGC – TTC – TCC – AC – 3’
  CD169 Reverse: 5’ – CAG – GTA – CAT – GCC – CTC – ATC – CT – 3’
  Annealing Temperature: 55°C

- FastStart Taq DNA polymerase dNTPack (Roche)

- Master mix 1 X (Roche):

Buffer + 20 mM $MgCl_2$	5 µl
dNTPs	1 µl
Primer forward	1 µl
Primer reverse	1 µl
dH_2O	40.6 µl
taq Polymerase 5 U/µl	0.4 µl

- LE Agarose (Biozym)

- 50 X TAE buffer
  - 2 M Tris
  - 50 mM EDTA
  - 2 M flacial acetic acid

  Dissolve solids in approximately 900 ml ddH_2O and adjust pH to 7.6 – 7.8 with HCl. Fill up with ddH_2O to 1000 ml.

- 1X TAE buffer: dilute 50x TAE buffer for electrophoresis.

- Ethidium bromide solution 10 mg/ml (Sigma)

- peqGold 100 bp DNA ladder (PeqLab)

- RNase free H_2O (Ampuwa®)

3.12.2. Method

The following PCR cycles were run with the Bio-Rad Thermal cycler:

Initial denaturation step	95°C	10 minutes	
Denaturation step	95°C	30 seconds	35 cycles
Primer Annealing step	56.5°C	30 seconds	
Extending step	72°C	30 seconds*	
Final extending step	72°C	10 minutes	

* VCAM1 primers give a longer product therefore elongation step is extended to 1 minute.

PCR products were loaded on a 2 % agarose gel and ran for 60 minutes at 100V. Using Gel Doc 2000 the gels were examined.

Results

In this study the recruitment of monocytes into the peri- and supraventricular area of the brain was investigated. This region is also known as the “fountain of microglia”, where amoeboid microglial cells are observed during perinatal development.

When isolated from the blood, monocytes constitute approximately 10% of buffy coat, which contains the peripheral blood mononuclear cells (Figure 11).

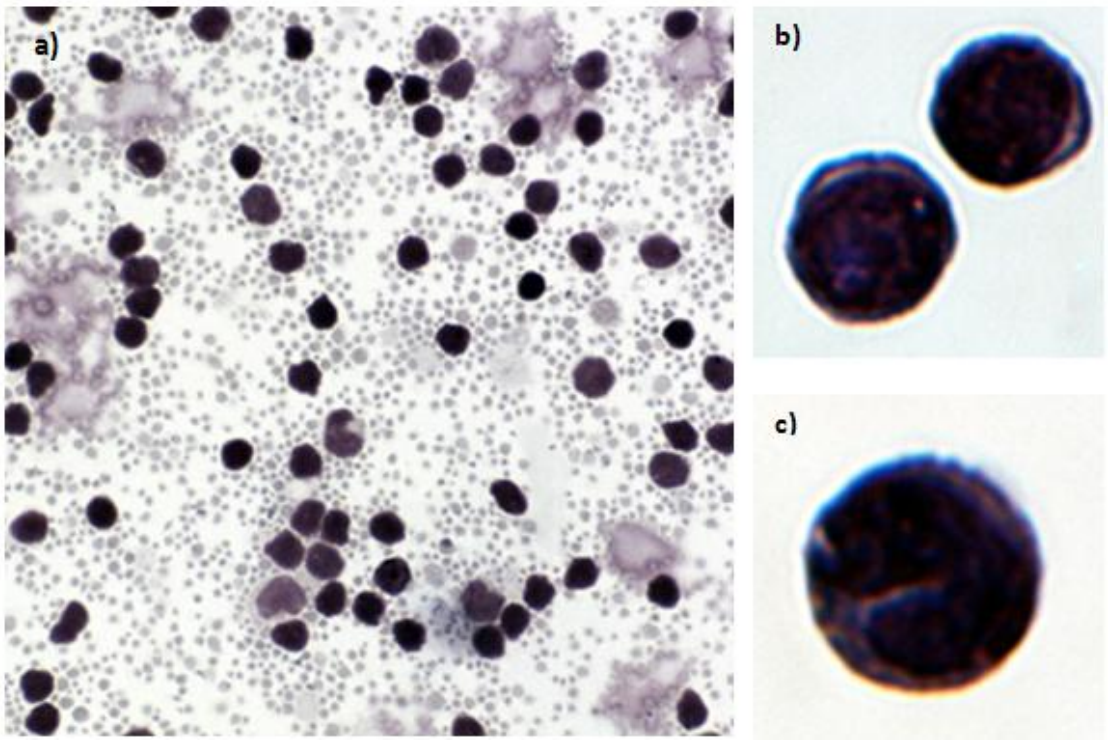

Figure 11: May Grünwald Giemsa staining of buffy coat. a) Buffy coat cells (× 250). b) Two lymphocytes with a large round nucleus (× 1000). c) Monocyte with a characteristically indented nucleus (× 1000).

In the first set of experiments, freshly isolated buffy coat of GFP-transgenic adult Lewis rats was injected into the peritoneum of neonatal Lewis rats (P0) to assess the migratory potential of monocytes into the CNS.

In order to determine the time window, when monocytes are entering into the brain, 5 different time points - P1, P3, P7, P10, and P14 - were investigated. The following tissues were immunohistochemically analyzed with an antibody recognizing GFP: the supraventricular corpus callosum, the spinal cord, and as a positive control for monocyte engraftment the peripheral organs, like thymus, heart, lung, liver, kidney, spleen, and intestines.

4.1. Immunohistochemistry of buffy coat-injected Lewis rats

At postnatal day 1, no GFP-positive cells could be found in the brain, nor in the spinal cord (Figure 12 a, b). A clear, positive signal was obtained from the spleen (Figure 12 d) and thymus (Figure 12 e). The liver exhibited ubiquitous, light brown staining over an extensive area which could also be detected in the negative control (not shown), thus the signal was unspecific. An unspecific signal was also detected in some goblet cells of the intestines (Figure 12 i).

On postnatal day 3, buffy coat-injected Lewis pups did not display GFP-expressing cells in the target region of the brain (Figure 13 a), nor in the spinal cord (Figure 13 b). However, a few positive cells were located in the liver (Figure 13 c), lung (Figure 13 g), heart (Figure 13 h), and kidney (Figure 13 i). In the spleen, a wave of positive cells infiltrated the white pulp and surroundings of the central arterioles. Many positive cells were also found in the thymus, throughout the medulla. An unspecific signal was derived from the goblet cells (Figure 13 j).

On postnatal day 7, no GFP signal was detected in the brain, except for an unspecific signal obtained from ependymal cells in the lateral ventricle (Figure 14 a). There were no GFP-positive cells located in the spinal cord (Figure 14 b). Single GFP-positive cells were found in the heart (Figure 14 g) and kidney (Figure 14 h). The spleen exhibited the highest number of positive cells (Figure 14 d). Lower numbers were found in thymus (Figure 14 e), however a light positive signal was also obtained from the thymus medulla of the negative control (Figure 36), making the result less reliable. The goblet cells of intestine displayed scattered positive cells, which were unspecifically stained (Figure 14 i).

At postnatal day 10, corpus callosum (Figure 15 a) and spinal cord (Figure 15 b) did not display any GFP-positive cells. Liver (Figure 15 c) and lung (Figure 15 h) displayed positive cells in the tissue. A few GFP-positive cells were detected in the thymic medulla (Figure 15 f). The spleen showed the highest amount of GFP-expressing cells around the central arteriole of the white pulp (Figure 15 e). The goblet cells of intestine displayed a light brown staining, which was unspecific (Figure 15 j).

On postnatal day 14, buffy coat-injected rats showed no positive cells in the supraventricular region of the brain and in the spinal cord (Figure 16 a, b). A single positive cell was located in the lung (Figure 16 f). The spleen (Figure 16 d) and thymus (Figure 16 e) displayed several GFP-expressing cells, but in lower numbers than in tissue of earlier time points. It is important to note that some positive cells, albeit fewer in number, were also found in the negative control of the thymus. Therefore the signal was partially unspecific and the actual number of real GFP-expressing cells was even lower (Figure 38).

In these initial experiments, buffy coat cell injections were assessed at different time points. No positive signal could be derived from the corpus callosum, however positive cells were found in the peripheral organs, particularly in lymphoid tissue. These findings indicated that buffy coat cells withstand the isolation procedure, and maintain their migratory competence.

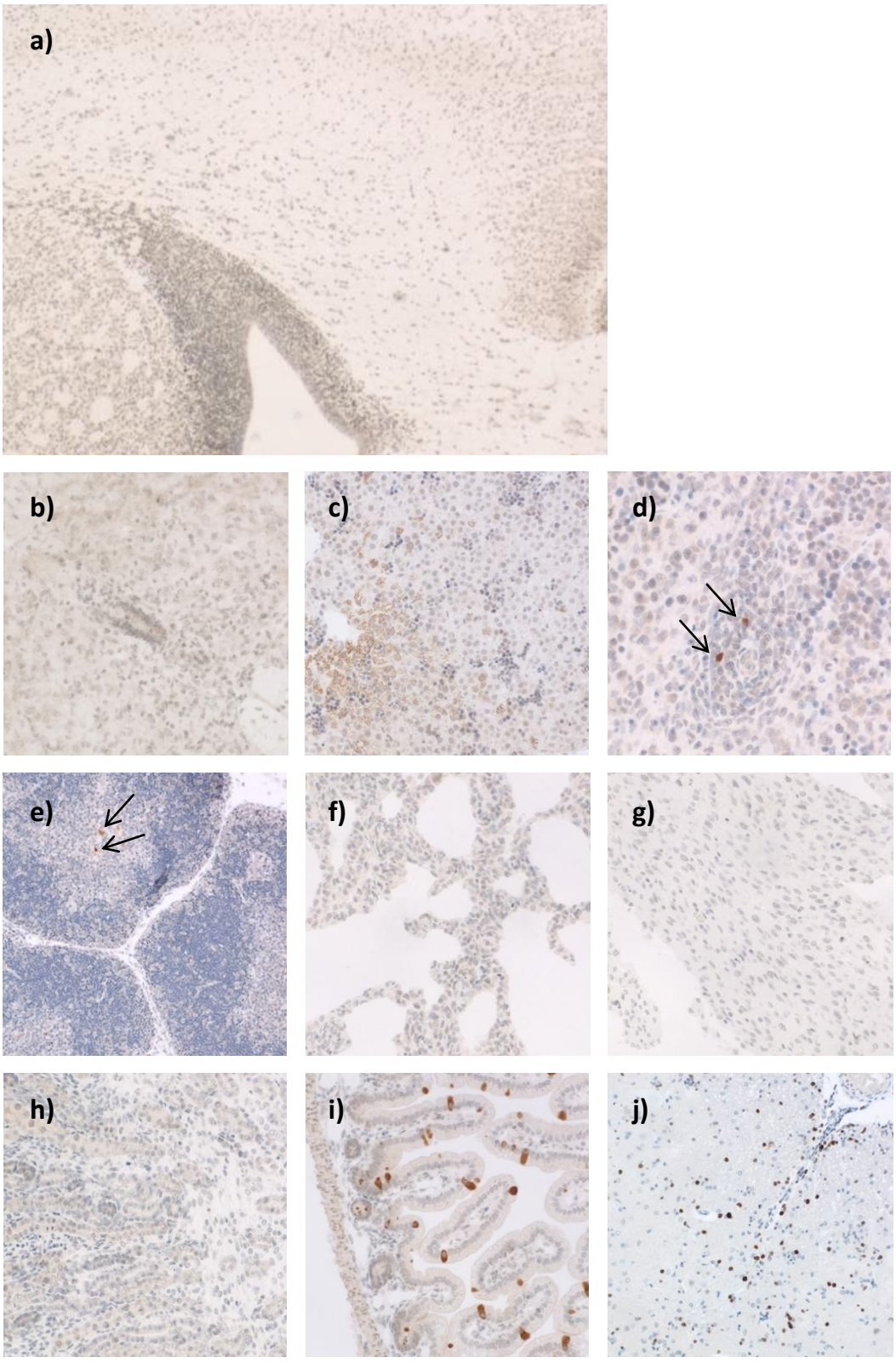

Figure 12: Buffy coat-injected P1 Lewis pup tissue, stained for GFP. Cell nuclei are encolored blue, intensely stained brown cells are GFP-positive. a) Brain section (× 40). b) Spinal cord section (× 100). c) Liver section displays cells that are unspecifically stained (× 100). d) Spleen tissue section displays single positive cells, indicated with black arrows (× 250) e) In thymus a positive signal is obtained from the medulla (× 100). f) Lung section (× 100). g) Heart section (× 100). h) Kidney section (× 100). i) Tissue of intestine section exhibits an unspecific signal (× 100). j) Spinal cord, infiltrated by GFP positive T lymphocytes serves as positive control for GFP stainings (× 100).

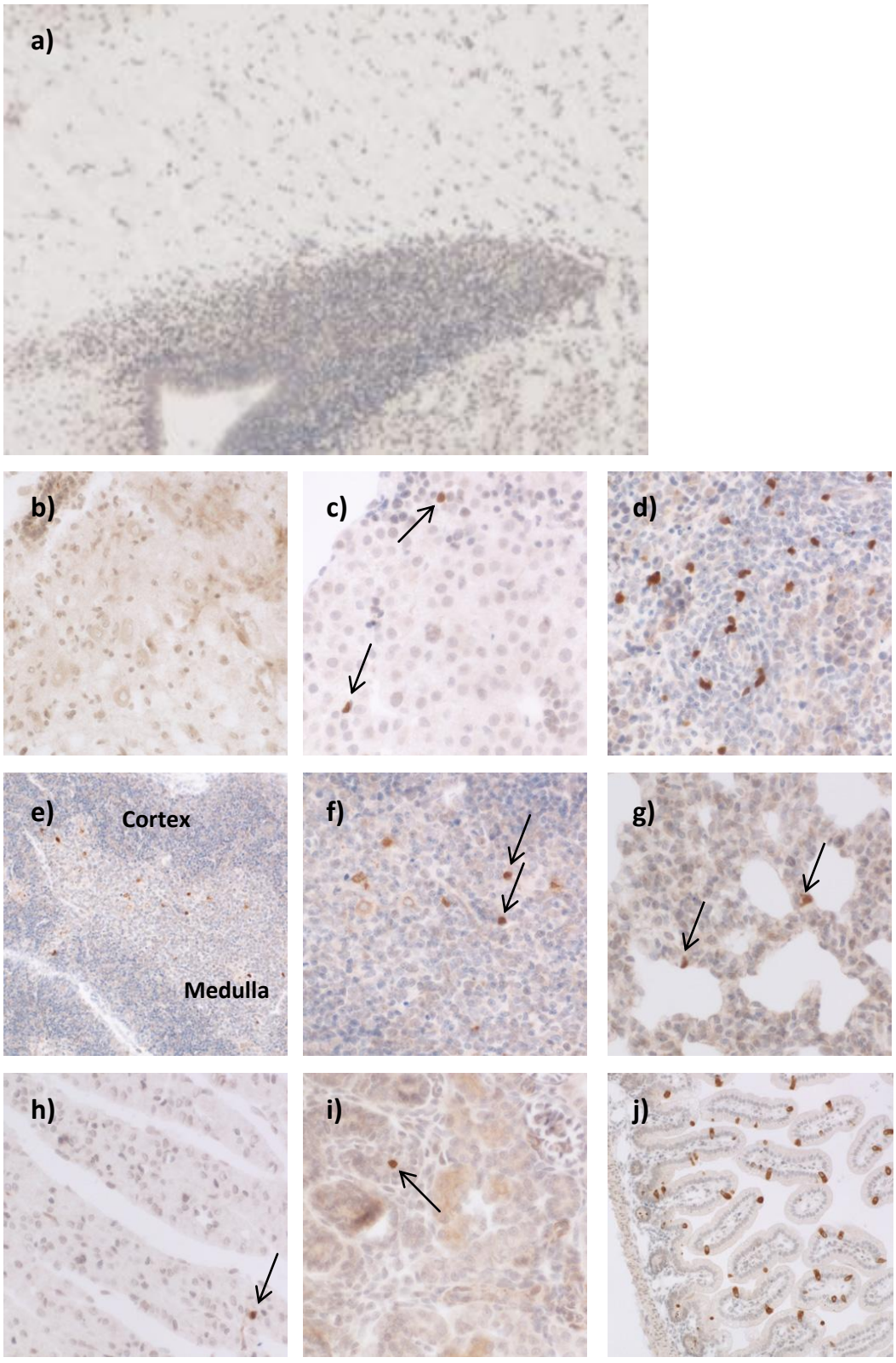

Figure 13: Buffy coat-injected P3 Lewis pup tissue, stained for GFP. Cell nuclei are encolored blue, brown staining indicates GFP-positive cells, which are highlighted with black arrows. a) Brain section (× 40). b) Spinal cord section (× 100) c) Liver tissue displays single positive cells, indicated with black arrows (× 100) d) Spleen exhibits many positive cells in the white pulp (× 100). e) Thymus displays several positive cells in the medulla (× 100). f) Higher magnification of a specific area in thymus (× 250). g) Lung shows few positive cells (× 250). h) Heart displays single positive cells (× 250). i) Kidney shows single positive cell in the tubules (× 250). j) Goblet cells of the intestines exhibit unspecific brown staining (× 100).

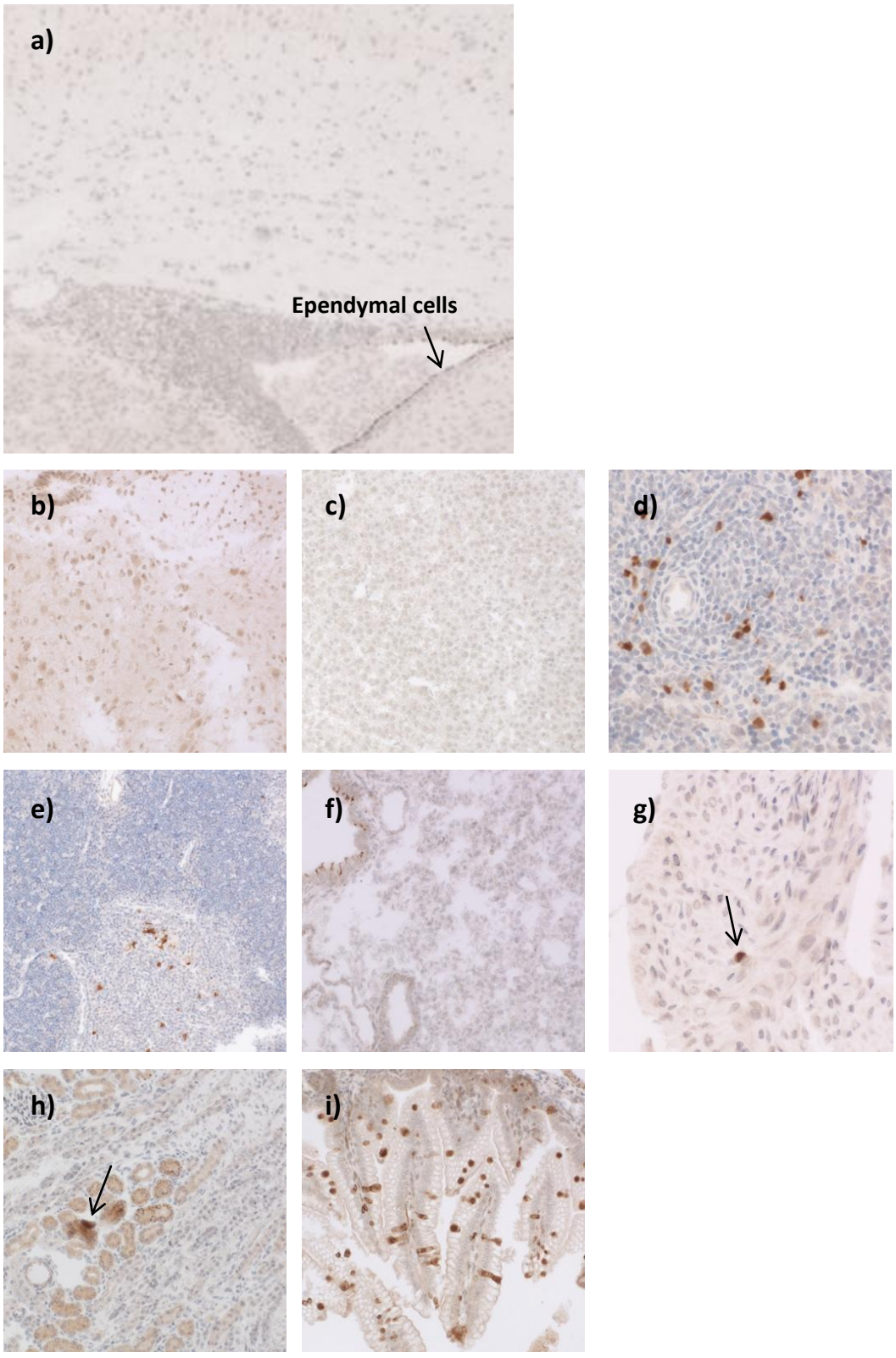

Figure 14: Buffy coat-injected P7 Lewis rat tissue, stained for GFP. Cell nuclei are stained blue, GFP-positive exhibit brown staining. Single GFP-positive cells are highlighted with black arrows. a) Brain tissue exhibits unspecific staining of ependymal cells (see black arrow) (× 40). b) Spinal cord section (× 100). c) Liver section (× 100). d) Spleen tissue shows many positive cells in the white pulp (× 250). e) Thymus tissue shows several positive cells in the medulla (× 100). f) Lung section (× 100). g) Heart displays single positive cells (× 250). h) Kidney displays single positive cells and unspecific staining of the tubules (× 100). i) Intestinal tissue displays unspecifically stained goblet cells (× 100).

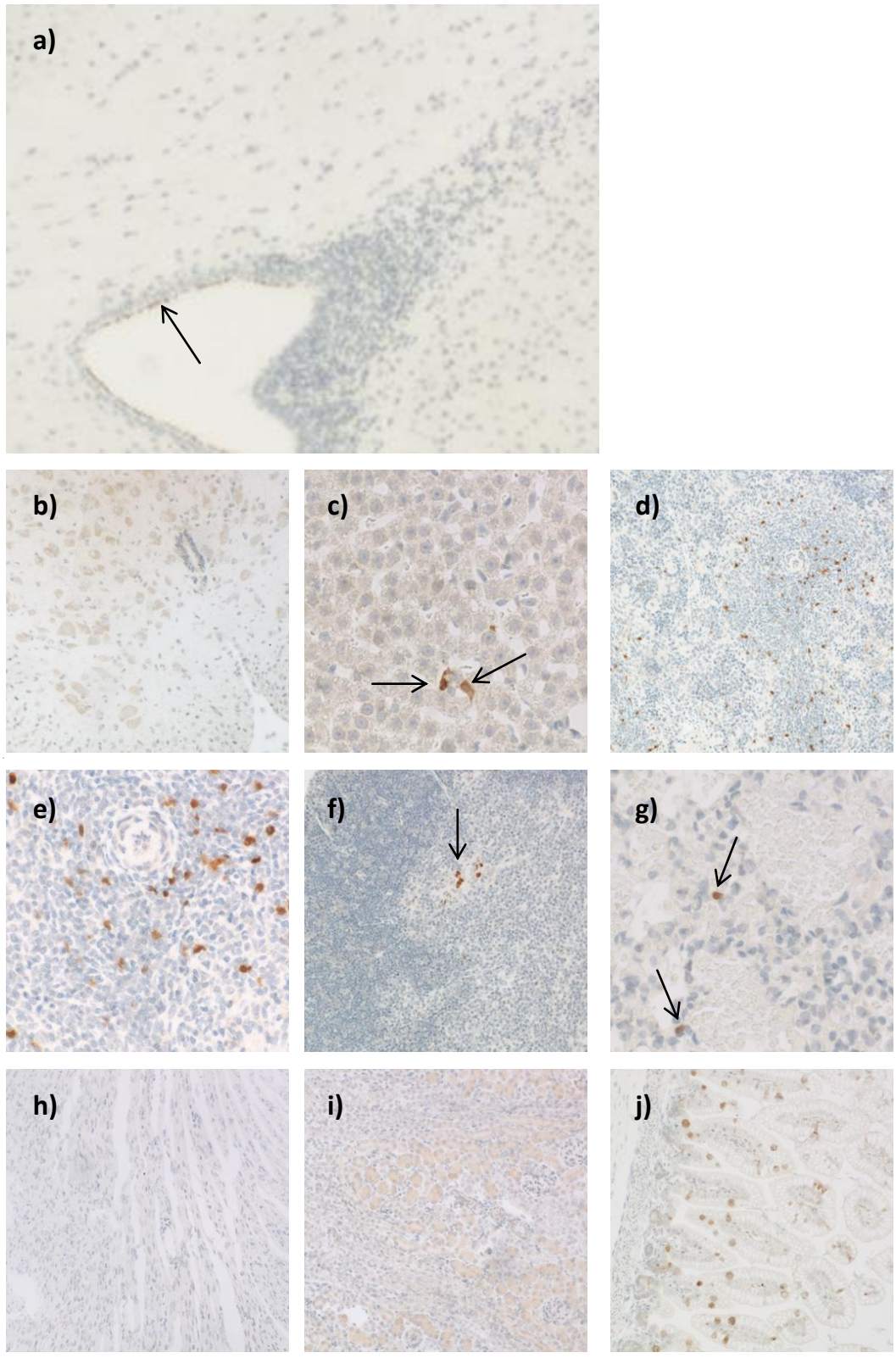

Figure 15: Buffy coat-injected P10 Lewis rat tissue, stained for GFP. Cell nuclei are stained blue, GFP-positive cells show brown staining. Single GFP-positive cells are highlighted with black arrows. a) Brain tissue shows unspecific staining of the ependymal cells (see black arrow) (× 40). b) Spinal cord section (× 100). c) Liver displays a few positive cells (× 100). d) Spleen exhibits many positive cells in the white pulp (× 250). e) Higher magnification of spleen tissue (× 250). Many positive cells are surrounding the central arteriole. f) Thymus displays positive cells in the medulla (× 100). g) Lung tissue shows single positive cells (× 250). h) Heart section (× 100). i) Kidney section (× 100). j) Intestinal goblet cells show unspecific staining (× 100).

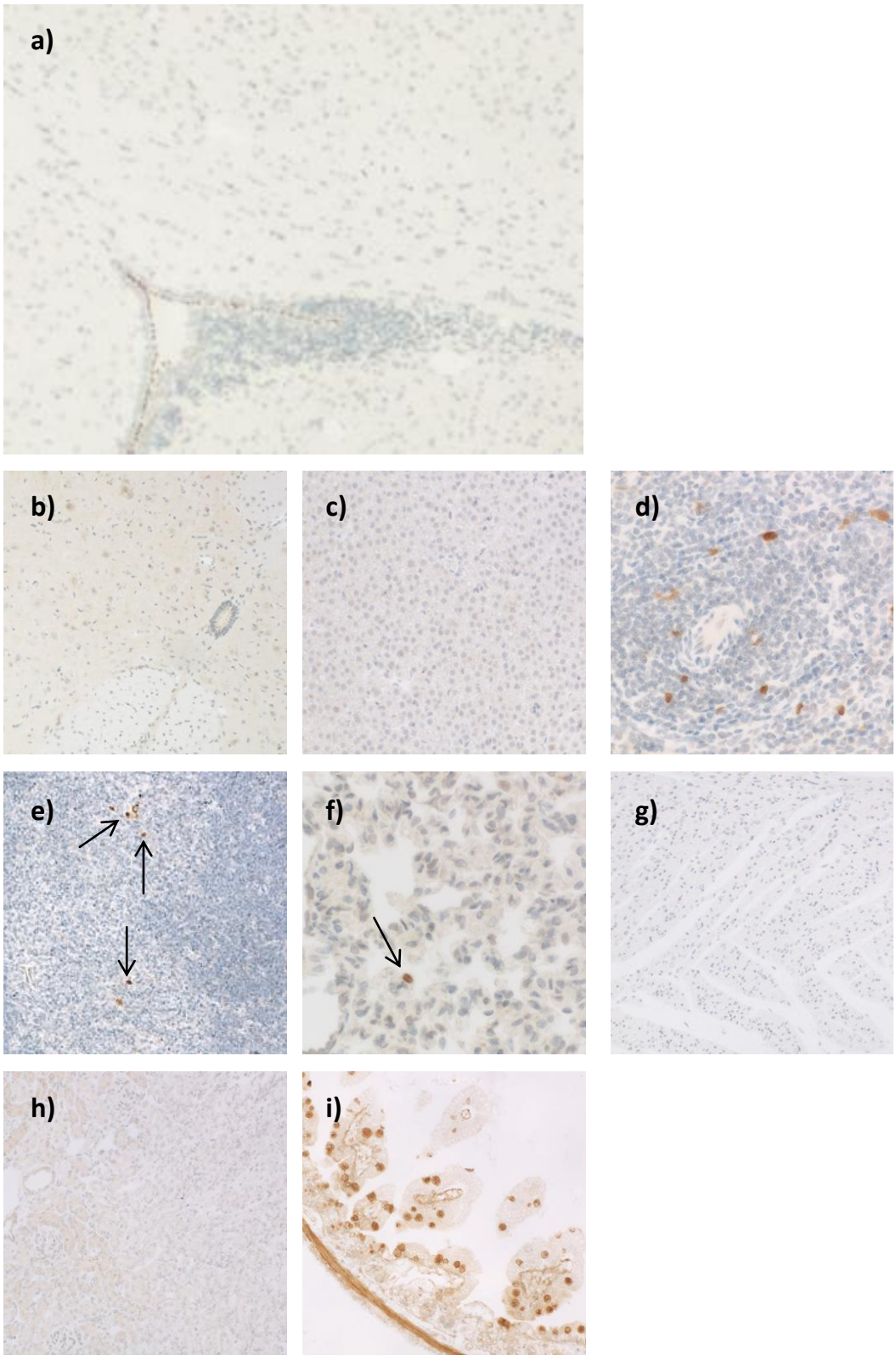

Figure 16: Buffy coat-injected P14 Lewis rat tissue, stained for GFP. Blue staining indicates cell nuclei. GFP-positive cells are stained intensely brown. Single GFP-positive cells are highlighted with black arrows. a) Brain tissue displays unspecific brown staining of ependymal cells (× 40). b) Spinal cord section (× 100). c) Liver section (× 100). d) Spleen displays several positive cells around the central arteriole of white pulp (× 250). e) In the thymus, positive cells are detected in the medulla (× 100). f) Lung tissue shows a single positive cell (× 250). g) Heart section (× 100). h) Kidney section (× 100). i) Intestinal tissue exhibits unspecific signal in goblet cells (× 100).

4.2. Double staining against GFP and CD43

Buffy coat cells contain approximately 10 % monocytes. Do these monocytes contribute at all to the tissue infiltrating GFP-positive cells, or is the tissue only infiltrated by GFP-positive T cells contained in the buffy coat preparation?

To answer this question the ratio of transgenic lymphocytes and monocytes were evaluated in a double staining experiment. Tissue section of buffy coat-injected P7 rats were incubated with antibodies targeting GFP and the lymphocyte marker CD43.

The double stainings allow to discriminate between cells derived from the endogenous, or from injected transgenic buffy coat, as endogenous cells are GFP-negative and engrafted cells are GFP-positive. In the liver (Figure 17 d), heart (Figure 17 e), and kidney (Figure 17 f) the endogenous lymphocyte population could be detected. In thymus, some double-positive lymphocytes were found. The spleen displayed both, double positive and a few single positive cells. The double positive cells were GFP-transgenic lymphocytes and the single positive cells, stained for GFP, were monocytes.

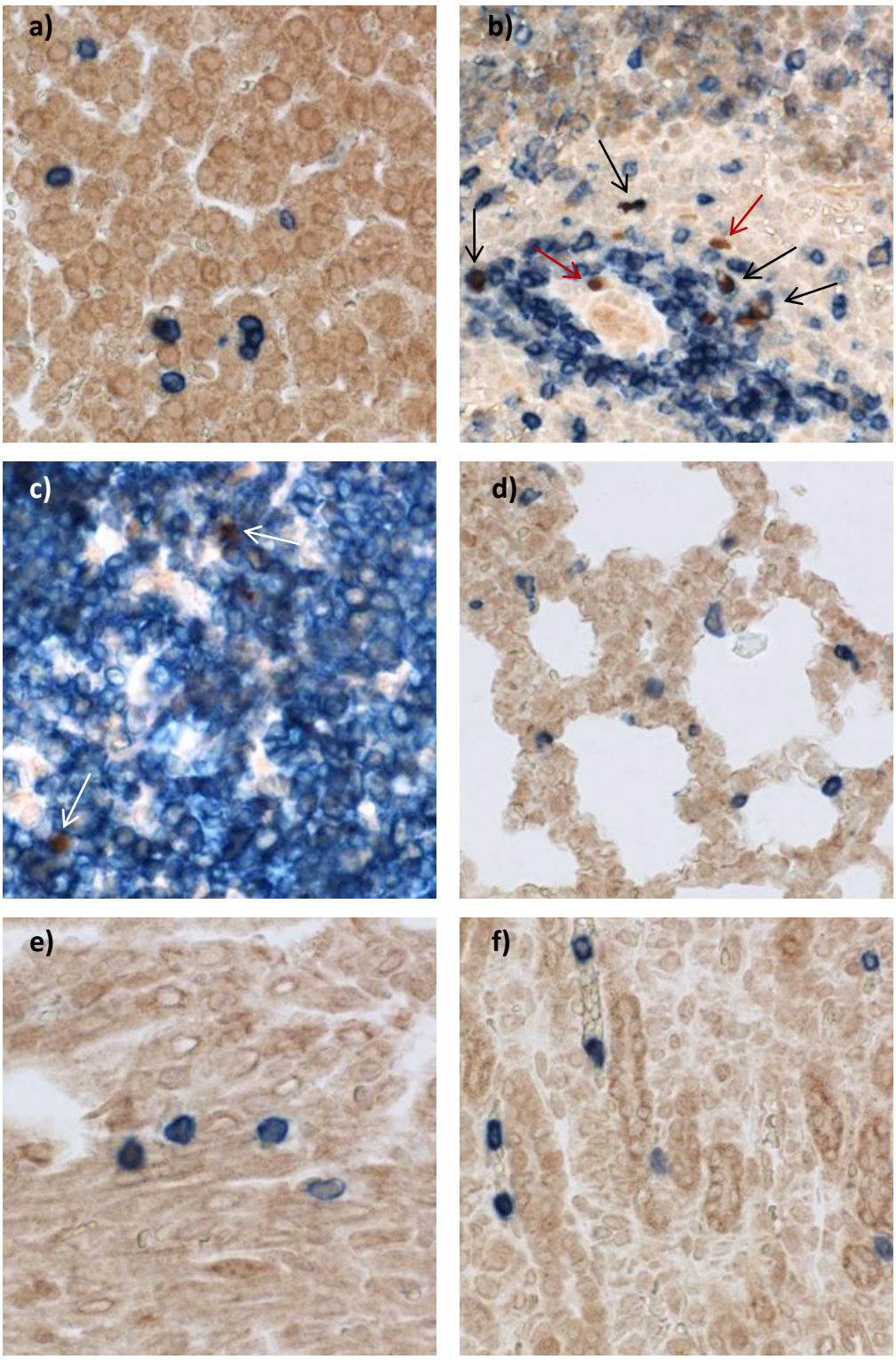

Figure 17: Double staining of P7 buffy coat-injected rat tissue for GFP (brown) and CD43 (blue). a) Liver shows positive staining for lymphocytes (× 250). b) Spleen tissue exhibits double positive cells (black arrow) and a few GFP-single-positive cells (red arrow) (× 250). c) Thymus shows a few double positive cells (white arrows) (× 250). d) Lung tissue is populated by some lymphocytes (× 250). e) A few lymphocytes are located in the heart (× 250). f) Kidney shows single-positive blue staining in the area of the tubules (× 250).

From a statistical point of view, merely 10 % of buffy coat cells are monocytes. This means that 90 % of GFP transgenic cells injected were “contaminating” cells, such as B and T lymphocytes, which was also shown with the previous double staining.

There are two obstacles transgenic monocytes have to overcome: First, a minor fraction of buffy coat cells enters into organs and only a vanishing number of these cells are monocytes. Secondly, they have to compete with endogenous monocytes, which are superior in number, in entering the tissue niches. Therefore, a high concentration of purified monocytes has to be introduced into the blood circulation, in order to provide numbers that are sufficient to enter into the CNS.

To exclude undesired cell types and purify monocytes to a high degree, the magnetic cell sorting technique by Miltenyi Biotec was established. The positive selection procedure offers an inexpensive, simple, gentle, and fast approach to obtain the desired cell population with high purity. The depletion method would have been an even more promising approach, reaching higher purity and recovering the cells “untouched”. However, it requires exact knowledge of the buffy coat composition, a large antibody cocktail and a higher retention capacity of the columns. With only 50 nm in diameter, the biodegradable MACS MicroBeads should not interfere with the migratory capacity or activity status of our cells. Therefore positive selection was our method of choice.[4]

4.3. Flow cytometry

For positive selection of monocytes, a FITC-conjugated mouse anti-rat CD11b antibody was used. In order to determine the optimal antibody dilution, a dilution series in the range of 1:10 to 1:500 was evaluated by flow cytometry.

According to the results from the titration experiment, the optimal antibody dilution, which is used as standard dilution for the MACS protocol is 1:100 (Figure 18).

To assess, whether the newly established MACS protocol is suitable to obtain monocytes in a highly enriched fraction, their purity was assessed in a FACS experiment (Figure 19).

Results from FACS analysis revealed a satisfactory monocyte yield of 80 %, making the MACS protocol an ideal technique for our purpose.

[4] http://www.miltenyibiotec.com/download/flyer_en/680/MACS_Technology_Flyer.pdf

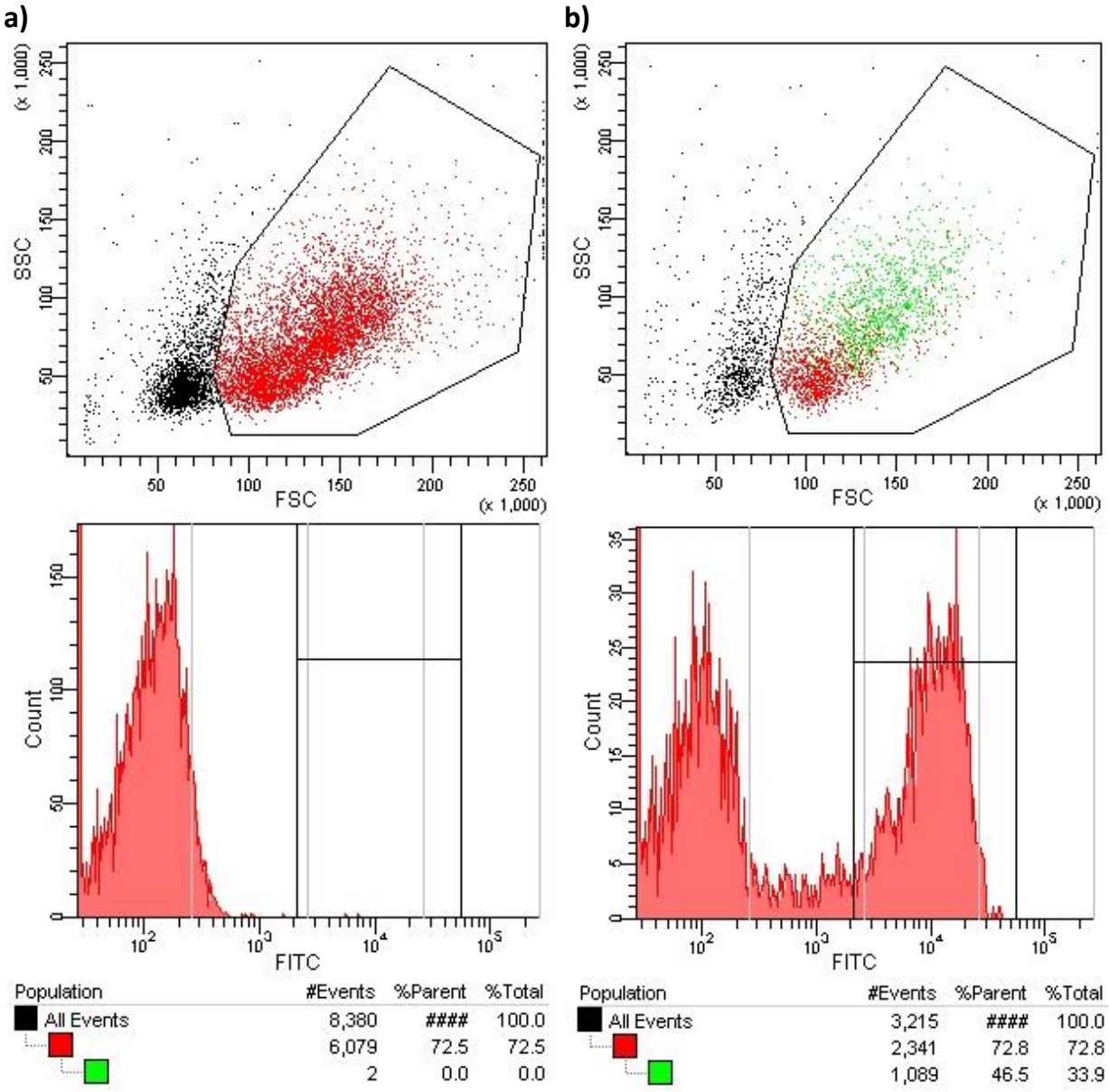

Figure 18: FACS dot blots and histogram. a) Unstained buffy coat. The red gate depicts living cell population. Histogram shows a peak derived from the gated unstained, living cells. b) CD11b stained buffy coat. The red gate depicts living cell population. The green gate represents the CD11b-positive cell population. The population histogram shows 2 peaks. The left one includes all the CD11b-FITC negative cells. The second peak represents CD11b-FITC positive buffy coat cells. The sharp peak separation denotes an ideally chosen antibody dilution of 1:100.

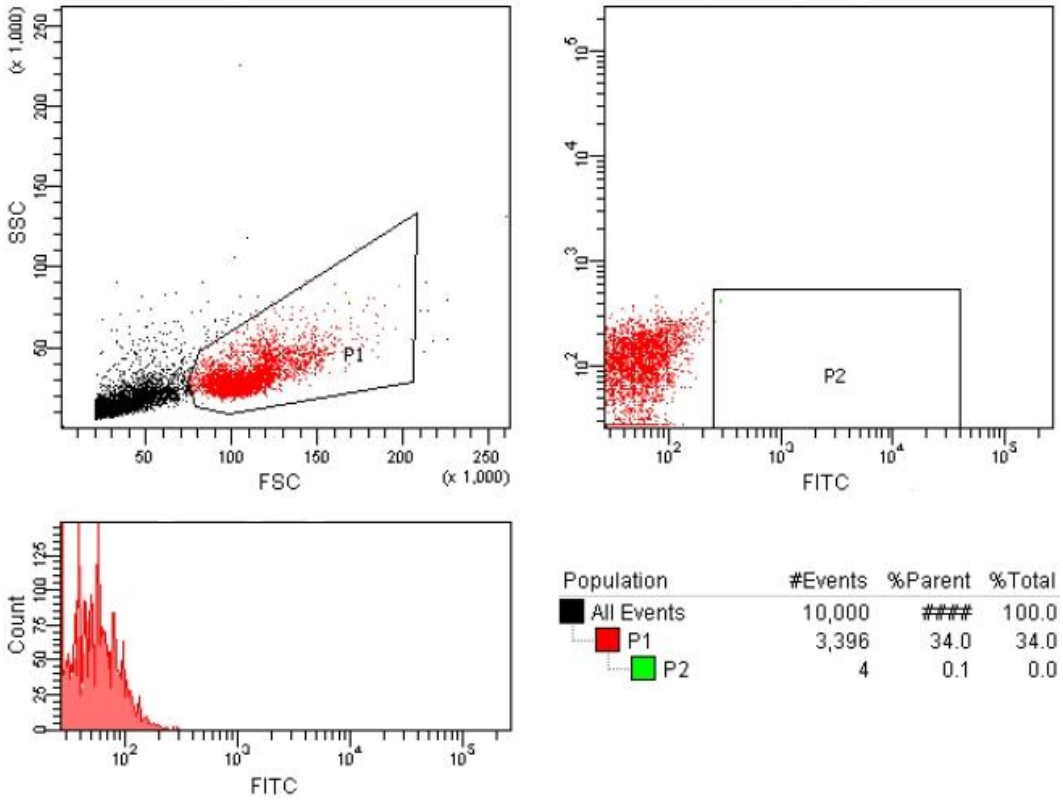

Figure 19: FACS dot blots and histogram of unstained buffy coat. The red gate depicts the living cell population. The population histogram shows a peak for the CD11b-negative population.

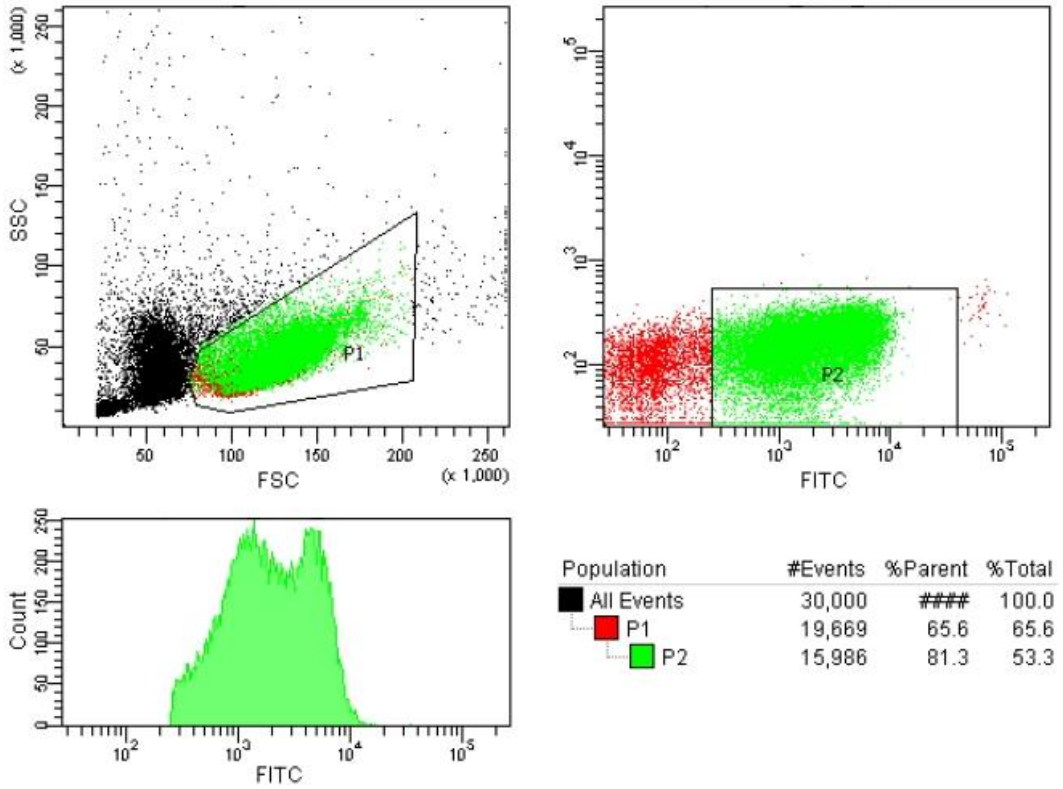

Figure 20: FACS dot blots and histogram of MACSed CD11b-FITC monocytes. Green gate represents CD11b-FITC positive monocytes. Population histogram shows gated CD11b-FITC monocytes (green). The two peaks most probably represent the different monocyte subsets.

4.4. Immunohistochemistry of monocyte-injected Lewis rats

In the second experiment, MACS-purified monocytes were injected intra peritoneally into new born Lewis rats. The results from the previous buffy coat injections suggested a peak in number of positive cells at P3 and P7, therefore the experiment was focused on these time points.

On postnatal day 3, supraventricular corpus callosum and spinal cord displayed no GFP-positive cells (Figure 21 a, b). The liver showed unspecific staining over an extensive area. Some cells displayed a stronger, irregular staining (Figure 21 c). The spleen showed single GFP-positive cells disseminated throughout the tissue (Figure 21 d) and located in blood vessels (e). In the thymus, positive cells were restricted to the medulla (Figure 21 f). The intestinal tissue showed unspecific staining of the goblet cells (Figure 21 j).

On postnatal day 7, the monocyte-injected rat did not display GFP-expressing cells in the brain region of interest, nor in the spinal cord (Figure 22 a, b). Cells in liver tissue showed extensive unspecific staining (Figure 22 c). Spleen tissue displayed light brown staining of cells located in blood vessels (Figure 22 d). Thymus showed positive cells in the medulla (Figure 22 e, f). Kidney tubules (Figure 22 i) and intestinal goblet cells (Figure 22 j) were unspecifically stained.

According to these results, monocytes do not enter into the CNS under the given circumstances and time points investigated.

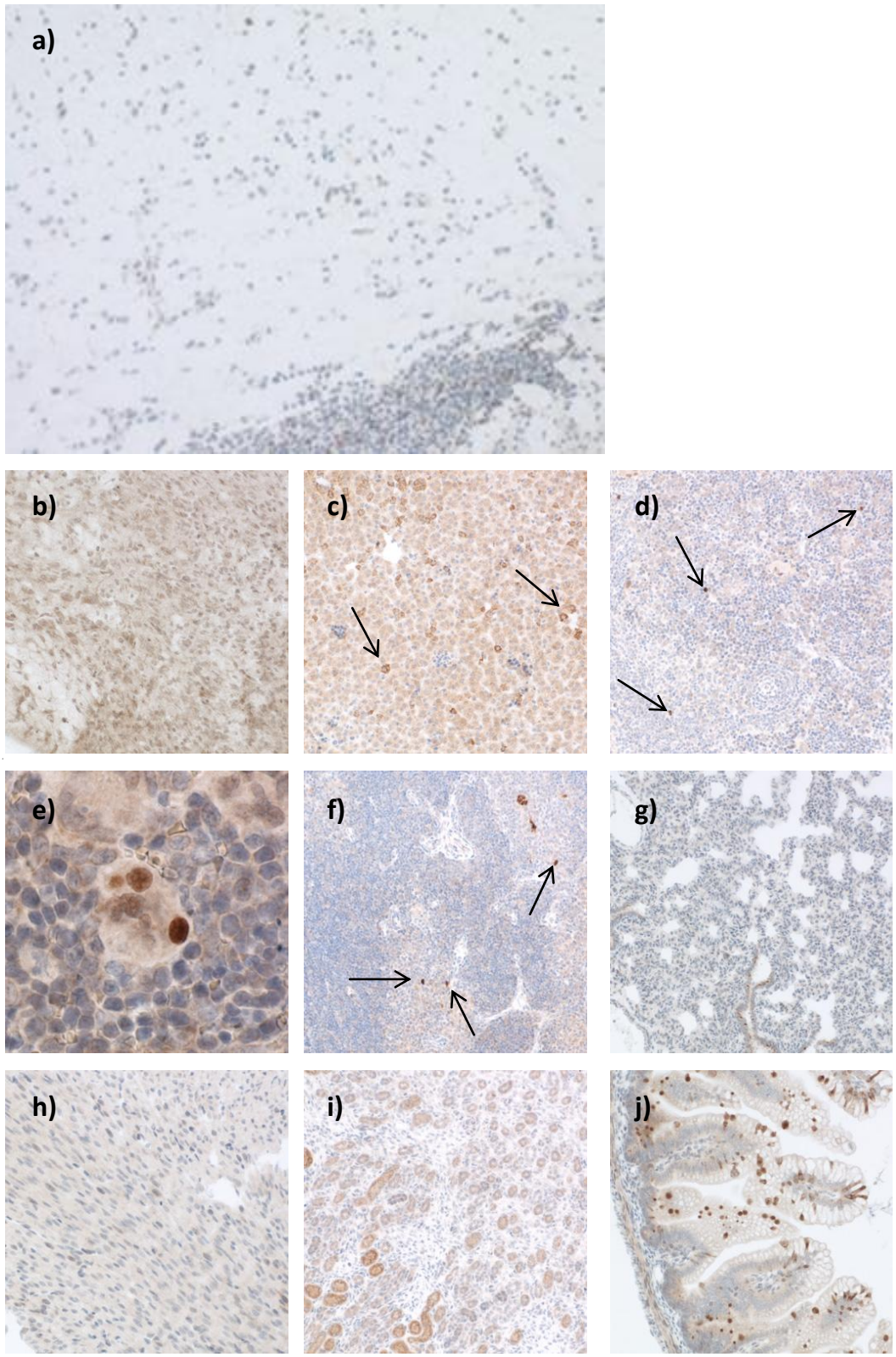

Figure 21: Monocyte-injected P3 Lewis pup tissue, stained for GFP. Cell nuclei are stained blue, GFP-positive cells are stained brown. Single positive cells are indicated with black arrows. a) Brain section (× 100). b) Spinal cord section (× 100). c) Liver shows unspecific and irregular, more intensely brown stained cells (see black arrows) (× 100). d) Spleen displays some positive cells (× 100). e) Few positive cells are detected in blood vessels of the spleen (× 400). f) Thymus shows positive cells in the medulla (× 100). g) Lung section (× 100). h) Heart section (× 100). i) Kidney shows unspecific staining in the tubules (× 100). j) Intestinal tissue displays unspecific signal in goblet cells (× 100).

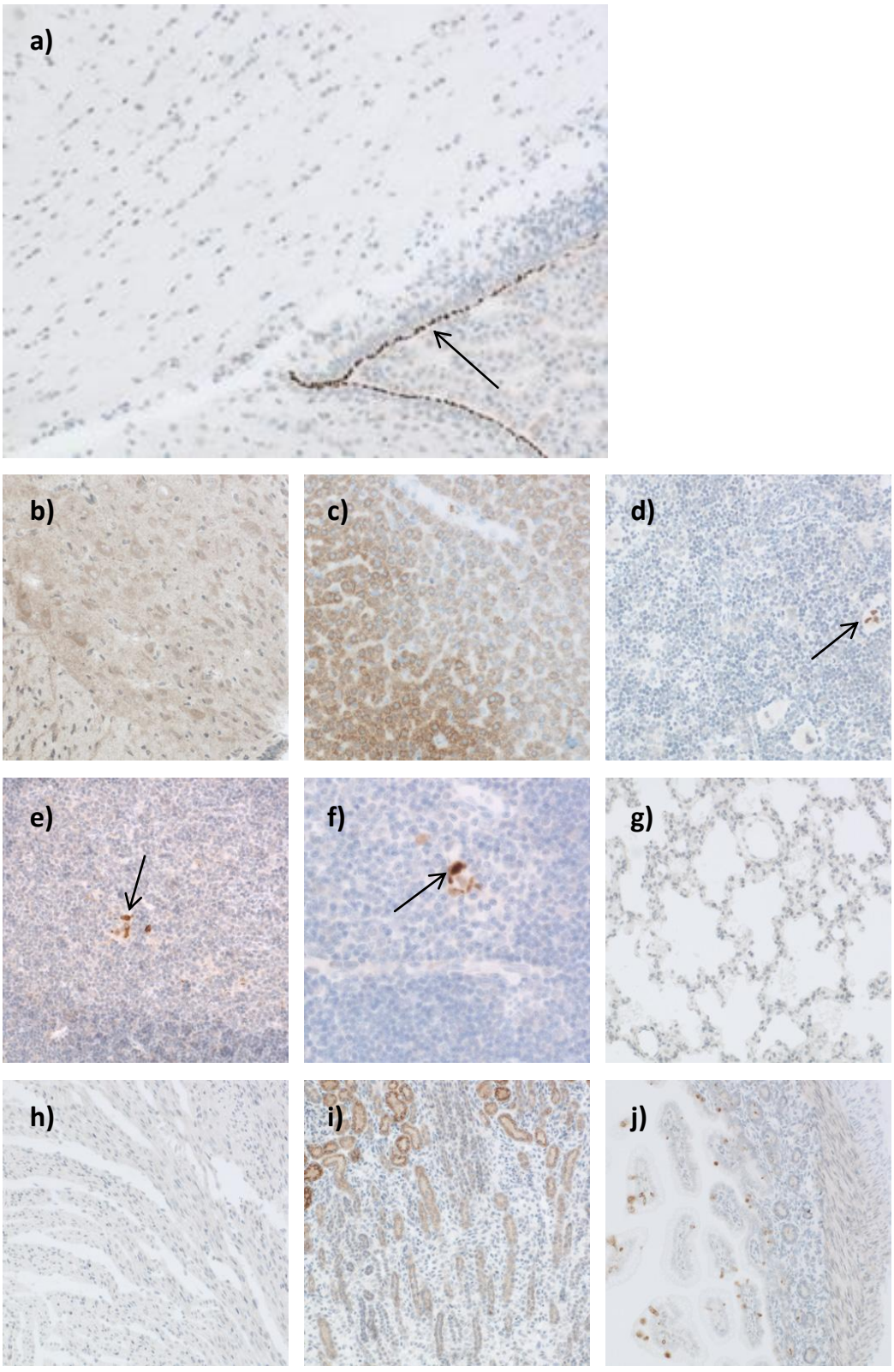

Figure 22: Monocyte-injected P7 Lewis rat tissue, stained for GFP. Cell nuclei are stained blue, GFP-positive cells are stained brown. a) Brain displays unspecific staining of ependymal cells (see black arrow) (× 100). b) Spinal cord section (× 100). c) Liver shows unspecifically stained cells (× 100). d) Spleen displays lightly stained cells in the blood vessel (× 100). e) Thymus shows positive cells in medulla (× 100). f) Higher magnification of positive cells in the thymic medulla (× 250). g) Lung section (× 100). h) Heart section (× 100). i) Kidney shows unspecific staining of the tubules (× 100). j) Intestinal tissue displays unspecific signal in the goblet cells (× 100).

4.5. Immunohistochemistry of spleen homogenate-injected Lewis rats

Preliminary data from our lab and studies conducted by others (Connor et al., 1995) suggest that the cells observed in the supraventricular white matter of postnatal rats contain iron. One organ that is notoriously populated by iron-containing cells, namely marginal metallophilic macrophages, is the spleen.

Consequently, in the third set of experiments it was investigated, whether these cells have the capability to enter into the respective area of the CNS. Therefore spleen homogenate was administered intra peritoneally and 2 time points, P7 and P14, were evaluated immunohistochemically.

On postnatal day 7, spleen homogenate-injected animals displayed no GFP-expressing cells in the supraventricular area of the brain (Figure 23 a), nor in the spinal cord (Figure 23 b). The liver and intestines exhibited unspecific cell staining (Figure 23 i). Many GFP-positive cells migrated into the white pulp of the spleen (Figure 23 d). The thymus exhibited some positive cells in the medulla and a few in the cortex (Figure 23 e). An unspecific signal was also obtained from the thymic medulla of the negative control (Figure 36). Therefore the results have to be interpreted cautiously.

The tissue of spleen homogenate-injected P7 animal was stained with DAB-enhanced Turnbull Blue to check for iron-containing cells. The staining of peripheral tissue showed that iron-containing cells could be detected in the liver (Figure 24 a), spleen (Figure 24 b), thymus (Figure 24 c), lung (Figure 24 d), and kidney (Figure 24 e).

On postnatal day 14, there were no GFP-positive cells located in the corpus callosum, nor spinal cord of the spleen homogenate-injected rat (Figure 25 a, b). GFP-positive cells were found in the thymus (Figure 25 e), however this result is not reliable, as a positive signal could also be detected in the negative control (Figure 38). The goblet cells of the intestine displayed unspecific staining (Figure 25 i).

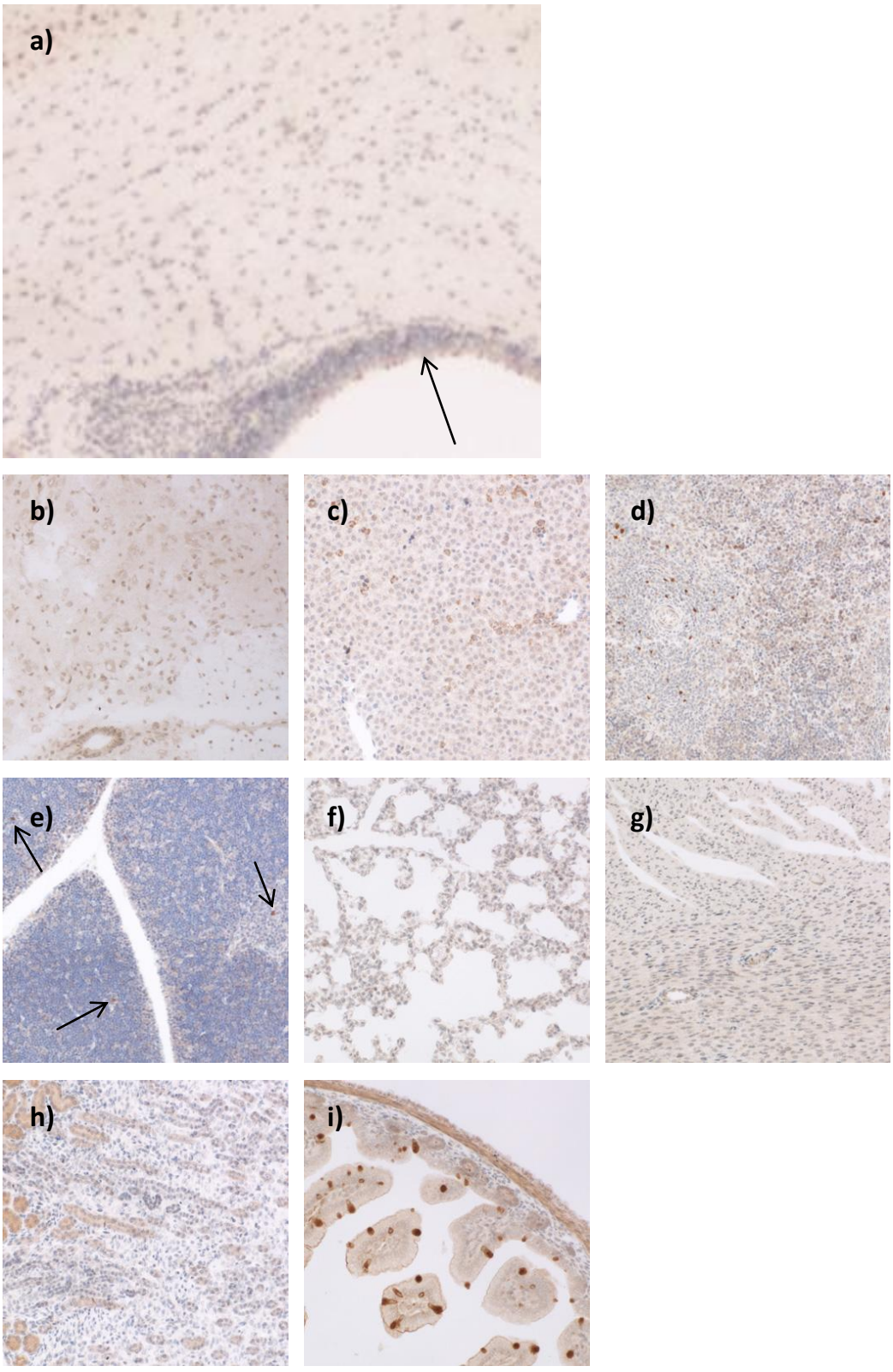

Figure 23: Spleen homogenate-injected P7 Lewis rat tissue, stained for GFP. Cell nuclei are stained blue, GFP-positive cells exhibit intense brown staining. a) Brain tissue shows slight unspecific staining of ependymal cells (see black arrow) (× 40). b) Spinal cord section (× 100). c) Liver exhibits unspecific staining (× 100). d) Spleen displays many GFP-positive cells in white pulp (× 40). e) Thymus displays some positive cells in medulla and cortex, indicated by black arrows (× 40). f) Lung section (× 100). g) Heart section (× 100). h) Kidney section (× 100) i) Intestinal tissue exhibits unspecific staining of goblet cells (× 100).

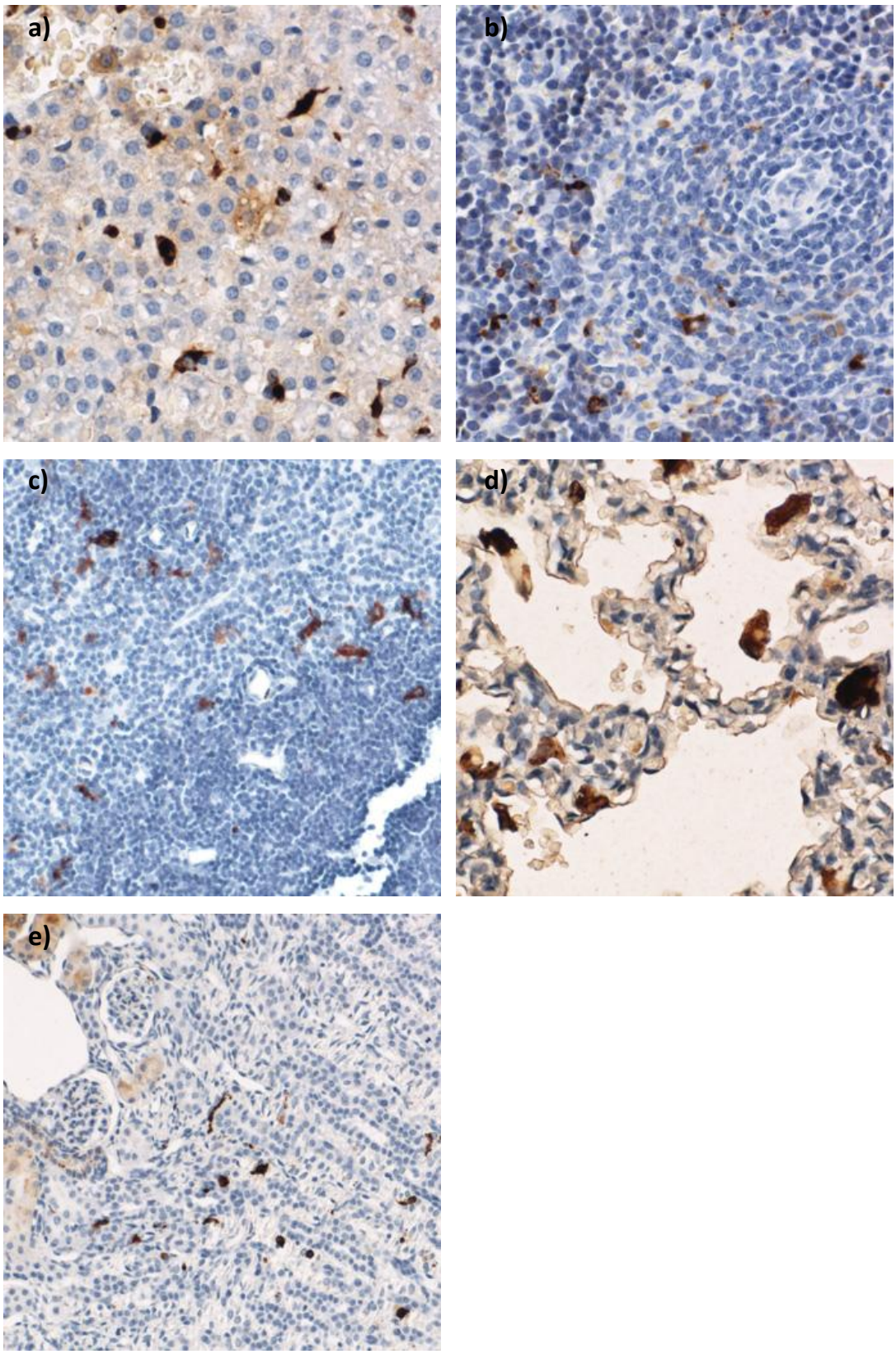

Figure 24: DAB-enhanced Turnbull Blue staining of peripheral tissue of spleen homogenate-injected P7 rats. Blue staining indicates cell nuclei. Iron containing cells are stained intensely brown. a) Liver section (× 250). b) Spleen section (× 250). c) Thymus section (× 100). d) Lung section (× 250). e) Kidney section (× 100).

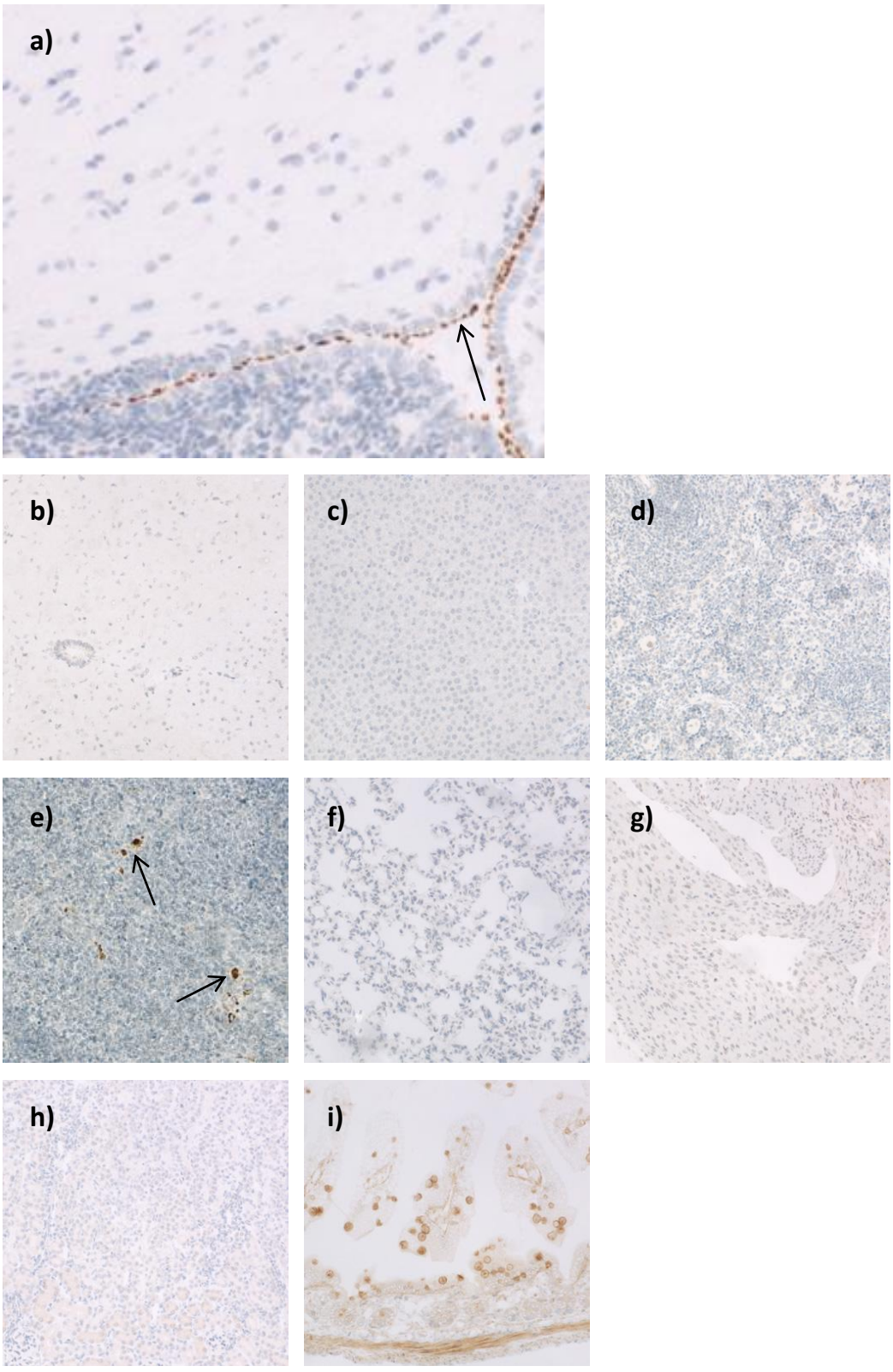

Figure 25: Spleen homogenate-injected P14 Lewis animal, stained for GFP. Cell nuclei are indicated in blue, GFP-positive cells are stained brown. a) Brain tissue exhibits unspecific staining of the ependymal cells (see black arrow) (× 100). b) Spinal cord section (× 100). c) Liver section (× 100). d) Spleen section (× 100). e) Thymus tissue shows positive cells in the medulla, highlighted with black arrows (× 100). f) Lung section (× 100). g) Heart section (× 100). h) Kidney section (× 100). i) Intestinal tissue shows unspecific staining (× 100).

4.6. Immunohistochemistry of iron-containing spleen cell-injected Lewis rats

By virtue of their iron content, metallophilic spleen cells could be retained and purified in a magnetic MACS column. The isolated iron-containing spleen cells were administered intra peritoneally into Lewis neonates (P0) to assess whether the highly enriched iron-positive cells find their way into the supraventricular corpus callosum. The recruitment of iron-positive cells was investigated in P3 Lewis pups.

On postnatal day 3, iron-positive spleen cell-injected pups displayed no positive cells in the supraventricular corpus callosum (Figure 26 a), nor spinal cord (Figure 26 b). However, GFP-expressing cells were located in great numbers in the blood vessels of the spleen (Figure 26 d, e). Several positive cells were found in the thymic medulla (Figure 26 f). Unspecific staining was observed in the liver (Figure 26 c), kidney tubules (Figure 26 i), and intestinal goblet cells (Figure 26 j).

According to these results, intra peritoneally injected iron-containing spleen cells are not contributing to the “fountain of microglia” in the corpus callosum during postnatal development.

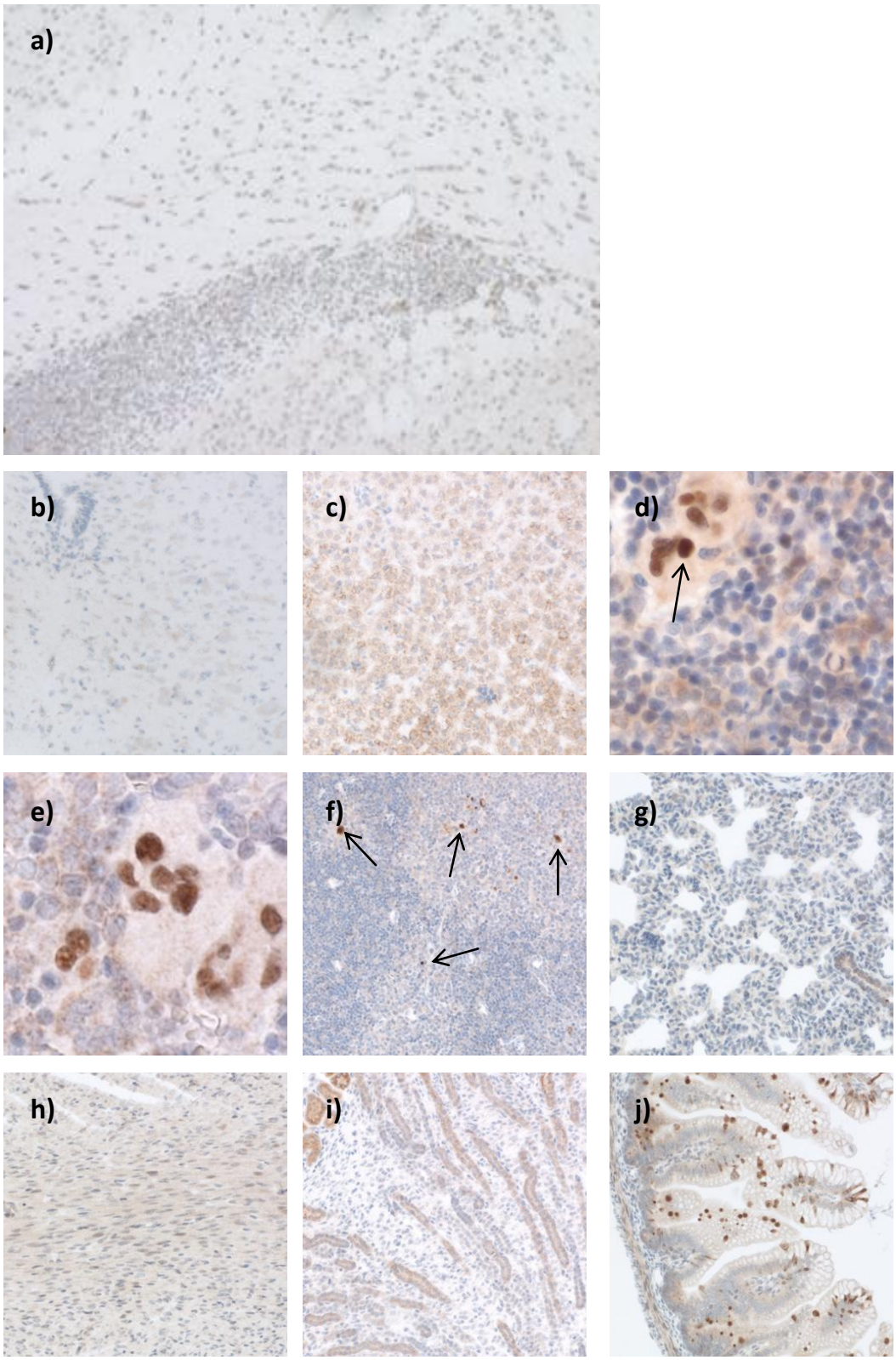

Figure 26: MACSed spleen cell-injected P3 Lewis rat tissue, stained for GFP. Cell nuclei indicate blue staining, GFP-positive cells exhibit intense brown staining. a) Brain section (× 100). b) Spinal cord section (× 100). c) Liver tissue displays unspecific staining (× 100). d) Spleen exhibits positive cells in the vasculature (× 100). e) Higher magnification of positive cells in a blood vessel of spleen (× 400). f) Thymus displays positive cells in the medulla (see black arrows) (× 100). g) Lung section (× 100). h) Heart section (× 100). i) Kidney exhibits unspecific staining in the tubules (× 100). j) Intestinal tissue shows unspecific staining of goblet cells (× 100).

4.7. Immunohistochemical analysis of cell surface markers

There is a possibility that the adult cells, which were used for injections, possess a receptor profile distinct from that in newborn rats. Thus it was investigated, whether monocytes and iron-containing spleen cells from adult animals lose their migratory capacity to enter the brain during postnatal development. MACS fractions of monocytes and iron-containing spleen cells from P3 pups and adult Lewis rats were stained for various receptors and adhesion molecules. Since only a small fraction of iron-containing spleen cells were obtained in the MACS eluate of P3 pups, the flow-through from MACS was used for immunohistochemical detection. The antigens, whose presence was assessed were Iba1, CX3CR1, CCR2, CD169 (recognized by ED3 antibody), and CD11b. Additionally cells were stained with Turnbull Blue to check their iron content.

Iba1 is a specific marker for macrophages and microglia. The marker was expressed in monocytes of adults (Figure 27 d-f) as well as in P3 pups (Figure 27 a-c), whereas the signal obtained from P3 pups was stronger than in adults. The spleen cells of adult and P3 animals displayed various signal intensities. The strongest signal was derived from large cells with anindented nucleus (Figure 27 k). The light stainings could be due to a lower level of marker expression. It could also be an unspecific signal, as macrophages carry many Fc receptors, which can bind to Fc region of antibodies, if not completely blocked.

ED3 stainings of P3 monocytes showed varying, but weak intensities (Figure 28 a-c). Spleen cells from P3 exhibited a weak signal for ED3 as well (Figure 28 d-e). Spleen cells of the eluate from an adult rat exhibited only a light brown surface staining (Figure 28 g-i). This observation is rather surprising, since the antibody is specific for CD169 (Sialoadhesin) on metallophilic spleen macrophages.

CCR2 is a chemokine receptor important for monocyte recruitment, as its alternative name MCP-1 (monocyte chemoattractant protein-1) suggests. CCR2 stainings of P3 monocytes showed varying and weak levels of brown staining (Figure 29 a-c). Adult monocytes exhibit stronger signals for CCR2 (Figure 29 d-f). Spleen cells of P3 pup exhibited intense as well as light staining, which might be an unspecific signal (Figure 29 g-i). MACSed spleen cell eluate from adult animals displayed many, strongly positive cells (Figure 29 j-l).

CD11b is a myeloid marker expressed on monocytes, granulocytes, macrophages, and natural killer cells. A strong CD11b signal was obtained from P3 monocytes (Figure 30 a-c). Spleen cells from P3 pups generally displayed irregular brown staining and larger cells with more intense brown staining (Figure 30 d-f). In adults, spleen cells from MACS eluate displayed little and abnormal cell surface staining, which could be due to variations in cell fixation (Figure 30 g-i).

CX3CR1 is a chemokine receptor, expressed on lymphocytes and monocytes. It is an important molecule for leukocyte migration[5]. Monocytes derived from an adult rat (Figure 31 d-f) showed a stronger staining for CX3CR1 than their P3 counterpart (Figure 31 a-c). The situation was similar for the MACSed spleen cells. Whereas spleen cells from a P3 pup displayed irregular and light surface staining (Figure 31 g-h), spleen cells from MACS eluate of an adult exhibited intense brown staining for CX3CR1 (Figure 31 i-k).

DAB-enhanced Turnbull Blue (TBB) stainings revealed that monocytes from a P3 pups do not contain iron (Figure 32 a-c). Light TBB staining in some monocytes derived from an adult rat indicated that monocytes are capable to accumulate low iron amounts (Figure 32 d-f). In spleen cells of a P3 rat, no iron-containing cells were detected (Figure 32 g-h). This data is consistent with the observation that only a low number of iron-containing spleen cells could be recovered by the MACS method, due to low amounts or lack of iron content. Spleen cells in the eluate from an adult rat were strongly positive for iron (Figure 32 j-l), which elegantly confirms the rationale that iron-containing macrophages are retained in the MACS column. The absence of TBB staining in the spleen cell flow-through (Figure 32 i) confirms that all iron-positive cells were efficiently isolated during the MACS procedure.

[5] http://www.ncbi.nlm.nih.gov/gene/1524

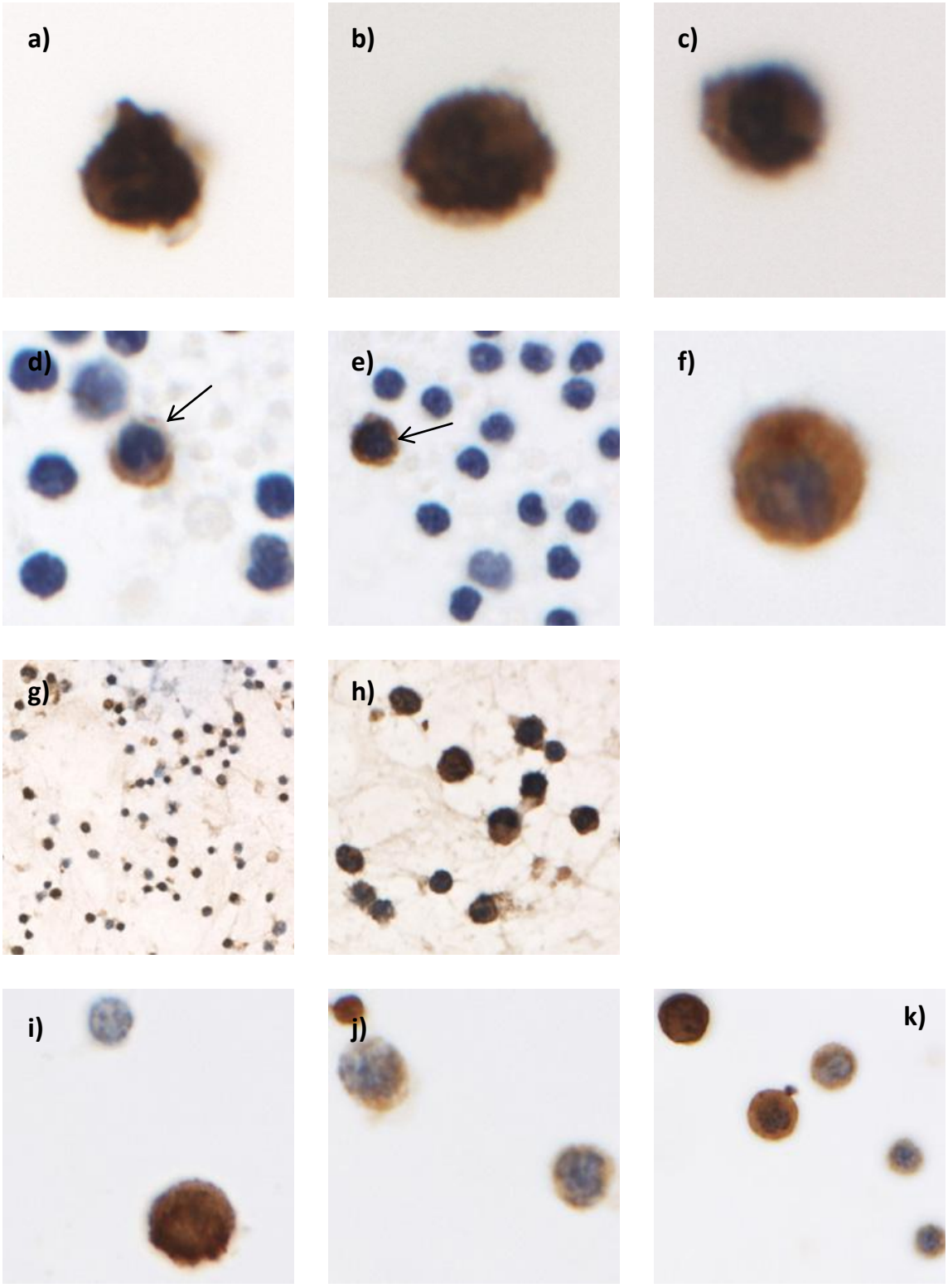

Figure 27: Iba1 cell surface stainings. Positive cells are stained brown. Cell nuclei are stained blue. a)-c) Monocytes of a P3 pup display intense brown staining (× 1000). d)-e) Buffy coat of an adult rat (× 400) with some positive cells (see black arrow). f) Monocyte of an adult rat shows light brown staining (× 1000). g)-h) Spleen cell flow-through of P3 pup shows different intensities of brown staining (× 250, × 1000, respectively). i)-k) Spleen MACS eluate of an adult rat shows cells of various sizes and morphologies, which exhibit different intensities of brown cell surface staining (× 400).

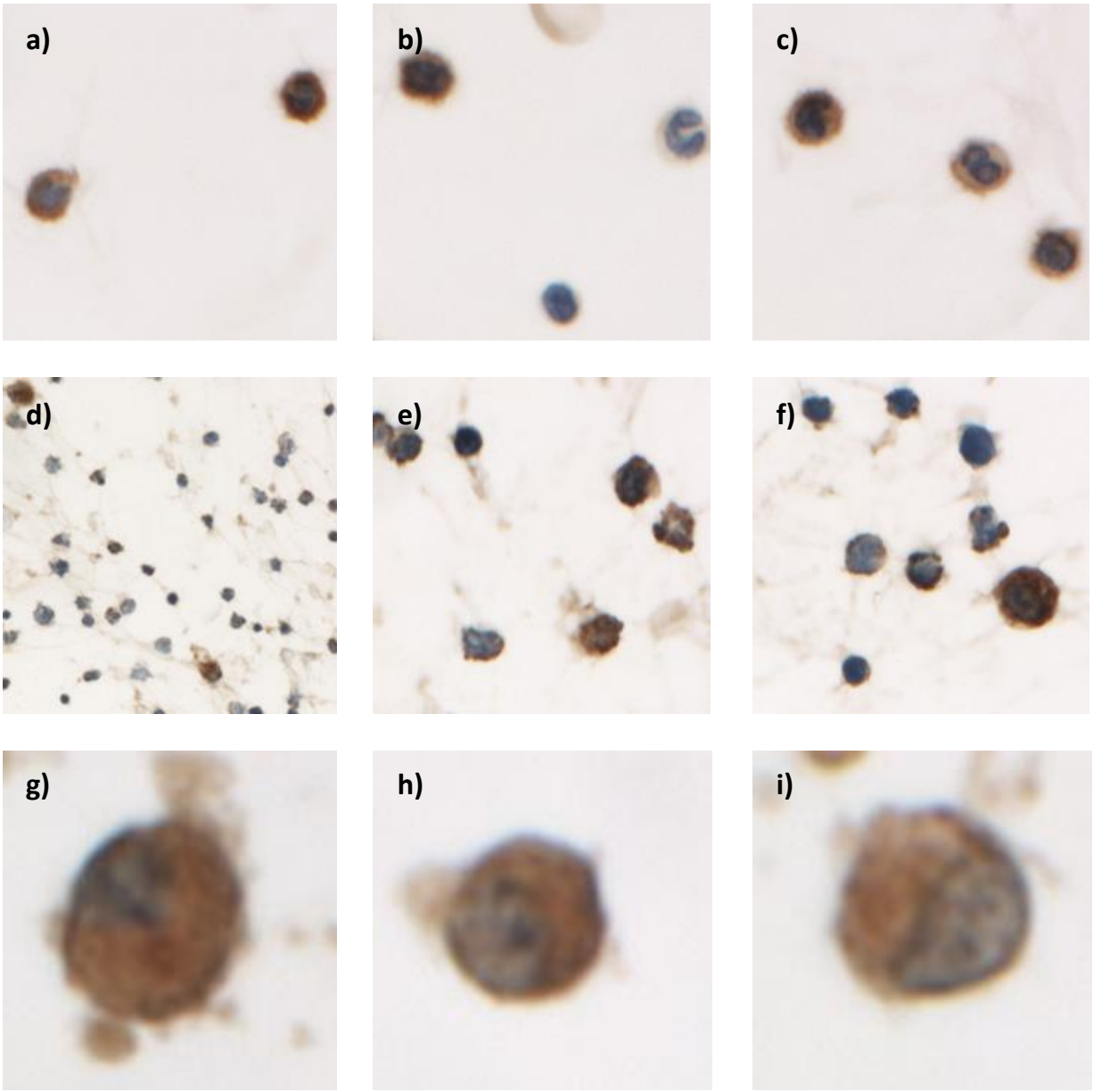

Figure 28: ED3 cell surface stainings. Positive cells are stained brown, cell nuclei are stained blue. a)-c) MACSed monocytes of a P3 pup show different intensities of brown staining (× 400). d)-f) Spleen cell flow-through of a P3 pup shows light and irregular brown staining (× 250, × 400, × 400, respectively). g)-i) Spleen cells of MACS eluate of an adult rat exhibit light brown staining (× 1000).

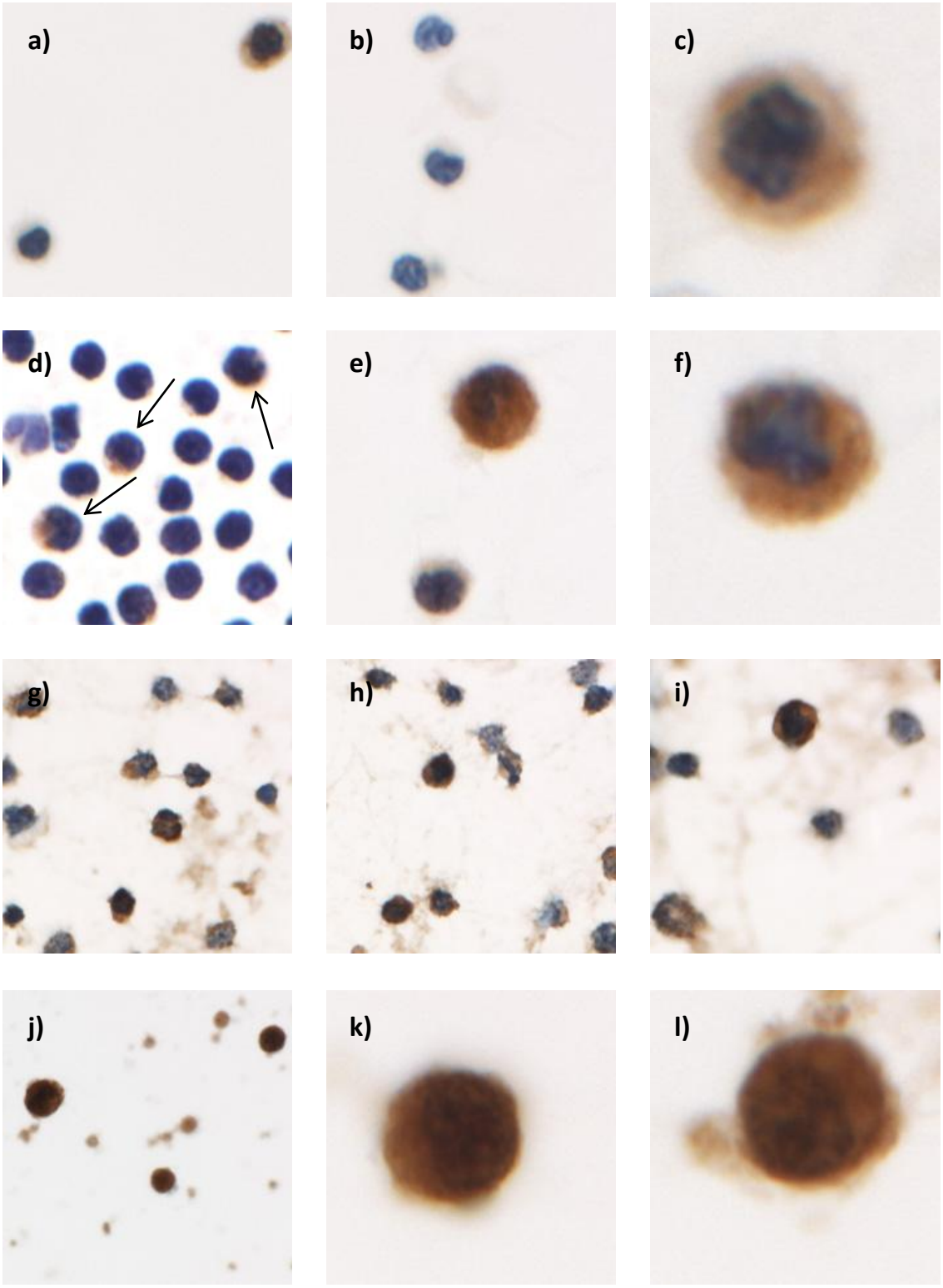

Figure 29: CCR2 cell surface stainings. Positive cells are stained brown, cell nuclei are stained blue. a)-c) MACSed monocytes of a P3 pup show different intensities of brown staining (× 400, × 400, × 1000, respectively). d) Some buffy coat cells of an adult rat with an indented nucleus display very light staining (× 400) (see black arrows). e)-f) MACSed monocytes of an adult rat display stronger brown staining (× 400, × 1000, respectively). g)-i) Spleen cell flow-through of a P3 pup show irregular staining (× 250, × 250, × 400, respectively). j)-l) Spleen cells of MACS eluate of an adult rat show intense brown staining (× 400, × 1000, × 1000, respectively).

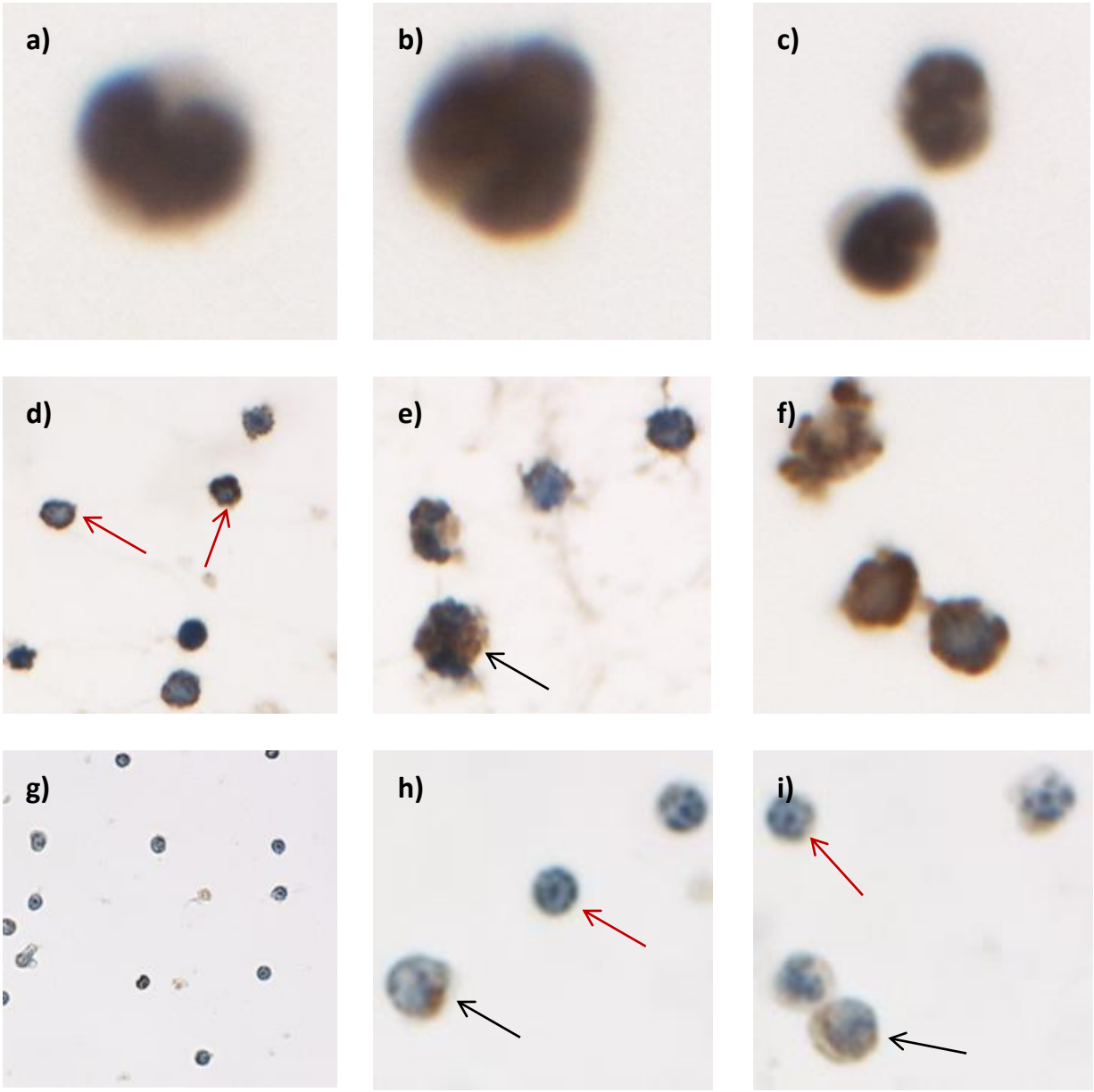

Figure 30: CD11b cell surface stainings. Positive cells are encolored brown. Cell nuclei are stained blue. a)-c) MACSed monocytes of a P3 pup show intense brown staining (× 1000, × 1000, × 400, respectively). d)-f) Spleen cell flow-through of a P3 pup show irregular (black arrow) and halo-like (red arrow) staining of various intensities (× 250, × 400, × 400, respectively). g)-i) Cells of MACSed spleen eluate of an adult rat show light brown (see black arrows), or no positive staining (see red arrows) (× 400, × 1000, × 1000, respectively).

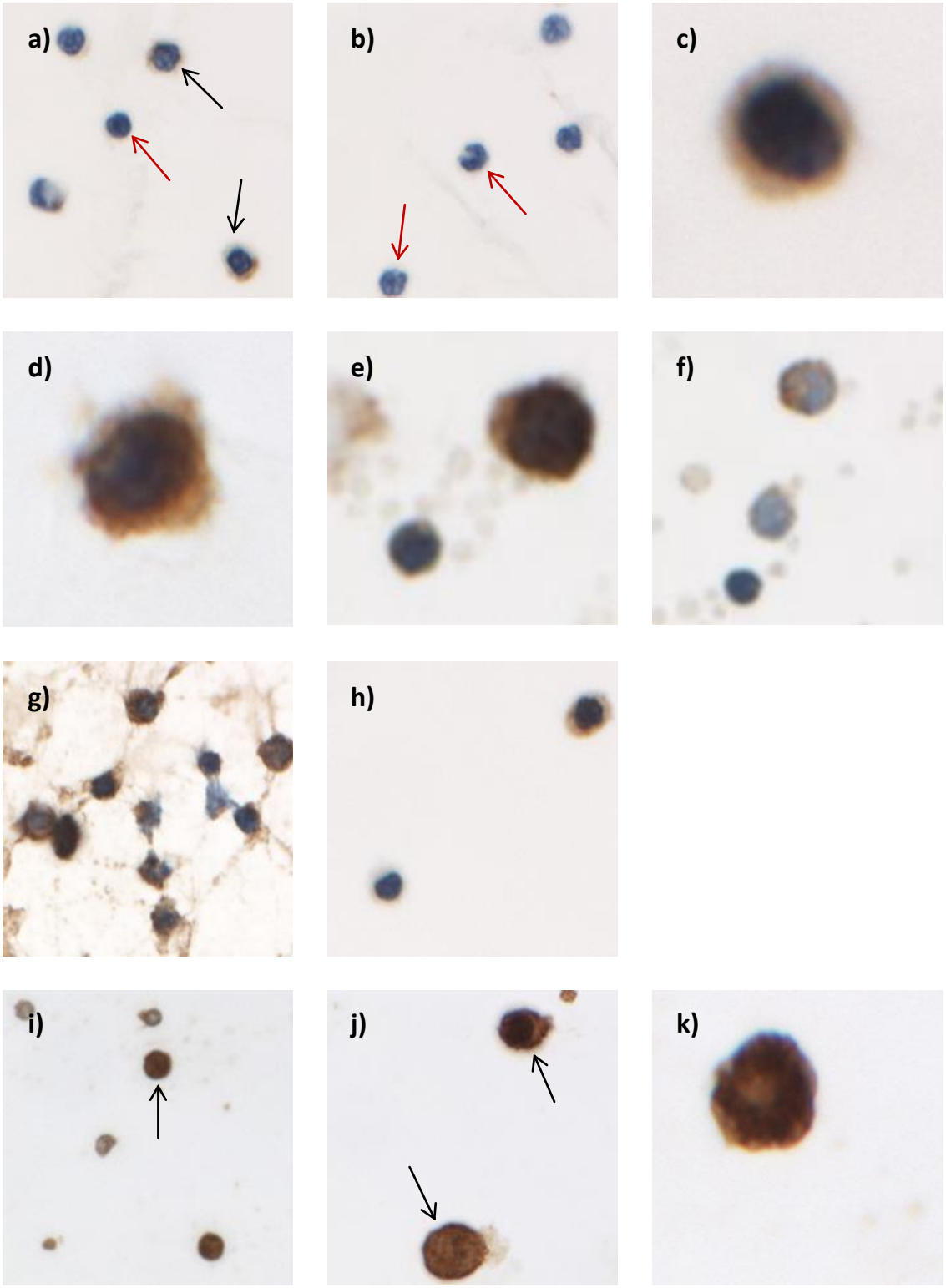

Figure 31: CX3CR1 cell surface stainings. Positive cells are stained brown. Cell nuclei are stained blue. a)-c) MACSed monocytes of a P3 pup show light (see black arrows), or no (see red arrrow) brown staining (× 250, × 250, × 1000 respectively). d)-f) MACSed monocytes of an adult rat show different intensities of brown staining (× 1000, × 1000, × 400, respectively). g)-h) Spleen cell flow-through of a P3 pup exhibit different nuances of brown staining (× 250). i)-k) Spleen cells of MACS eluate of an adult rat show different intensities of brown staining. Large cells display a very intense brown staining (see black arrows) (× 250, × 400, × 1000, respectively).

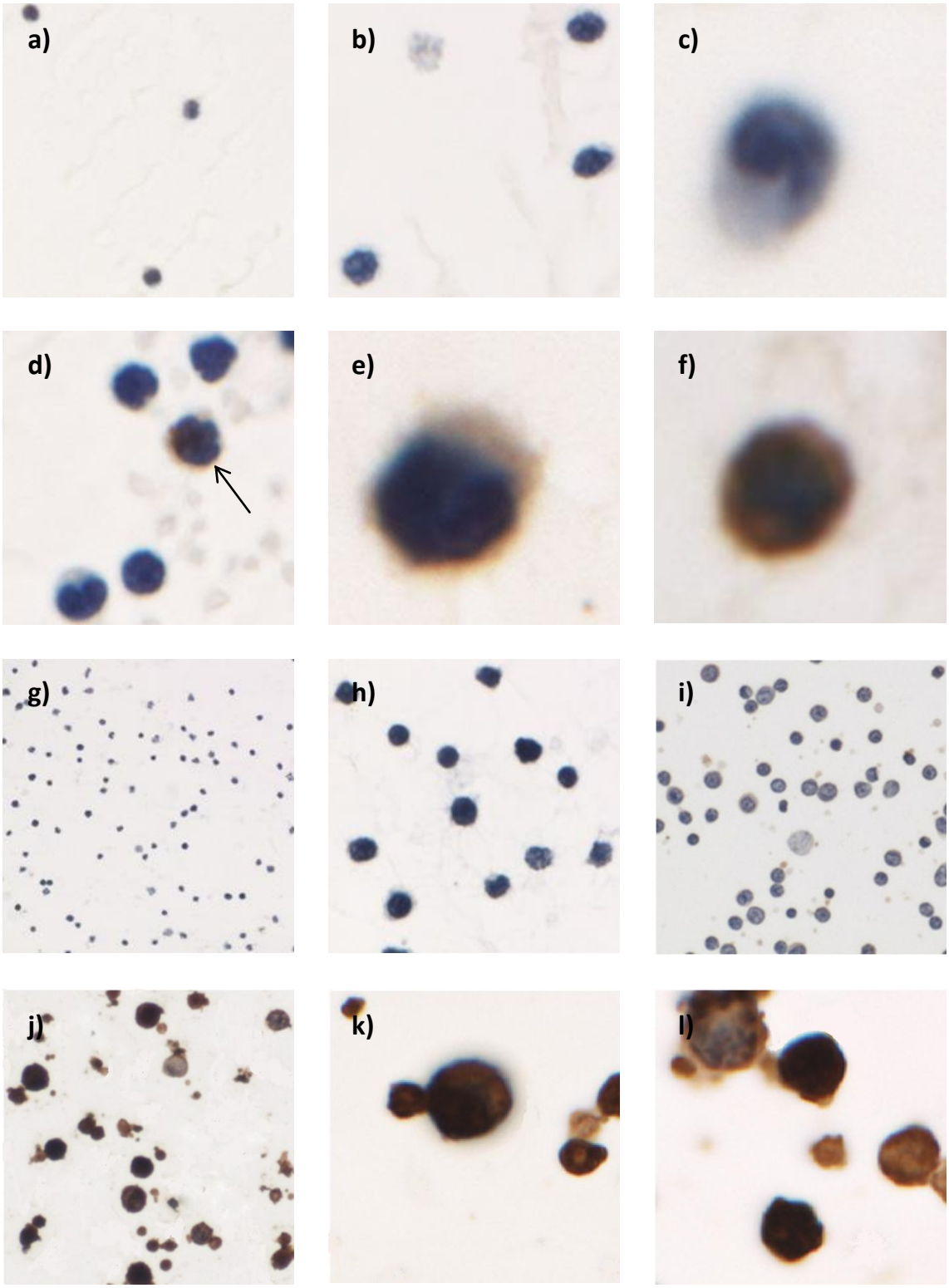

Figure 32: DAB-enhanced Turnbull Blue stainings. Iron-containing cells are stained brown, indicated in blue are the cell nuclei. a)-c) MACSed monocytes of a P3 pup display no brown staining (× 250, × 400, × 1000, respectively). d) Some buffy coat cells of an adult rat exhibit a brown staining pattern (see black arrow) (× 250). e)-f) MACSed monocytes of adult rats display light brown staining (× 1000). g)-h) Spleen cell flow-through of a P3 pup indicates no iron-positive cells (× 250, × 400, respectively). i) Spleen cell flow-through of an adult rat displays no iron positive cells (× 400) j)-l) Spleen cells of MACS eluate from an adult rat show intense brown staining (× 400, × 1000, × 1000, respectively).

4.8. PCR of adhesion molecules

In order to investigate the expression of adhesion molecules on monocytes of MACSed buffy coat and magnetically sorted spleen cells on messenger RNA level, in vitro experiments were performed. RNA was isolated from corpus callosum of P2 Lewis rat, from MACSed spleen cells and monocytes of P3 and adult Lewis rats. Polymerase chain reactions (PCR) with CCR2, CX3CR1, Integrin α_4, Integrin α_L, and Sialoadhesin (CD169) were conducted on cell eluates. The results allow a comparison of expression level of these adhesion molecules and receptors. Additionally, PCRs with CCL2, ICAM-1, VCAM-1 of P2 corpus callosum material were performed to investigate, which of these adhesion molecules are expressed in the early postnatal development.

GAPDH bands of cell eluate cDNAs showed the same intensities, with exception of adult buffy coat eluate, which indicates that equal amounts of sample were loaded. Since the intensity was higher in one sample, differences in band intensities have to be interpreted cautiously. CCR2 expression was slightly lower in spleen eluate of the adult animal than in the P3 pup and maintained at equal levels in Buffy coat eluates of P3 and adult rats. CX3CR1 was expressed at same levels in all eluates of adult and P3 rats. Sialoadhesin (CD169) displayed a higher expression in spleen eluate derived from adult rat than in the P3 pup, whereas it could not be detected in either of the buffy coat eluates. Integrin α_4 and α_L were expressed at same levels in all cell eluates.

Corpus callosum tissue of a P2 Lewis pup showed a strong signal for GAPDH. CCL2 exhibited a very low expression level in comparison to the other genes. VCAM-1 was strongly expressed, whereas ICAM-1 displayed a low expression level. Due to the excision method of corpus callosum it is not certain, whether the material used for RNA isolation contained the desired region exclusively. Surrounding, “contaminating” tissue may lead to distortion of the results.

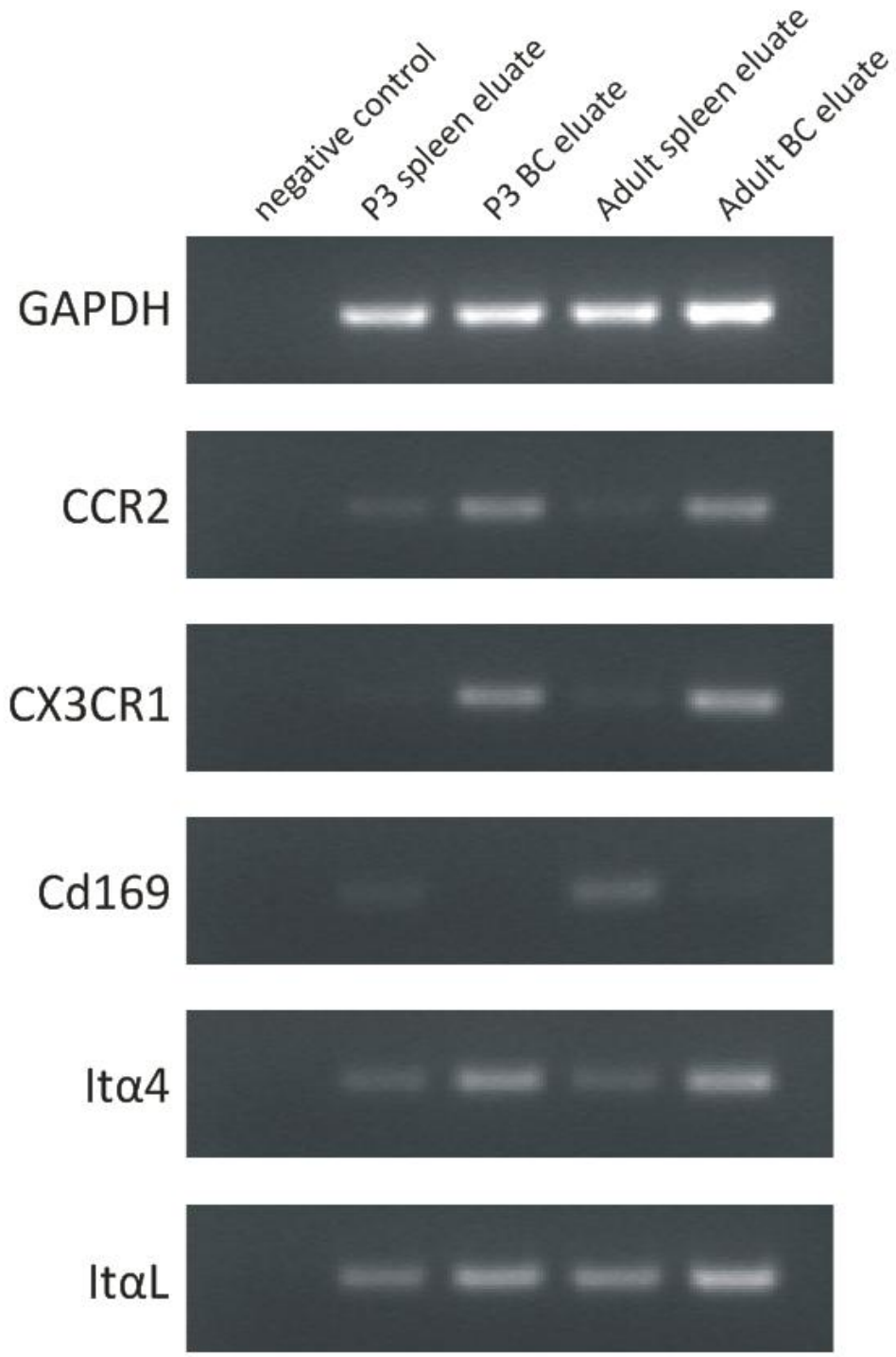

Figure 33: Expression levels of MACSed spleen and buffy coat eluate from adult and P3 rat. Markers which were investigated are CCR2 (229 bp), CX3CR1 (216 bp), CD169 (155 bp), Itα4 (189 bp), ItαL (203 bp) and the housekeeping gene GAPDH (311 bp). PCR was run with 35 cycles to obtain results which are quantifiable.

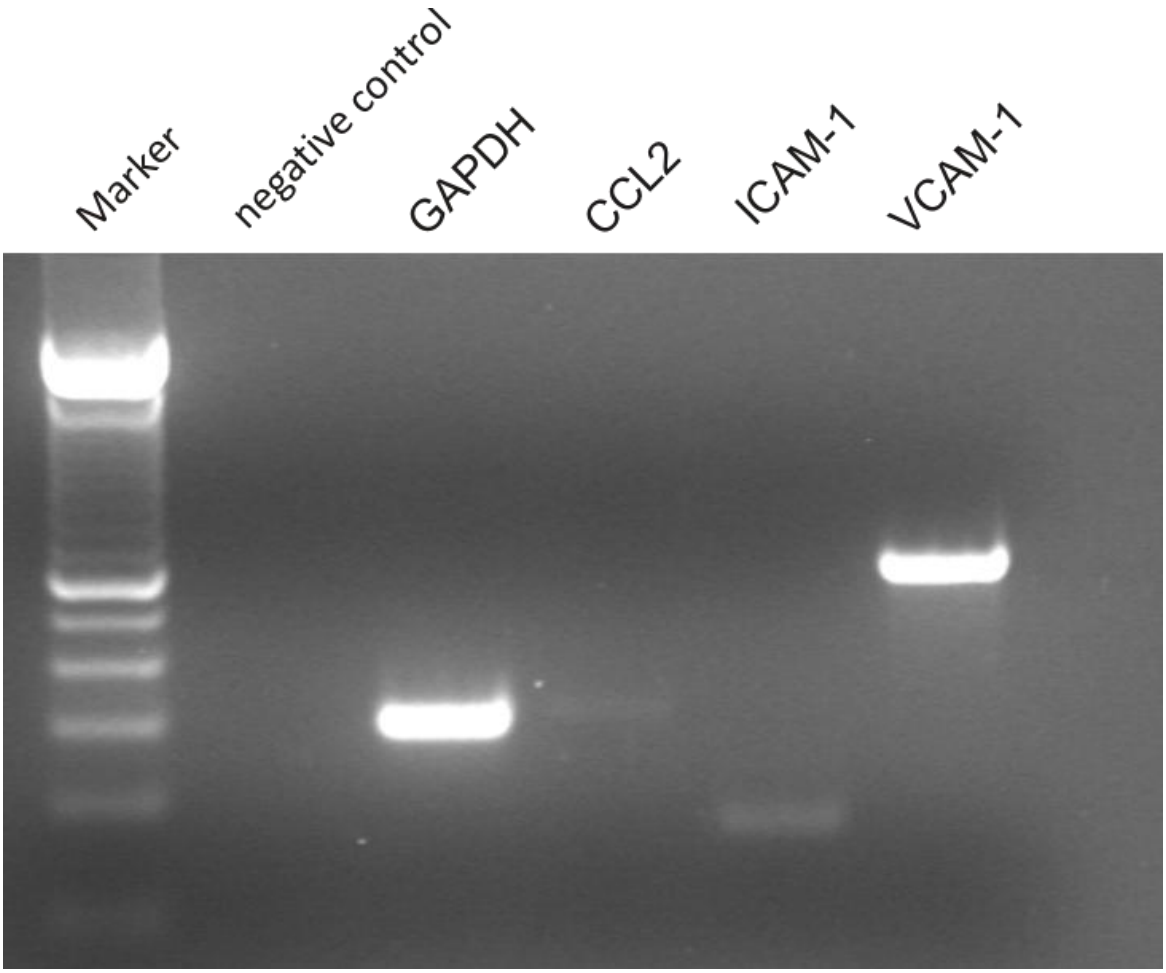

Figure 34: Expression levels of P2 corpus callosum. Markers which were investigated are CCL2 (320 bp), ICAM-1 with (182 bp), VCAM-1 (635 bp), and the housekeeping gene GAPDH (311 bp). PCR was run with 35 cycles to obtain quantifiable results.

Discussion

The “fountain of microglia”, or the appearance of amoeboid microglia-like cells in the perinatal region of the supra - and periventricular corpus callosum, has been investigated extensively in the past (Hirasawa et al., 2005; Hristova et al., 2010; Wu et al., 1992).

In this study, we aimed at investigating the origin of these phagocytes in the corpus callosum. We addressed the question, whether amoeboid microglial cells are recruited from the periphery or whether they are derived from the resident, cortical microglia population.

The purpose of the local accumulation of phagocytic cells in the periventricular corpus callosum has not been elucidated yet. One hypothesis is that the microglial precursors are recruited to help in developmental processes, such as axon pruning and clearance of dead neurons during synapse formation, before the onset of myelination (Marin-Teva et al., 2004; Neumann et al., 2009). Interleukin-1 (IL-1) is produced by activated, amoeboid microglia and serves as mitogen to astrocytes, which are crucial for axon guidance and the formation of neuronal circuits. A decline in amoeboid cells during development correlates with a decrease in IL-1 production (Giulian et al., 1988).

Preliminary data from our lab shows that the amoeboid microglia-like cells contain iron. A peak in appearance of these iron positive phagocytic cells occurs concomitantly with the onset of axon myelination at postnatal day 14. Iron is a critical transitional metal during normal neuronal development, therefore uptake of iron is increased during neonatal development. Iron deficiency is associated with hypomyelination, which strongly suggests that oligodendrocytes require iron for myelinogenesis (Connor et al., 1995). This observation raised the concept that the recruited cells serve as iron suppliers.

Microglia-like cells might pick up the iron on their way to the CNS. This theory is based on the observation that choroid plexi of postnatal rats stain for iron (unpublished data) (Redzic and Segal, 2004). Iba1-positive, but iron-negative, round cells were detected in the blood vessels of choroid plexus. These cells might pick up iron en route to the stem cell zone of the ventricle and subsequently migrate to the corpus callosum as iron-positive cells (unpublished data).

The blood-brain barrier, the endothelium of the CNS, can be stimulated by cell mediators, subsequently changing their permeability status. This allows passage of specific cells, carrying the appropriate adhesion molecules.

Especially two cell adhesion molecules are involved in the recruitment of leukocytes from the blood circulation into the tissue, lymphocyte function-associated antigen-1α (LFA-1α) and intercellular adhesion molecule-1 (ICAM-1). ICAM-1 expression on vascular endothelium

is induced by tumor necrosis factor-α (TNF-α) and IL-1. The highest concentration of IL-1 in normal developing rat cerebral cortex was observed from embryonal day 18 until birth (Dalmau et al., 1997; Giulian et al., 1988). The IL-1 expression peak in the perinatal phase correlates with the peak of LFA-1α-positive monocyte-like cells in parenchyma, ICAM-1 positive blood vessels, and the increase in microglial cell numbers, which was reported in other studies (Dalmau et al., 1997). Therefore Dalmau and his colleagues proposed that LFA-1 and ICAM-1 adhesion molecules may participate in recruitment of microglial cell precursors in the developing rat brain.

In this study, we tested the recruitment of GFP-expressing monocytes into the postnatal CNS. We also evaluated the hypothesis whether GFP-expressing, myeloid cells of the spleen, representing a cell pool which not only gives rise to iron positive cells in the spleen, is also able to populate other organs like the brain. The immunohistochemical data suggests that these cells only enter into peripheral tissues, particularly the lymphoid organs, but not into the CNS.

There are several possibilities to explain the absence of GFP-expressing cells in the CNS upon intra peritoneal monocyte and spleen cell injection. First it is possible that adult and newborn rats possess different receptor profiles on monocytes and myeloid spleen cells. It was confirmed on two levels, namely immunohistochemical and in vitro analysis, that there are no apparent differences in expression of adhesion molecules and receptors between monocytes and myeloid spleen cells at both time points tested.

Corpus callosum tissue displays strong expression of VCAM-1. The respective adhesion molecule, integrin α_4, was expressed at higher levels in monocytes than in spleen cells. Integrin α_L, or LFA - 1α is also expressed at equal levels in P3 and adult myeloid cells. Integrin α_L expression in monocytes is slightly higher than in spleen cells. The respective ligand, ICAM-1, shows only a low expression in corpus callosum tissue of a P2 pup. From all adhesion molecules tested, CCL2 displays the lowest expression level in the corpus callosum. This is not a novel finding, since unpublished microarray data from our lab suggests that CCL2 is not expressed in cortical tissue of P0 Lewis rats.

According to Mildner and his colleagues, monocytes can enter the brain under defined conditions by virtue of CCR2 expression (Mildner et al., 2007). Our data derives from postnatal animals, but as the onset of amoeboid microglia accumulation in the corpus callosum occurs earlier in development about one week before birth (Hristova et al., 2010), it cannot be excluded that CCL2 is expressed in higher levels during embryonal development. However, the number of amoeboid microglia-like cells in the corpus callosum continues to rise during postnatal development, with a peak between P0 and P7 and a subsequent decline (Chugani et al., 1991b; Hirasawa et al., 2005; Wu et al., 1992; Wu et al., 2006). For this, the brain has to be accessible for blood-derived precursors also in the postnatal development.

A considerable amount of studies conducted by others suggest that blood monocytes migrate to the inflamed and irradiated brain tissue. During the course of acute experimental autoimmune encephalitis (EAE), the animal model of multiple sclerosis, high numbers of monocytes are found to infiltrate the CNS, transform into ramified microglial cells and persist in the CNS for several weeks. Their fate, however, still remains unknown (Flugel et al., 2001). There are reports suggesting that they undergo apoptosis (Nguyen et al., 1994), while others found only small numbers of apoptotic macrophages (Smith et al., 1996). In direct trauma and stroke models, blood-brain barrier disruption facilitated recruitment of blood-borne cells from the circulation (Jones et al., 2000; Priller et al., 2001). In peripheral facial nerve axotomy, a model that conserves blood-brain barrier integrity, only a few blood-derived leukocytes traffic into the CNS (Raivich et al., 1998). The blood leukocytes are attracted to sites of inflammation, or injury as a consequence of upregulated cell mediators in the challenged tissue (Karpus et al., 1995).

Upon irradiation, Mildner et al. observed monocytic recruitment into the brain. The influx was enhanced under pathological conditions, combined with an irradiation dose. It turned out that the recruitment of CCR2+ monocytes into the brain was an irradiation artifact, because no engraftment occurred in brains which were protected from irradiation (Mildner et al., 2007). Likewise under pathological conditions, irradiation leads to CCL2 production by brain endothelium, enabling the entry of CCR2-bearing monocytes (Holman et al., 2011; Klopp et al., 2007).

Monocyte entry has been described under supposedly physiological, non-traumatic conditions. Ling et al. observed the entry of monocytes, labeled with colloidal carbon particles, into the corpus callosum during postnatal development. However, these results could not be reproduced by other exogenous labeling techniques of monocytes. This fortifies the assumption that the carbon labeling altered the activity status of the blood leukocytes and triggered their entry into the brain (Hristova et al., 2010). A non-manipulative model used by Ajami et al., which does not require irradiation nor transplantation, were parabiotic animals. They observed no monocytic recruitment into the CNS, suggesting local proliferation and maintenance of microglia under steady state conditions (Ajami et al., 2007).

The data collected from the intra peritoneal injection experiments so far did not show a recruitment of microglia precursors from the periphery. There is a possibility that the concentration of injected cells is still too low. However, Wu and his colleagues observed cells in the CNS when injecting 10^6 monocytes, which is an amount equal to our experiments. Thus the low number of injected cells is most probably not the decisive factor for the absence of GFP-expressing cells in the CNS.

In the future, our experiment can be optimized by choosing an alternative injection site. Wu et al. assessed 3 different sites of administration: the peritoneum, tail vein and carotid vein.

The intra-peritoneal route proved to be the most inefficient, followed by tail vein injection. A highly efficient application route, yielding the most cells in the CNS, was intravenous injection into the carotid vein (Wu et al., 2006).

In case the outcome does not point to a recruitment of myeloid precursors from the periphery, we will have to reconsider our theory about the origin of the “fountain of microglia”. The accumulation of amoeboid microglia-like cells could be also explained by reorganization of cortical microglia, which have the capacity to dedifferentiate into amoeboid microglia upon stimulation, a property called “functional plasticity” (Tambuyzer et al., 2008).

In conclusion, this postnatal recruitment of microglial cells is not only interesting from a developmental perspective, but also regarding therapeutical prospects. The blood-brain barrier poses a major obstacle to gene therapy. Microglial engraftment from the periphery allows these cells to be exploited as a biological and non-invasive tool for cell therapy by introducing therapeutical genes to the diseased CNS (Flugel et al., 2001; Priller et al., 2001).

Acknowledgements

I want to thank everybody who supported and contributed to my diploma thesis.

First, I want to thank my supervisor, Monika Bradl for the opportunity to work in her lab and for her guidance, constructive input, and kind words throughout this project.

By inviting me to join her group she enabled me to enrich my knowledge in many different fields. I was introduced to various techniques, including immunohistochemical, biochemical, in vitro and in vivo methods, as well as microscopy. I also gained an insight into rat anatomy and the general handling of laboratory animals.

I want to acknowledge Marianne Leisser, Ulrike Köck and Angela Kury for great technical assistance.

Further, I want to express my gratitude to the rest of the staff of our department for creating such a pleasant working atmosphere. I feel lucky to have been part of such a harmonical, benevolent group of people.

My special thanks go out to Isabella Wimmer for her stimulating input, new ideas, and motivation. Thank you for your support and sharing your knowledge even on tricky technical questions.

I want to thank my family, especially my parents, Helga and Manfred, and my sister, Marianne, for their unconditional love and support. Their encouragement always kept me going, especially through tough times.

Finally I want to thank Jan for always standing by my side, enduring my mood swings and cheering me up whenever necessary.

Supplementary Data

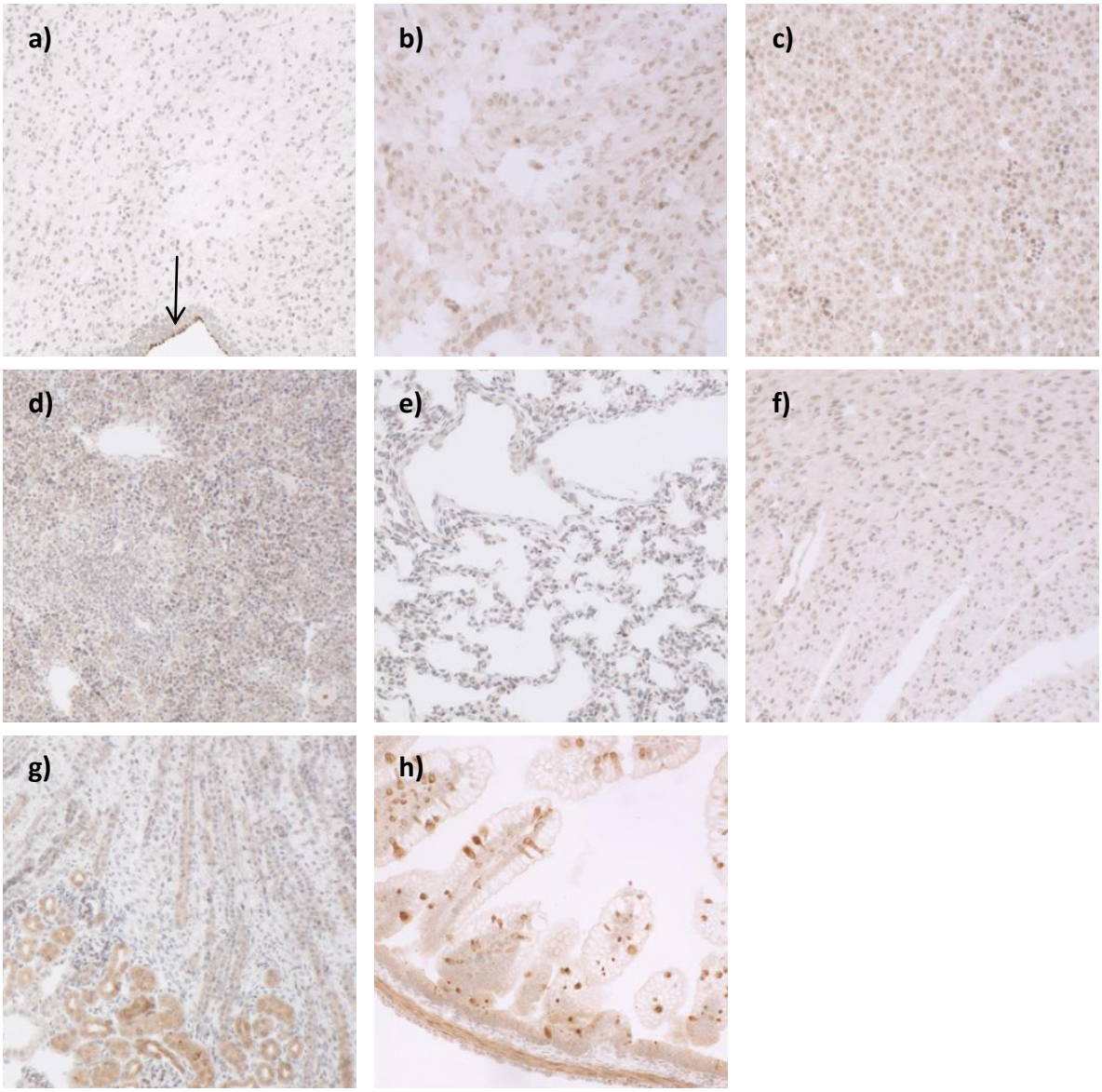

Figure 35: Negative control of Buffy coat-injected P3 pups, stained for GFP. P3 Lewis pup was injected with RPMI/1% rat serum. a) Brain section. Ependymal cells display unspecific GFP staining (see black arrow) (× 100). b) Spinal cord section (× 100). c) Liver section (× 100). d) Spleen section (× 100). e) Lung section (× 100). f) Heart section (× 100). g) Kidney tissue shows unspecific staining of the tubules (× 100). h) Intestinal tissue displays unspecific brown staining of goblet cells (× 100).

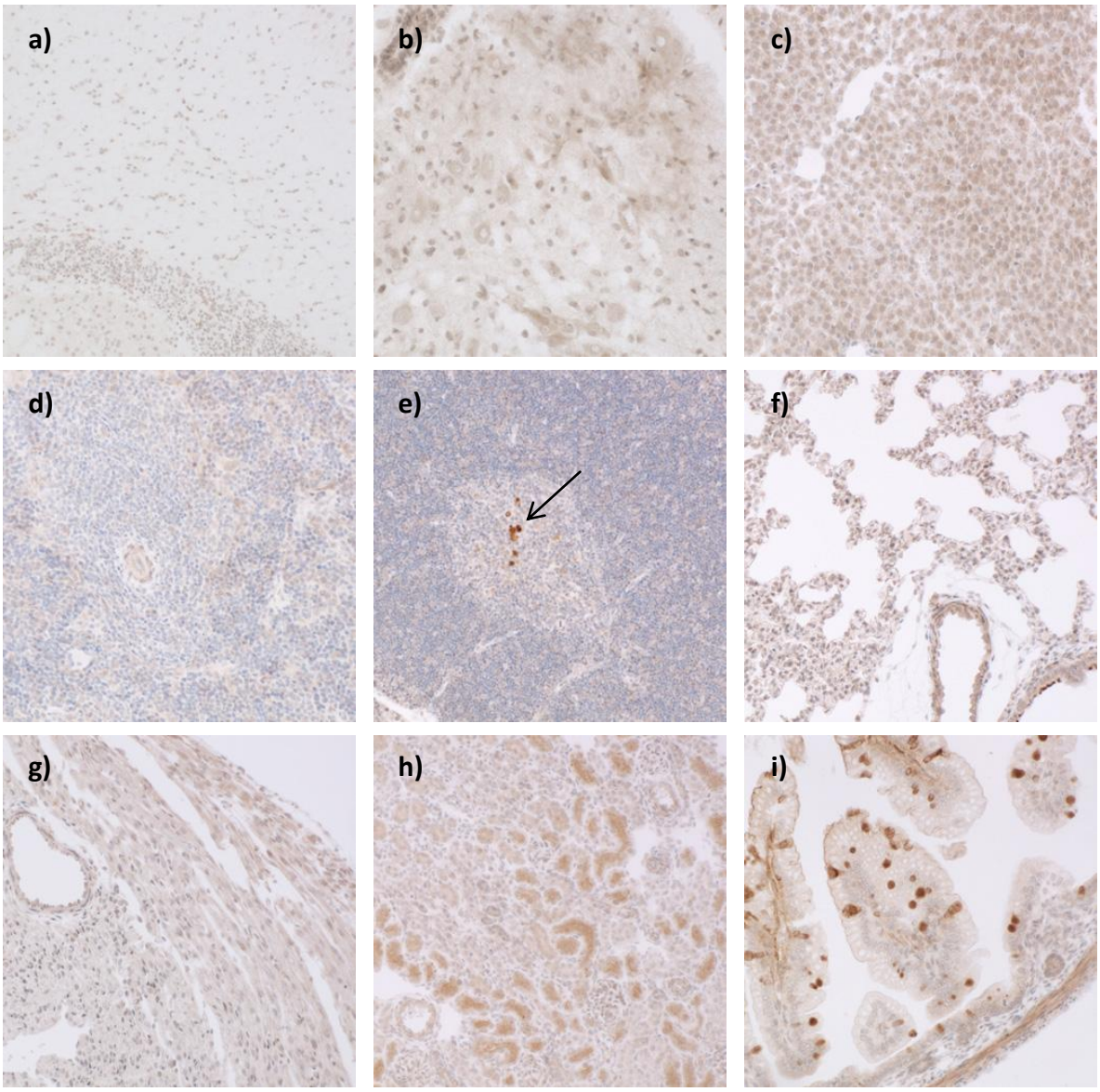

Figure 36: Negative control of Buffy coat and spleen homogenate-injected P7 rats. P7 Lewis rat was injected with RPMI/1% rat serum. a) Brain section (× 100). b) Spinal cord section (× 100). c) Liver section (× 100). d) Spleen section (× 100). e) Thymus shows unspecific staining in the medulla (see black arrow) (× 100). f) Lung section (× 100). g) Heart section (× 100). g) Kidney shows unspecific staining of the tubules (× 100). h) Intestinal tissue exhibits unspecific staining of the goblet cells (× 100).

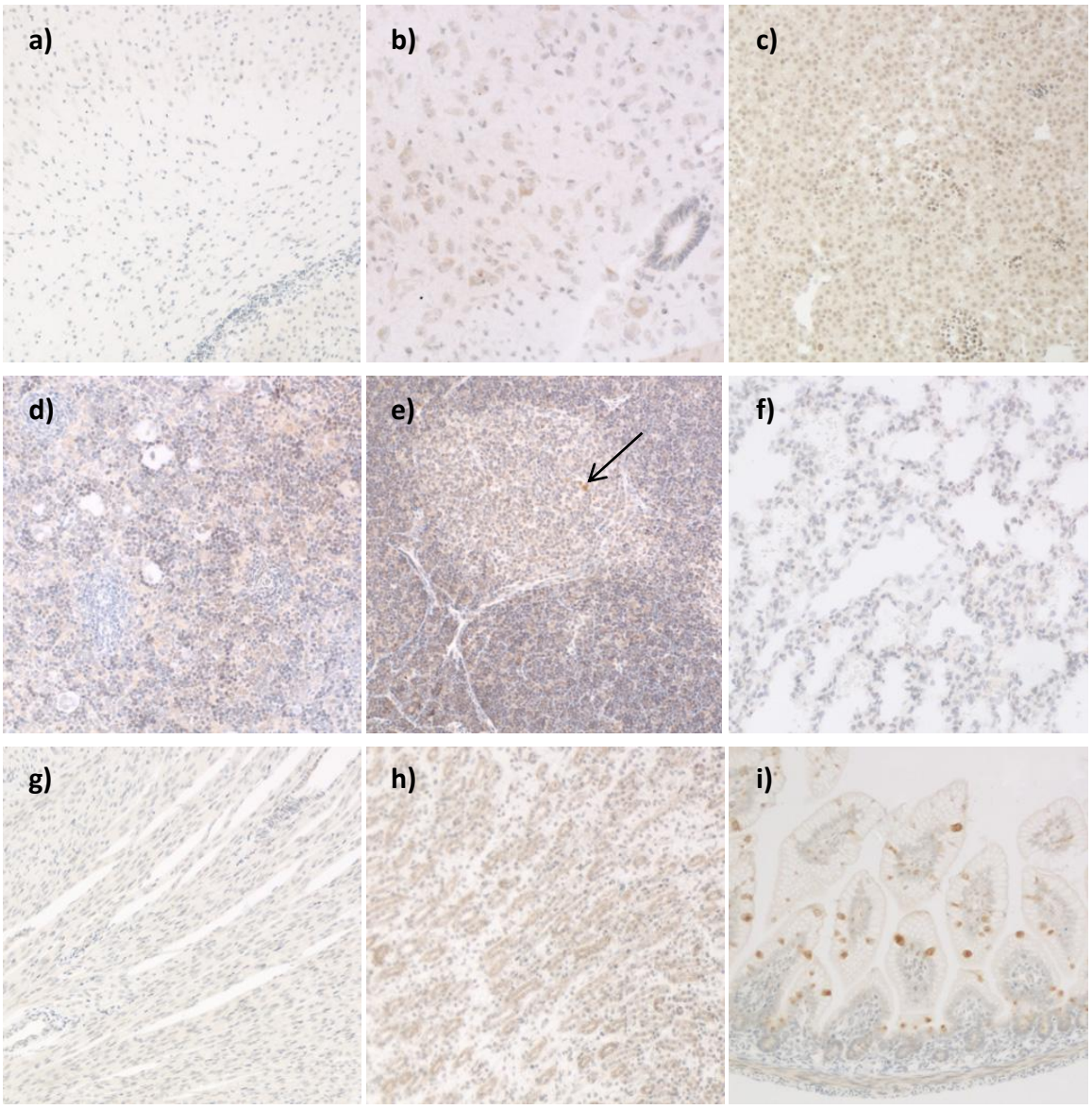

Figure 37: Negative control of Buffy coat-injected P10 rats. P10 Lewis rat was injected with RPMI/1% rat serum. a) Brain section (× 100). b) Spinal cord section (× 100). c) Liver section (× 100). d) Spleen section (× 100). e) Thymus shows light unspecific staining in the medulla (see black arrow) (× 100). f) Lung section (× 100). g) Heart section (× 100). g) Kidney section (× 100). h) Intestinal tissue exhibits unspecific staining of the goblet cells (× 100).

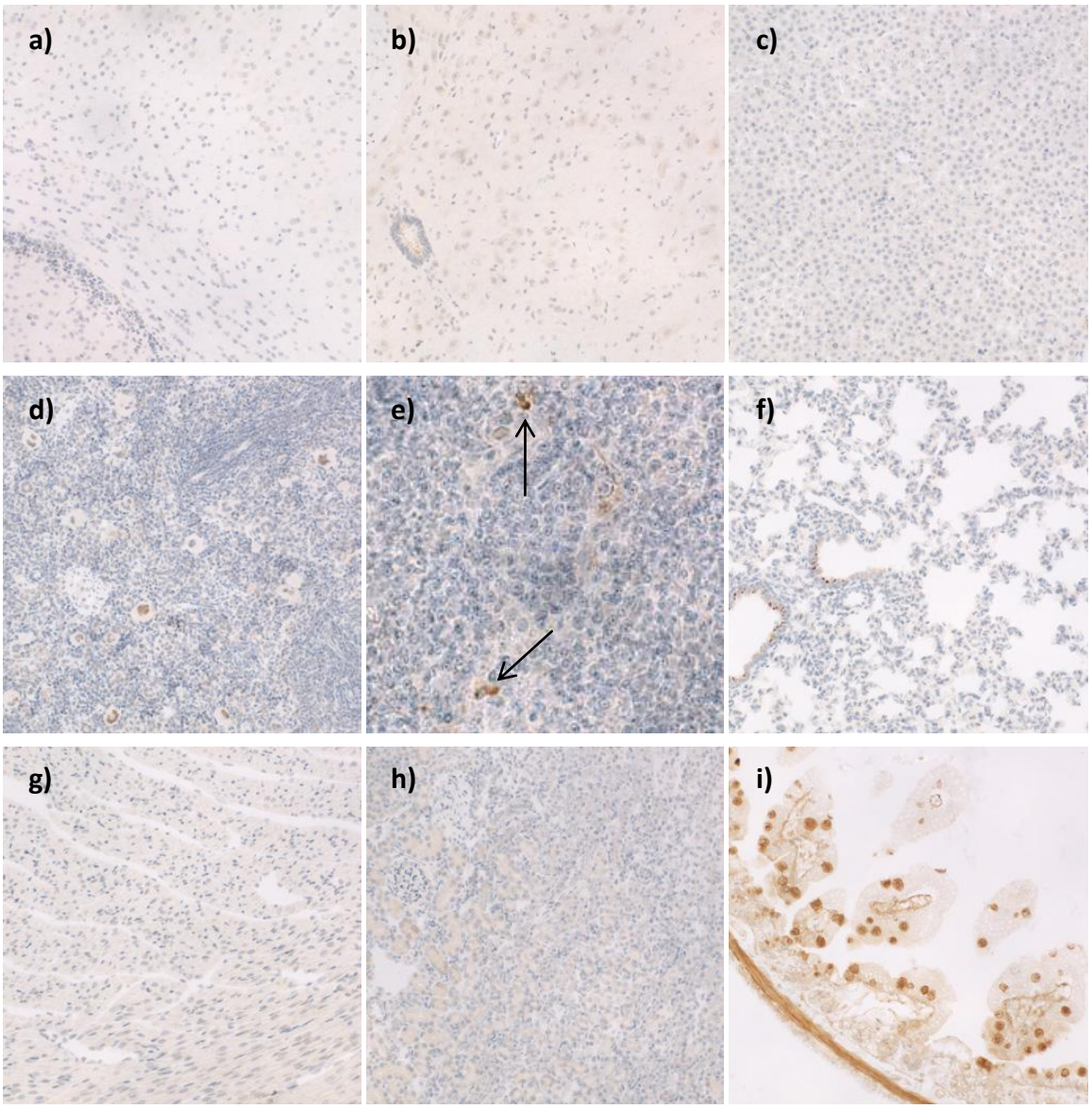

Figure 38: Negative control of Buffy coat and spleen homogenate-injected P14 rats. P14 Lewis animal was injected with RPMI/1% rat serum. a) Brain section (× 100). b) Spinal cord section (× 100). c) Liver section (× 100). d) Spleen section (× 100). e) Thymus shows unspecific staining, indicated by black arrows (× 100). f) Epithelium of lung tissue displays unspecific staining (see black arrow) (× 100). g) Heart section (× 100). g) Kidney shows unspecific staining of the tubules (× 100). h) Intestinal tissue exhibits unspecific staining of the goblet cells (× 100).

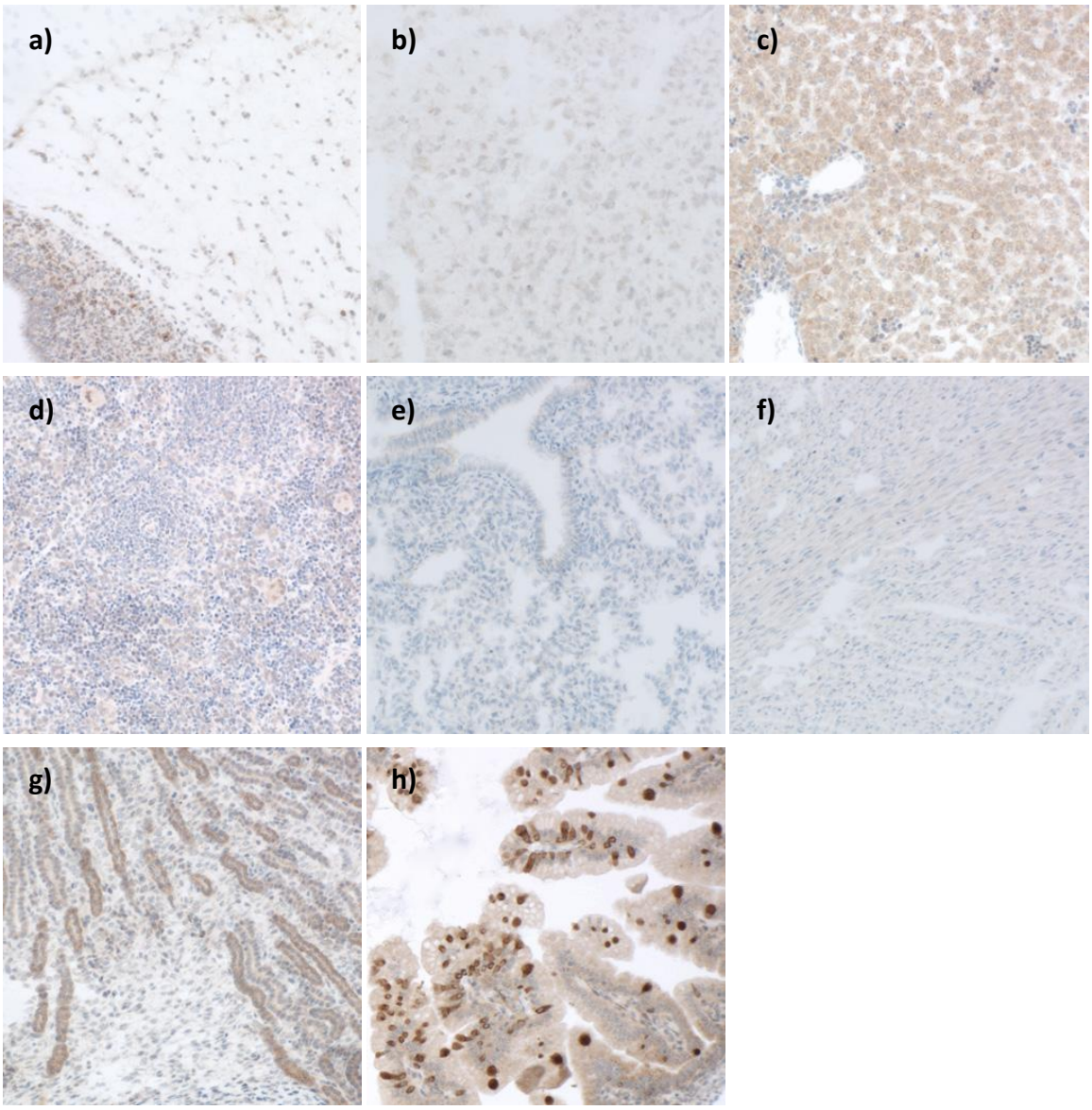

Figure 39: Negative control of monocyte and iron containing spleen cell-injected P3 pups. P3 Lewis pup was injected with RPMI/1% rat serum. a) Brain section (× 100). b) Spinal cord section (× 100). c) Liver shows unspecific staining throughout the tissue (× 100). d) Spleen section (× 100). e) Lung section (× 100). f) Heart section (× 100). g) Kidney shows unspecific staining of the tubules (× 100). h) Intestinal tissue exhibits unspecific staining of the goblet cells (× 100).

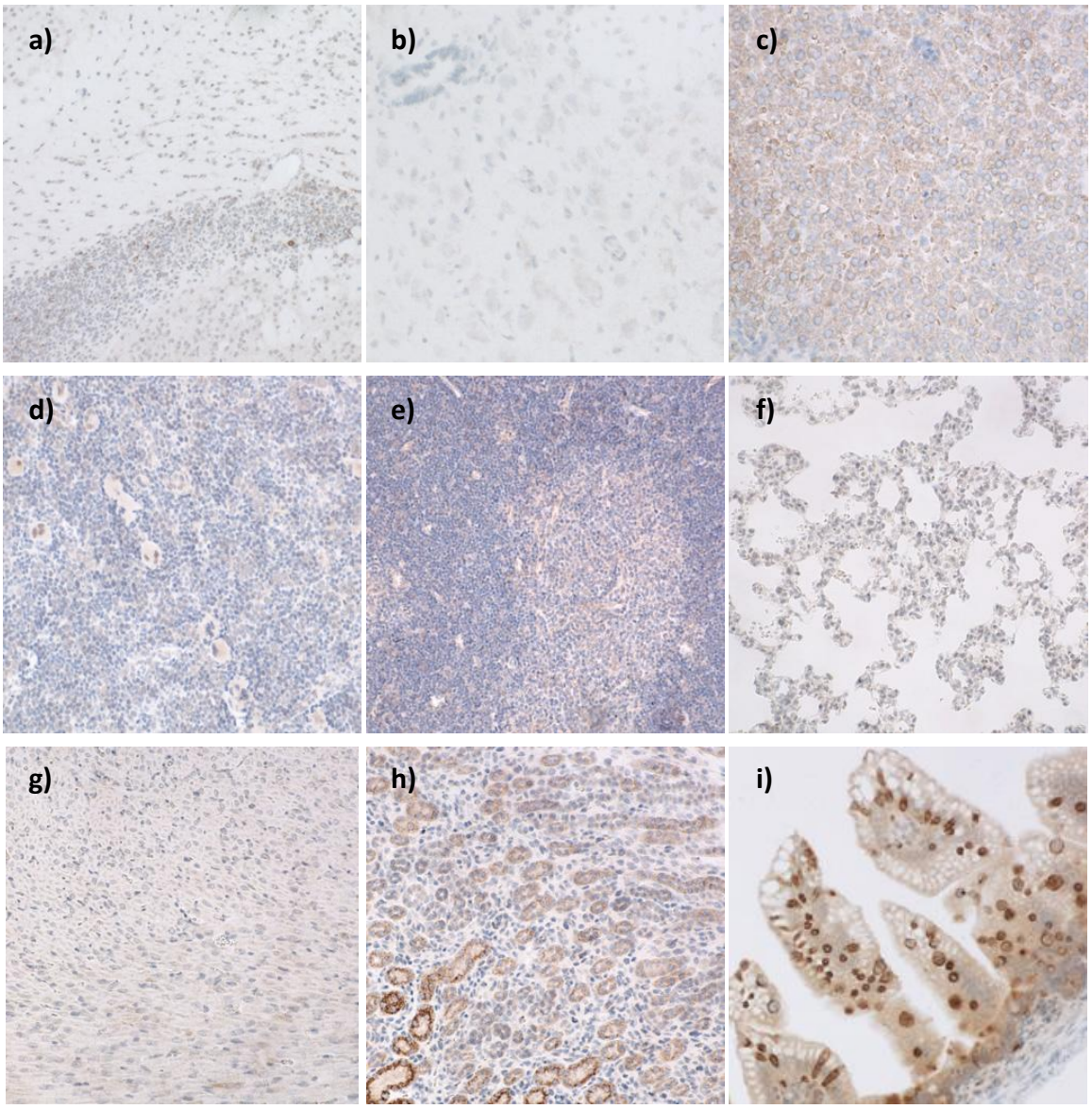

Figure 40: Negative control of monocyte-injected P7 pups. P3 Lewis pup was injected with RPMI/1% rat serum. a) Brain section (× 100). b) Spinal cord section (× 100). c) Liver shows ubiquitous unspecific staining (× 100). d) Spleen section (× 100). e) Thymus section (× 100). f) Lung section (× 100). g) Heart section (× 100). h) Kidney displays unspecific staining of the tubules (× 100). i) Intestinal tissue shows unspecific staining of the goblet cells (× 100).

Reference List

Ajami, B., Bennett, J.L., Krieger, C., Tetzlaff, W., and Rossi, F.M. (2007). Local self-renewal can sustain CNS microglia maintenance and function throughout adult life. Nat Neurosci *10*, 1538-1543.

Akashi, H., Tayama, K., Fujino, T., Fukunaga, S., Tanaka, A., Hayashi, S., Tobinaga, S., Onitsuka, S., Sakashita, H., and Aoyagi, S. (2000a). Cerebral protection selection in aortic arch surgery for patients with preoperative complications of cerebrovascular disease. Jpn J Thorac Cardiovasc Surg *48*, 782-788.

Akashi, K., Traver, D., Miyamoto, T., and Weissman, I.L. (2000b). A clonogenic common myeloid progenitor that gives rise to all myeloid lineages. Nature *404*, 193-197.

Alliot, F., Godin, I., and Pessac, B. (1999). Microglia derive from progenitors, originating from the yolk sac, and which proliferate in the brain. Brain Res Dev Brain Res *117*, 145-152.

Alliot, F., Lecain, E., Grima, B., and Pessac, B. (1991). Microglial progenitors with a high proliferative potential in the embryonic and adult mouse brain. Proc Natl Acad Sci U S A *88*, 1541-1545.

Auffray, C., Fogg, D., Garfa, M., Elain, G., Join-Lambert, O., Kayal, S., Sarnacki, S., Cumano, A., Lauvau, G., and Geissmann, F. (2007). Monitoring of blood vessels and tissues by a population of monocytes with patrolling behavior. Science *317*, 666-670.

Chan, W.Y., Kohsaka, S., and Rezaie, P. (2007). The origin and cell lineage of microglia—New concepts. Brain Research Reviews *53*, 344-354.

Chugani, D.C., Kedersha, N.L., and Rome, L.H. (1991a). Vault Immunofluorescence in the Brain - New Insights Regarding the Origin of Microglia. Journal of Neuroscience *11*, 256-268.

Chugani, D.C., Kedersha, N.L., and Rome, L.H. (1991b). Vault immunofluorescence in the brain: new insights regarding the origin of microglia. J Neurosci *11*, 256-268.

Conductier, G., Blondeau, N., Guyon, A., Nahon, J.L., and Rovere, C. (2010). The role of monocyte chemoattractant protein MCP1/CCL2 in neuroinflammatory diseases. J Neuroimmunol.

Connor, J.R., Pavlick, G., Karli, D., Menzies, S.L., and Palmer, C. (1995). A histochemical study of iron-positive cells in the developing rat brain. J Comp Neurol *355*, 111-123.

Dalmau, I., Vela, J.M., Gonzalez, B., and Castellano, B. (1997). Expression of LFA-1alpha and ICAM-1 in the developing rat brain: a potential mechanism for the recruitment of microglial cell precursors. Brain Res Dev Brain Res *103*, 163-170.

Davalos, D., Grutzendler, J., Yang, G., Kim, J.V., Zuo, Y., Jung, S., Littman, D.R., Dustin, M.L., and Gan, W.B. (2005). ATP mediates rapid microglial response to local brain injury in vivo. Nat Neurosci *8*, 752-758.

Flugel, A., Bradl, M., Kreutzberg, G.W., and Graeber, M.B. (2001). Transformation of donor-derived bone marrow precursors into host microglia during autoimmune CNS inflammation and during the retrograde response to axotomy. J Neurosci Res *66*, 74-82.

Geissmann, F., Jung, S., and Littman, D.R. (2003). Blood monocytes consist of two principal subsets with distinct migratory properties. Immunity *19*, 71-82.

Geissmann, F., Manz, M.G., Jung, S., Sieweke, M.H., Merad, M., and Ley, K. (2010). Development of monocytes, macrophages, and dendritic cells. Science *327*, 656-661.

Ginhoux, F., Greter, M., Leboeuf, M., Nandi, S., See, P., Gokhan, S., Mehler, M.F., Conway, S.J., Ng, L.G., Stanley, E.R.*, et al.* (2010). Fate mapping analysis reveals that adult microglia derive from primitive macrophages. Science *330*, 841-845.

Giulian, D., Young, D.G., Woodward, J., Brown, D.C., and Lachman, L.B. (1988). Interleukin-1 is an astroglial growth factor in the developing brain. J Neurosci *8*, 709-714.

Hickey, W.F., and Kimura, H. (1988). Perivascular microglial cells of the CNS are bone marrow-derived and present antigen in vivo. Science *239*, 290-292.

Hirasawa, T., Ohsawa, K., Imai, Y., Ondo, Y., Akazawa, C., Uchino, S., and Kohsaka, S. (2005). Visualization of microglia in living tissues using Iba1-EGFP transgenic mice. Journal of Neuroscience Research *81*, 357-362.

Hoftberger, R., Aboul-Enein, F., Brueck, W., Lucchinetti, C., Rodriguez, M., Schmidbauer, M., Jellinger, K., and Lassmann, H. (2004). Expression of major histocompatibility complex class I molecules on the different cell types in multiple sclerosis lesions. Brain Pathol *14*, 43-50.

Holman, D.W., Klein, R.S., and Ransohoff, R.M. (2011). The blood-brain barrier, chemokines and multiple sclerosis. Biochim Biophys Acta *1812*, 220-230.

Hristova, M., Cuthill, D., Zbarsky, V., Acosta-Saltos, A., Wallace, A., Blight, K., Buckley, S.M., Peebles, D., Heuer, H., Waddington, S.N.*, et al.* (2010). Activation and deactivation of periventricular white matter phagocytes during postnatal mouse development. Glia *58*, 11-28.

Jones, L.L., Liu, Z., Shen, J., Werner, A., Kreutzberg, G.W., and Raivich, G. (2000). Regulation of the cell adhesion molecule CD44 after nerve transection and direct trauma to the mouse brain. J Comp Neurol *426*, 468-492.

Karpus, W.J., Lukacs, N.W., McRae, B.L., Strieter, R.M., Kunkel, S.L., and Miller, S.D. (1995). An important role for the chemokine macrophage inflammatory protein-1 alpha in the pathogenesis of the T cell-mediated autoimmune disease, experimental autoimmune encephalomyelitis. J Immunol *155*, 5003-5010.

Kennedy, D.W., and Abkowitz, J.L. (1997). Kinetics of central nervous system microglial and macrophage engraftment: analysis using a transgenic bone marrow transplantation model. Blood *90*, 986-993.

Klopp, A.H., Spaeth, E.L., Dembinski, J.L., Woodward, W.A., Munshi, A., Meyn, R.E., Cox, J.D., Andreeff, M., and Marini, F.C. (2007). Tumor irradiation increases the recruitment of circulating mesenchymal stem cells into the tumor microenvironment. Cancer Res *67*, 11687-11695.

Kreutzberg, G.W. (1996). Microglia: a sensor for pathological events in the CNS. Trends Neurosci *19*, 312-318.

Marin-Teva, J.L., Dusart, I., Colin, C., Gervais, A., van Rooijen, N., and Mallat, M. (2004). Microglia promote the death of developing Purkinje cells. Neuron *41*, 535-547.

Mikkola, H.K., and Orkin, S.H. (2006). The journey of developing hematopoietic stem cells. Development *133*, 3733-3744.

Mildner, A., Schmidt, H., Nitsche, M., Merkler, D., Hanisch, U.-K., Mack, M., Heikenwalder, M., Brück, W., Priller, J., and Prinz, M. (2007). Microglia in the adult brain arise from Ly-6ChiCCR2+ monocytes only under defined host conditions. Nature Neuroscience *10*, 1544-1553.

Neumann, H., Kotter, M.R., and Franklin, R.J. (2009). Debris clearance by microglia: an essential link between degeneration and regeneration. Brain *132*, 288-295.

Nguyen, K.B., McCombe, P.A., and Pender, M.P. (1994). Macrophage apoptosis in the central nervous system in experimental autoimmune encephalomyelitis. J Autoimmun *7*, 145-152.

Ohno, K., Miyoshi, S., Minami, M., Akashi, A., Maeda, H., Nakagawa, K., Matsumura, A., Nakamura, K., Matsuda, H., and Ohashi, S. (2000). Ipsilateral recurrence frequency after video-assisted thoracoscopic surgery for primary spontaneous pneumothorax. Jpn J Thorac Cardiovasc Surg *48*, 757-760.

Perry, V.H., Matyszak, M.K., and Fearn, S. (1993). Altered antigen expression of microglia in the aged rodent CNS. Glia *7*, 60-67.

Polazzi, E., and Monti, B. (2010). Microglia and neuroprotection: from in vitro studies to therapeutic applications. Prog Neurobiol *92*, 293-315.

Polfliet, M.M., Goede, P.H., van Kesteren-Hendrikx, E.M., van Rooijen, N., Dijkstra, C.D., and van den Berg, T.K. (2001). A method for the selective depletion of perivascular and meningeal macrophages in the central nervous system. J Neuroimmunol *116*, 188-195.

Priller, J., Flugel, A., Wehner, T., Boentert, M., Haas, C.A., Prinz, M., Fernandez-Klett, F., Prass, K., Bechmann, I., de Boer, B.A.*, et al.* (2001). Targeting gene-modified hematopoietic cells to the central nervous system: use of green fluorescent protein uncovers microglial engraftment. Nat Med *7*, 1356-1361.

Raivich, G., Jones, L.L., Kloss, C.U., Werner, A., Neumann, H., and Kreutzberg, G.W. (1998). Immune surveillance in the injured nervous system: T-lymphocytes invade the axotomized mouse facial motor nucleus and aggregate around sites of neuronal degeneration. J Neurosci *18*, 5804-5816.

Ransohoff, R.M. (2007). Microgliosis: the questions shape the answers. Nat Neurosci *10*, 1507-1509.

Redzic, Z.B., and Segal, M.B. (2004). The structure of the choroid plexus and the physiology of the choroid plexus epithelium. Adv Drug Deliv Rev *56*, 1695-1716.

Repnik, U., Knezevic, M., and Jeras, M. (2003). Simple and cost-effective isolation of monocytes from buffy coats. J Immunol Methods *278*, 283-292.

Rezaie, P. (2004). Microglia in the Cerebral Wall of the Human Telencephalon at Second Trimester. Cerebral Cortex *15*, 938-949.

Rezaie, P., and Male, D. (1999). Colonisation of the developing human brain and spinal cord by microglia: a review. Microsc Res Tech *45*, 359-382.

Scriba, A., Luciano, L., and Steiniger, B. (1996). High-yield purification of rat monocytes by combined density gradient and immunomagnetic separation. J Immunol Methods *189*, 203-216.

Serbina, N.V., and Pamer, E.G. (2006). Monocyte emigration from bone marrow during bacterial infection requires signals mediated by chemokine receptor CCR2. Nat Immunol *7*, 311-317.

Shang, X.Z., Lang, B.J., and Issekutz, A.C. (1998). Adhesion molecule mechanisms mediating monocyte migration through synovial fibroblast and endothelium barriers: role for CD11/CD18, very late antigen-4 (CD49d/CD29), very late antigen-5 (CD49e/CD29), and vascular cell adhesion molecule-1 (CD106). J Immunol *160*, 467-474.

Smith, T., Schmied, M., Hewson, A.K., Lassmann, H., and Cuzner, M.L. (1996). Apoptosis of T cells and macrophages in the central nervous system of intact and adrenalectomized Lewis rats during experimental allergic encephalomyelitis. J Autoimmun *9*, 167-174.

Stoll, M., Capper, D., Dietz, K., Warth, A., Schleich, A., Schlaszus, H., Meyermann, R., and Mittelbronn, M. (2006). Differential microglial regulation in the human spinal cord under normal and pathological conditions. Neuropathol Appl Neurobiol *32*, 650-661.

Sunderkotter, C., Nikolic, T., Dillon, M.J., Van Rooijen, N., Stehling, M., Drevets, D.A., and Leenen, P.J. (2004). Subpopulations of mouse blood monocytes differ in maturation stage and inflammatory response. J Immunol *172*, 4410-4417.

Swirski, F.K., Nahrendorf, M., Etzrodt, M., Wildgruber, M., Cortez-Retamozo, V., Panizzi, P., Figueiredo, J.L., Kohler, R.H., Chudnovskiy, A., Waterman, P.*, et al.* (2009). Identification of

splenic reservoir monocytes and their deployment to inflammatory sites. Science *325*, 612-616.

Tacke, F., and Randolph, G.J. (2006). Migratory fate and differentiation of blood monocyte subsets. Immunobiology *211*, 609-618.

Takahashi, K., and Naito, M. (1993). Development, differentiation, and proliferation of macrophages in the rat yolk sac. Tissue Cell *25*, 351-362.

Tambuyzer, B.R., Ponsaerts, P., and Nouwen, E.J. (2008). Microglia: gatekeepers of central nervous system immunology. Journal of Leukocyte Biology *85*, 352-370.

Van Furth, R., and Cohn, Z.A. (1968). The origin and kinetics of mononuclear phagocytes. Journal of experimental medicine *128*, 415 - 435.

Van Furth, R., Cohn, Z.A., Hirsch, J.G., Humphrey, J.H., Spector, W.G., and Langevoort, H.L. (1972). The mononuclear phagocyte system: a new classification of macrophages, monocytes, and their precursor cells. Bulletin of the World Health Organization (WHO) *46*, 845 - 852.

Varol, C., Yona, S., and Jung, S. (2009). Origins and tissue-context-dependent fates of blood monocytes. Immunol Cell Biol *87*, 30-38.

Wu, C.H., Wen, C.Y., Shieh, J.Y., and Ling, E.A. (1992). A quantitative and morphometric study of the transformation of amoeboid microglia into ramified microglia in the developing corpus callosum in rats. J Anat *181 (Pt 3)*, 423-430.

Wu, J., Yang, S., Luo, H., Zeng, L., Ye, L., and Lu, Y. (2006). Quantitative evaluation of monocyte transmigration into the brain following chemical opening of the blood-brain barrier in mice. Brain Res *1098*, 79-85.

Yona, S., and Jung, S. (2010). Monocytes: subsets, origins, fates and functions. Current Opinion in Hematology *17*, 53-59.

Yrlid, U., Jenkins, C.D., and MacPherson, G.G. (2006). Relationships between distinct blood monocyte subsets and migrating intestinal lymph dendritic cells in vivo under steady-state conditions. J Immunol *176*, 4155-4162.

Zassler, B., and Humpel, C. (2006). Transplantation of NGF secreting primary monocytes counteracts NMDA-induced cell death of rat cholinergic neurons in vivo. Exp Neurol *198*, 391-400.

Ziegler-Heitbrock, H.W. (2000). Definition of human blood monocytes. J Leukoc Biol *67*, 603-606.

Curriculum Vitae

Personal Data

Name:	Magdalena Heninger
Date of birth:	September 18th, 1987
Place of birth:	Vienna, Austria
Citizenship:	Austrian
Contact:	leni.heninger@hotmail.com

Education

1994 – 1998	Primary school VS Rittingergasse 29A, Vienna VS Lavantgasse 35, Vienna
1998 – 2006	Secondary school GRG21 Ödenburgerstrasse 74
Since October 2006	Study of Molecular Biology University of Vienna